U.S.NRC
United States Nuclear Regulatory Commission
Protecting People and the Environment

NUREG/CR-7201

Characterizing Explosive Effects on Underground Structures

Office of Nuclear Security and Incident Response

AVAILABILITY OF REFERENCE MATERIALS IN NRC PUBLICATIONS

NRC Reference Material

As of November 1999, you may electronically access NUREG-series publications and other NRC records at NRC's Library at www.nrc.gov/reading-rm.html. Publicly released records include, to name a few, NUREG-series publications; *Federal Register* notices; applicant, licensee, and vendor documents and correspondence; NRC correspondence and internal memoranda; bulletins and information notices; inspection and investigative reports; licensee event reports; and Commission papers and their attachments.

NRC publications in the NUREG series, NRC regulations, and Title 10, "Energy," in the *Code of Federal Regulations* may also be purchased from one of these two sources.

1. **The Superintendent of Documents**
   U.S. Government Publishing Office
   Mail Stop IDCC
   Washington, DC 20402-0001
   Internet: bookstore.gpo.gov
   Telephone: (202) 512-1800
   Fax: (202) 512-2104

2. **The National Technical Information Service**
   5301 Shawnee Rd., Alexandria, VA 22312-0002
   www.ntis.gov
   1-800-553-6847 or, locally, (703) 605-6000

A single copy of each NRC draft report for comment is available free, to the extent of supply, upon written request as follows:

Address: **U.S. Nuclear Regulatory Commission**
Office of Administration
Publications Branch
Washington, DC 20555-0001
E-mail: distribution.resource@nrc.gov
Facsimile: (301) 415-2289

Some publications in the NUREG series that are posted at NRC's Web site address www.nrc.gov/reading-rm/doc-collections/nuregs are updated periodically and may differ from the last printed version. Although references to material found on a Web site bear the date the material was accessed, the material available on the date cited may subsequently be removed from the site.

Non-NRC Reference Material

Documents available from public and special technical libraries include all open literature items, such as books, journal articles, transactions, *Federal Register* notices, Federal and State legislation, and congressional reports. Such documents as theses, dissertations, foreign reports and translations, and non-NRC conference proceedings may be purchased from their sponsoring organization.

Copies of industry codes and standards used in a substantive manner in the NRC regulatory process are maintained at—

The NRC Technical Library
Two White Flint North
11545 Rockville Pike
Rockville, MD 20852-2738

These standards are available in the library for reference use by the public. Codes and standards are usually copyrighted and may be purchased from the originating organization or, if they are American National Standards, from—

American National Standards Institute
11 West 42nd Street
New York, NY 10036-8002
www.ansi.org
(212) 642-4900

Legally binding regulatory requirements are stated only in laws; NRC regulations; licenses, including technical specifications; or orders, not in NUREG-series publications. The views expressed in contractorprepared publications in this series are not necessarily those of the NRC.

The NUREG series comprises (1) technical and administrative reports and books prepared by the staff (NUREG–XXXX) or agency contractors (NUREG/CR–XXXX), (2) proceedings of conferences (NUREG/CP–XXXX), (3) reports resulting from international agreements (NUREG/IA–XXXX), (4) brochures (NUREG/BR–XXXX), and (5) compilations of legal decisions and orders of the Commission and Atomic and Safety Licensing Boards and of Directors' decisions under Section 2.206 of NRC's regulations (NUREG–0750).

U.S.NRC
United States Nuclear Regulatory Commission
Protecting People and the Environment

NUREG/CR-7201

Characterizing Explosive Effects on Underground Structures

Manuscript Completed: September 2013
Date Published: September 2015

Prepared by
A. H. Chowdhury, CNWRA
T. E. Wilt, CNWRA

Center for Nuclear Waste Regulatory Analyses
Southwest Research Institute®
6220 Culebra Road
San Antonio, Texas 78238-5166

Kris Jamgochian, NRC Project Manager
Peter S. Lee, NRC Technical Monitor

NRC Job Code N4128

Office of Nuclear Security and Incident Response

ABSTRACT

A literature review and finite element analyses were conducted to characterize the effects of explosions on underground structures for explosive charges located close to and on the ground surface. Explosive charge weights were selected to be consistent with Vehicle Borne Improvised Explosive Devices (VBIEDs) terrorists make mostly using chemicals and available precursor materials. The phenomena associated with air and surface explosions of VBIEDs, propagation of their dynamic waves through air, crater formation, and propagation through subsurface media are similar to those of conventional high explosive military weapons. Empirical equations for predicting these blast-induced effects and designing underground structures under explosive loads are available in the literature. These empirical equations, however, do have a specific range of applicability. Numerical analysis techniques (e.g., finite element) also require specific assumptions and idealizations. A limited finite element parametric study was used to investigate the influence of important parameters. These influences include the explosive charge weight and how the distance of a point in the subsurface soil from the location of explosion affects the explosion-generated pressure distribution in the underground soil. The blast-induced pressure wave in the soil surrounding an underground structure results in time-dependent loading (pressure or impulse force) of the underground structure. The current methodology for the designing underground structures subjected to explosive loads uses concepts and provisions of other specific codes, standards, and design manuals commonly used in designing reinforced concrete, prestressed concrete, masonry, and steel structures. An underground structure that may be subjected to both explosive and seismic loads should consider both types of loads in appropriate combinations.

CONTENTS

CONTENTS (continued)

FIGURES

TABLES

EXECUTIVE SUMMARY

The blast-induced dynamic loads explosions generate above ground and in contact with the ground surface can damage underground structures. Underground structures that are designed to protect against high explosive charges mostly include sensitive military facilities, civil defense facilities, and, most recently, nuclear power plants (e.g., proposed small modular reactors). The military facilities include bunkers, missile silos, command and control facilities, and communication facilities. The blast-induced shock exerted on an underground structure will vary with the type of explosive; the explosive charge weight; whether the explosive charge is in direct contact with the ground surface; the distance from the explosion to the underground structure (i.e., burial depth); and the characteristics of the underground media, such as the soil and/or rock types, presence of different layers of soil, and drainage conditions affecting the moisture content and pore water pressure of the underground media.

The objective of this report is to review and conduct numerical analyses to characterize the effects explosions close to the ground surface and in contact with the ground surface have on underground structures, with emphasis on the Vehicle Borne Improvised Explosive Devices (VBIEDs). The activities include (i) identifying the characteristics and properties of VBIEDs; (ii) reviewing the dynamics of explosion propagation through air, underground soil medium, and underwater; (iii) identifying the empirical equations for the propagation of the blast-induced shock wave through the air, underground soil medium, and underwater; (iv) conducting a limited finite element parametric study to determine the explosion-generated pressure distribution in the underground soil; (v) identifying the empirical equations for evaluating the structural response; (vi) identifying structural design standards or guidance for underground structures subjected to explosive loads; and (vii) reviewing and identifying the differences between explosive and seismic load effects on an underground structure and the differences in the required structural design.

Explosives are terrorists' most popular choice for damaging human lives and property. Although military explosives can be illegally obtained and are used by terrorists to make VBIEDs, they are difficult to obtain, and terrorists often choose to make their own explosives using chemicals and precursor materials available to them. This report provides a sample of homemade explosives and ingredients used to prepare the VBIEDs. The VBIEDs use a vehicle as the package, container, and means of delivery. The types of vehicle used for the detonation of VBIEDs determine the aboveground height of detonation. The U.S. National Counterterrorism Center has identified the trinitrotoluene (TNT)-equivalent explosive capacities for different vehicle sizes. The maximum TNT-equivalent explosives' holding capacities in U.S. vehicles range from 227 to 27,215 kg [500 to 60,000 lb].

Because the VBIEDs are conventional weapons, the phenomena of the air and surface explosions of the VBIEDs, propagation of their dynamic waves through air, crater formation, and propagation through subsurface media are similar to those of conventional military and commercial weapons. The magnitude and distribution of the dynamic loads on the underground structures created by near-ground surface detonation of VBIEDs are affected by the strength of the explosive charge and its distance from the buried structure, the properties of the soil and rock between the detonation point and the structure, and the orientation of structural members with respect to the direction of propagation of the dynamic waves. This dynamic load on the underground structures will also be affected by engineered site-specific conditions, such as the presence of an explosion-protected concrete slab, a rock barrier, or a surface building floor slab between the point of detonation and the underground structures.

Empirical equations are available for calculating explosion-induced effects in the air, on the ground surface, and under water and are primarily based on the assumption of a spherical-shaped explosive charge. The empirical equations are used for calculating important parameters that affect the underground structures, such as explosion wave arrival time at a given location; duration of the explosion wave; peak free-field pressure; impulse force; and particle displacement, velocity, and acceleration. Only a limited amount of test data is available to predict the pressures on the underground structures primarily from conventional weapons. The empirical and experimental information is aided by various numerical analysis techniques, with appropriate assumptions, idealizations, and simplifications that have been implemented in various restricted-use codes (i.e., defense related and commercially available computer codes, such as ABAQUS and LS-DYNA).

Empirical equations are also available for the analysis and design of underground concrete and steel structures that are subjected to the surface and subsurface explosion-generated pressure on the soil that surrounds the underground structures. These empirical equations are based on experimental investigations and aided by analytical investigations. These empirical equations provide a means to calculate forces imposed on structures, including bending moment and shear capacity, beam-column effects, energy absorption capacity under shock loads, cracking, and spall of concrete components.

A finite element parametric study has been conducted on the subsurface effects from a surface burst. A Lagrangian approach was used with the blast loading calculated using the Conventional Weapons (CONWEP) algorithm available in ABAQUS/Explicit. The size of the TNT-equivalent charge was varied, and the resulting soil pressures and apparent crater size were predicted. Charge weights varied from 45.3 to 27,216 kg [100 to 60,000 lb]. For the case of a 100-kg [220-lb] TNT-equivalent charge, the finite element soil pressures correlated well with the pressures calculated from empirical relationships. The finite-element-predicted apparent crater dimensions were within the range of the empirically derived dimensions for most of the TNT-equivalent charge sizes considered. For the larger charge sizes {4,536; 9,072; 18144; and 27,216 kg [10,000; 20,000; 40,000; and 60,000 lb]}, the predicted apparent crater radius was just below the empirically calculated lower limit. However, for these larger charge sizes, conventional Lagrangian analysis results in excessive mesh distortion. Thus, for these larger explosive charges it was necessary to use the element deletion technique with a specified soil failure criterion. It was recommended that additional parametric analyses be performed to further investigate the choice of the soil failure criterion. The Lagrangian element-to-particle conversion technique available in ABAQUS/Explicit was also investigated. However, it was determined that element-to-particle techniques in ABAQUS/Explicit are currently not possible due to documented code errors. Finally, an Eulerian analysis was performed for a 454-kg [1,000-lb] explosive charge, which predicted an apparent crater depth also within the range calculated using empirical equations of Gould (1981). However, this was less than the crater depth the Lagrangian analysis predicted, which used the CONWEP algorithm to calculate the blast pressure. The smaller apparent crater depth may be the result of the Eulerian analysis underpredicting the ground surface blast loading pressure. It was recommended that a finer mesh be used in modeling the air domain.

The design codes and guidelines the military developed constitute the principal guidance documents for the design of underground structures subjected to dynamic forces generated by explosions in air, ground surface explosions, and underground detonation of high explosive charges. They use concepts and provisions of other specific codes, standards, and design manuals commonly used in the design of reinforced concrete, prestressed concrete, masonry, and steel structures.

An underground structure may be subjected to both explosive loads and seismic loads and should be designed to perform its intended function considering these loads. The energy source for the explosive load is quite different from that of the seismic load, although both of them produce P-waves, S-waves, and surface waves. Despite similarities, explosions result in higher P/S ratios than similarly located earthquakes, making the energy spectrum very different. In addition, there may be a significant difference in the magnitude of spectral quantities. As a result, one spectrum will not reasonably envelope another spectrum. However, an approach similar to that of combining internal accidental missile load with other loads, as specified in the commonly used concrete and steel design codes, will be a reasonable approach for combining the external explosive load with other loads for the design of underground structures.

ACKNOWLEDGMENTS

The activities reported here were performed on behalf of the U.S. Nuclear Regulatory Commission (NRC), Office of New Reactors. This report is an independent product of the Center for Nuclear Waste Regulatory Analyses (CNWRA®) and does not necessarily reflect the views or regulatory position of NRC. The authors would like to thank L. Howard for the technical review and W. Patrick for the programmatic review. The authors would like to acknowledge the input provided by S. Hsiung and A. Ghosh to this report. The authors also appreciate L. Naukam for providing word processing support and L. Mulverhill for editorial support in preparation of this document.

QUALITY OF DATA, ANALYSES, AND CODE DEVELOPMENT

DATA: All CNWRA-generated original data contained in this report meet the quality assurance requirements described in the Quality Assurance Manual. Data used in this report are primarily obtained from other sources. Each data source is cited in this report and should be consulted for determining the level of quality for those cited data. The work presented in this report is documented in Scientific Notebook 1160E (Wilt, 2013).

ANALYSES AND CODES: CNWRA conducted finite element analyses using the commercial computer code ABAQUS/Explicit Version 6.12 (Dassault Systèmes Simulia Corp., 2012b). ABAQUS/Explicit Version 6.12 (Dassault Systèmes Simulia Corp., 2012b) is controlled under the software quality assurance procedure Technical Operating Procedure–018, Control, Development, and Modification of Scientific and Engineering Software. Spreadsheet calculations were accomplished using Microsoft® Excel® (Microsoft Corporation, 2012).

References

Dassault Systèmes Simulia Corp. "ABAQUS Analysis User's Manual, Version 6.12." Providence, Rhode Island: Dassault Systèmes Simulia Corp. 2012.

Microsoft Corporation. "Microsoft Excel 2007." Redmond, Washington: Microsoft Corporation. 2007.

Wilt, T.E. "Characterizing Explosive Effects on Underground Structures." Electronic Scientific Notebook 1160E. San Antonio, Texas: Center for Nuclear Waste Regulatory Analyses. 2013

ACRONYMS

ACI	American Concrete Institute
AISC	American Institute of Steel Construction
ANSYS	
ASCE	American Society of Civil Engineers
CONWEP	Conventional Weapons
DOD	U.S. Department of Defense
DOE	U.S. Department of Energy
EFG	element free Galerkin
EOS	equations-of-state
EPIC	Elastic-Plastic Impact Computations
ERDA	Energy Research and Development Administration
GM	General Motors
HOB	height-of-burst
IED	Improvised Explosive Device
JWL	Jones-Wilkens-Lee
LSTC	Livermore Software Technology Corporation
MDOF	multiple-degree-of-freedom
PETN	pentaerythritol tetranitrate
PP	peak pressure
PTX	Picatinny Ternary Explosive
RDX	Cyclotrimethlenetrinitramine
SDOF	single-degree-of-freedom
SPH	smoothed particle hydrodynamics
SSI	soil-structure interaction
TNT	trinitrotoluene
UFC	Unified Facilities Criteria
VBIED	Vehicle Borne Improvised Explosive Device

1. INTRODUCTION

1.1 Background

The dynamic waves generated in the subsurface media by surface explosions and underground explosions may exert dynamic loads on the underground structures and severely damage them. An explosion above but near the ground surface produces overpressure in the air that is transmitted underground through refraction at the ground surface. Explosions at the ground surface and underground near the ground surface couple more directly, and may produce a crater and then propagate dynamic waves through the underground media. Baker (1973), American Society of Civil Engineers (ASCE, 1985), and Cooper (1996) detail propagation of waves due to these explosions.

Explosives are the most popular choice of terrorists to harm or kill people and damage property (Rostberg, 2005). The characteristics and properties of military and commercial explosives are well documented (Department of Army, 2008; Department of Navy, 1947; Cooper, 1996). As military explosives become more difficult to obtain, terrorists may choose to make their own explosives using chemicals and precursor materials available to them. The conventional homemade explosive devices that are used in terrorist attacks are called Improvised Explosive Devices (IEDs). The IEDS fall into three categories: (i) Vehicle Borne Improvised Explosive Device (VBIED), (ii) Package-Type IED, and (iii) Suicide Bomb IED (U.S. National Counterterrorism Center, 2006). VBIEDs use a vehicle as the package, container, and means of delivery.

In general, VBIEDs are detonated near the ground surface. The types of vehicles used to convey VBIEDs to the target location determine the aboveground height of detonation. Thus, the damage delivered by a VBIED explosion on an underground structure depends on the resulting air blast of the VBIED, propagation of blast waves through air, crater formation, and propagation of waves through subsurface soil and rock.

The magnitude of the dynamic load on the underground structures created by near-surface (above ground) detonation of VBIEDs is affected by the strength of the explosive charge and its distance from the underground structure; the properties of the soil and rock between the detonation point and the structure; and the orientation of structural members with respect to the direction of propagation of the dynamic waves. This dynamic load on the underground structures also are affected by engineered site-specific conditions, such as the presence of an explosion protection concrete slab, a rock barrier, or a surface building floor slab between the point of detonation and the underground structures (DOD, 2008, 1986).

The VBIEDs are conventional weapons. The phenomena of the air and surface explosions of the VBIEDs, propagation of their dynamic waves through air, crater formation, and propagation through subsurface media are similar to those of conventional military weapons and commercial explosives (Baker, 1973; Cooper, 1996). The explosive loads generated from the detonation of nuclear weapons (ASCE, 1985) also are discussed herein to the extent applicable for VBIEDs.

Various investigators have developed empirical equations for calculating explosion-induced effects in the air, on the ground surface, in the subsurface, and under water (ASCE, 1985; Baker, 1973; Brode, 1954; Cooper, 1996; Larcher, 2007; Kinney and Graham, 1985; Krauthammer and Altenberg, 2000; Smith and Hetherington, 1994). These empirical equations are based primarily on the assumption of a spherically shaped explosive charge. However, limited empirical equations also are available for non-spherical explosive charges. The

empirical equations are for calculating important parameters that affect the underground structures, such as explosion wave arrival time at a given location; duration of the explosion wave; peak free field pressure; impulse force; and particle displacement, velocity, and acceleration. Only a limited amount of test data is available to predict the pressures on the underground structures primarily from conventional weapons (DOD, 2008). Empirical and experimental information is supported by various numerical analysis techniques, with appropriate assumptions, idealizations, and simplifications implemented in Department of Defense (DOD, 2008) and commercial computer codes (Dassault Systèmes Simulia Corp., 2012a; LSTC, 2013).

Empirical equations are available for the analysis and design of underground concrete and steel structures that are subjected to the surface and subsurface explosion-generated pressure on the soil that surrounds the underground structures (DOD, 2008, 2002, 1986; Smith and Hetherington, 1994). These empirical equations are based on experimental investigations aided by analytical investigations. These empirical equations provide a means to calculate factors such as bending moment and shear capacity of various structural components, beam-column effects, energy absorption capacity under shock loads, and cracking and spall of concrete components. Various computer codes are also available to model underground structures subjected to explosive loads (e.g., Dassault Systèmes Simulia Corp., 2012a; LSTC, 2013).

In addition to possible explosive loads, underground structures may be subjected to dynamic waves generated by natural earthquakes. In broad terms, earthquakes occur from the sudden release of strain energy caused by ruptures at plate boundaries or at faults. Many investigators and authors (e.g., Das, 1993; Kramer, 1996; Gere and Shah, 1984; Newmark and Rosenblueth, 1971; Kana, et al., 1991) have discussed the propagation of seismic waves through underground media. There are important differences between the characteristics of explosion induced and earthquake-induced responses of the geologic media, which influence the characteristics of the input loads on the underground structures. These result from differences in parameters such as source dimension, source time function, source mechanism, and focal depth (Dahy and Hassib, 2009). Explosive loads to underground structures are P-wave dominated short duration loads, whereas earthquakes loads are S-wave dominated long duration loads. For underground structures that may be subjected to both explosive loads and seismic loads, consideration of the differences between explosion-induced and seismic-induced loads on underground structures is important in the design of underground structures as discussed in Chapter 6 of this report.

1.2 Objectives

The overall objective of this report is to identify and evaluate potential effects on underground structures of a VBIED explosion that is assumed to occur in air near or on the ground surface. This report describes the characteristics of VBIEDs; dynamics of explosion propagation through air, underground soil medium, and underwater; computational methods to quantify blast-induced pressures; empirical relationships and numerical analyses to calculate soil pressure distribution and estimate crater formation; computational methods to evaluate underground structural response; and relevant design standards and guidance applicable to underground structures. This report also provided numerical determination of the “zones of influence” in the underground medium due to air and surface explosions of different magnitudes. The explosive and seismic loads to which an underground structure may be subjected are compared. The report includes a qualitative assessment of the design of an underground structure that will need to be done for (i) two individual design spectra (one for explosive load and the other for seismic load) or (ii) only one of these two design spectra that may envelope the other spectrum.

2. EXPLOSIVE EFFECTS

The physical phenomena and resulting effects of detonation of high explosive charges in air near the ground surface and at the ground surface are reviewed and summarized to provide a basis for evaluating potential threats to shallow buried underground structures. The discussion emphasizes Vehicle Borne Improvised Explosive Devices (VBIEDs). The mechanism of propagation of blast waves caused by conventional weapons (i.e., high explosives) is examined using available information from the literature. Because of the limited amount of information on this topic, publicly available information related to nuclear explosions also is considered (ASCE, 1985). Nuclear-explosion information is included because the shock-wave propagation mechanism is similar to that for conventional weapons (Baker, 1973).

For purposes of this discussion, a surface burst is associated with detonation of an explosive charge that is in contact with the ground. An air burst is a detonation in which the explosive charge is not in contact with the ground surface. The discussion includes transmission of explosion-generated pressure waves through air and underground media, as well as the analytical tools available for modeling explosive yields and explosive effects in air, underground, and in water. The available information summarized here is used to characterize the physical phenomena of surface and air burst effects on underground structures.

2.1 Fundamentals of Explosives

Explosives are the most popular choice of terrorists for inflicting damage to infrastructure and taking lives (Rostberg, 2005). Explosive materials may be solids, liquids, or gases (DOD, 2008). Detonation occurs when the rate of reaction exceeds the speed of sound in the explosive material, creating a shock wave and rapid release of energy (Baker, 1973), which proceeds through the explosive material at a supersonic speed, called the detonation velocity.

The blast pressure produced by an explosion depends on the physical and chemical characteristics of the explosive materials; the methods and procedures used in manufacturing, storing, and handling of the explosive; and the properties of the medium in which it explodes and/or propagates.

2.1.1 Vehicle-borne Improvised Explosive Devices

Conventional explosive devices used in terrorist attacks are called Improvised Explosive Devices (IEDs). An IED is a homemade device that is usually unique in nature because its builder has had to improvise by creating it with the materials at hand. These materials could be explosives alone or used in combination with toxic chemicals, or biological or radiological materials. IEDs can vary in size and have different functioning methods, containers, and delivery methods. IEDs fall into three categories: (i) VBIED, (ii) Package-Type IED, and (iii) Suicide Bomb IED (U.S. National Counterterrorism Center, 2006). In general, IEDs become more difficult to detect and protect against as they become more sophisticated.

The most common materials used for making IEDs, particularly in battlefield situations or where access otherwise is available, are military munitions. Thefts from U.S. military bases and depots are potential sources, as are illegal cross-border transfers. As military explosives become more difficult to obtain, terrorists make their own explosives from available chemicals and precursor materials. Commonly available agricultural, mining, and civilian munitions manufacturing are readily available sources. Chemical precursors to explosives have wide variety of uses and include such chemicals as acetone, ammonia, glycol, nitric acid, peroxide,

butane, benzene, ether, glycerin, iodine, methane, sulfuric acid, urea and certain highly reactive metals (Rostberg, 2005). Explosives derived from these common chemicals are relatively easy to manufacture. Table 2-1 provides a sample of homemade explosives and ingredients (Nardin, 2005). Table 2-2 contains information on characteristics of U.S. military and commercial explosives (Cooper, 1996; Department of Army, 2008; Department of Navy, 1947).

Table 2-1 Homemade Explosives and Ingredients*

Explosive	Synonyms	Raw Ingredients
Nitroglycerin	Nitroglycerine; trinitroglycerin; glyceryl trinitrate. Product may be mixed with ethylene glycol dinitrate and stored chilled until ready to use.	Glycerin is slowly added to a 50:50 mix of concentrated nitric and sulfuric acid under controlled temperature conditions; wash with sodium bicarbonate solution. Potassium nitrate may be used instead of nitric acid.
Acetone peroxide	Tricycloacetone peroxide	30% (preferred) or 3% hydrogen peroxide; acetone; sulfuric or hydrochloric acid.
Methyl ethyl ketone peroxide	MEKAP	Methylethylketone, 30% hydrogen peroxide, sulfuric or hydrochloric acid.
DDNP	4,6-Dinitrobenzene-2-diazo-1-oxide; diazodinitrophenol	Picric acid, potassium or sodium nitrite; more than 85% sulfuric acid, sodium hydroxide, sulfur.
Silver acetylide	Double salts $Ag_2C_2 \cdot Ag_2NO_3$	Silver metal; acetylene or calcium carbide+water; 70% nitric acid; alcohol.
Copper acetylide		Copper sulfate; sodium hydroxide; acetylene or calcium carbide + water.
Trimercury chlorate acetylide	Chloate-trimercury acetylide	Mercuric nitrate; sodium chlorate; acetylene or calcium carbide + water.
HMTD	hexamethylenetriperoxidediamine	Hydrogen peroxide; hexamine; citric acid. Alternative procedure uses 37% formaldehyde solution, 3% hydrogen peroxide, and ammonium sulfate.
Lead azide		Sodium azide (also an explosive); dextrin; sodium hydroxide; lead nitrate.
Sodium azide		85% hydrazine hydrate; butyl nitrite or isopropyl nitrite; ethyl alcohol; sodium hydroxide.
TACC	Tetraaminecopper chlorate	Ammonium hydroxide, copper sulfate, sodium chlorate, alcohol.
Lead picrate		Picric acid, lead monoxide, methanol
Mercury fulminate		Mercury metal, 70% nitric acid, ethanol.
Nitrated milk powder	Milk booster; casein nitrate	Milk; 70% nitric acid; conc. Sulfuric acid; vinegar; baking soda.
Nitromannite	Mannitol hexanitrate	Mannose; conc. nitric acid; conc. sulfuric acid; ethanol; sodium chloride; sodium bicarbonate (baking soda).

Table 2-1 Homemade Explosives and Ingredients* (continued)		
Explosive	**Explosive**	**Explosive**
Armstrong's explosive	Chlorate impact explosive	Mix almost any chlorate salt (e.g., potassium chlorate) with sulfur and then add red phosphorous while very wet; mixture when dry explodes upon touch.
Diaminesilver chlorate		Silver nitrate; sodium chlorate; 25% ammonium hydroxide; produces shock-sensitive dark crystals
Potassium chlorate primer	Friction primer	Mix potassium chlorate with antimony sulfate, wet, in 5% gum Arabic solution; some preparations add sulfur and ground glass, sometimes also calcium carbonate and/or meal powder.
Nitrogen trichloride	Chloride of azode	Ammonium chloride or ammonia and hydrogen chloride or mix ammonium hydroxide with hydrochloric acid; carbon or lead rods from battery; electrolyze solution using battery charger; nitrogen trichloride explodes above 60 °C or on shock or in contact with dust or organic material.
Nitrogen triiodide		Iodine crystals; conc. ammonium hydroxide; nitrogen triiodide crystals will settle in mixture. Very unstable explosive.
Silver fulminate		70% nitric acid, silver metal, ethanol.
Mixture of potassium nitrate, potassium carbonate	Yellow powder	If mixture is heated resulting in melting especially in a metal container or with trace metal salts it may detonate.
Lead nitroanilate		Lead nitrate; sodium nitrite; salicylic acid; hydrochloric acid; potassium chlorate; ethanol. Easily detonated.
Nitrogen sulfide	Nitrogen sulfide may be mixed with dry potassium chlorate	Sulfur; chlorine (generated from bleach or swimming pool chemicals); hydrochloric acid; oil; sodium chloride; manganese dioxide; benzene; anhydrous ammonia.
*Nardin, J. "Homemade Explosives." Laramie, Wyoming: Arista Tek, Inc. 2005.		

Table 2-2 Characteristics of U.S. Explosives*						
		Detonation Velocity			**Heat of Detonation**	
Name	**Applications**	**m/sec**	**ft/sec**	**RE Factor**	**MJ/kg**	**ft-lb/lb**
Ammonium nitrate	Earthmoving	2,700	8,900	0.42	—	—
Nitroguanidine	Gun propellants	7,437	24,400	—	—	—
PETN	Detonating cord, blasting caps, demolition charges	8,300	27,200	1.66	6.90	2.31×10^6

Table 2-2 Characteristics of U.S. Explosives* (continued)						
		Detonation Velocity			Heat of Detonation	
Name	Applications	m/sec	m/sec	RE Factor	MJ/kg	ft-lb/lb
RDX	Blasting caps, composition explosive	8,350	27,400	1.60	6.78	2.27×10^6
Torpex	Torpedo war heads, depth bombs, mines	7,315	24,000	—	—	—
TNT	Demolition charge composition explosive	6,900	22,600	1.00	5.90	1.97×10^6
Tetryl	Booster charge composition explosive	7,100	23,300	1.25	6.32	2.11×10^6
Haleite	EDNATOL constituent	7,620	25,000	—	—	—
Nitroglycerin	Commercial dynamite	7,700	25,200	1.50	—	—
Black powder	Time fuse	400	1,300	0.55	—	—
Amatol 80/20	Bursting charge	4,900	16,000	1.17	—	—
Composition A3	Booster charge Bursting charge	8,100	26,500	—	—	—
Composition B	Bursting charge	7,800	25,600	1.35	6.44	2.15×10^6
Composition C4 (M112)	Cutting charge Breaching charge	8,040	26,400	1.34	6.65	2.22×10^6
Mercury fulminate	Blasting cap, Primer	5,029	16,500	—	—	—
Composition H6	Cratering charge	7,190	23,600	1.33	—	—
Ammonium nitrate	Cratering charge	2,700	8,900	0.42	—	—
Tetrytol 75/25	Demolition charge	7,000	23,000	1.20	—	—
Pentolite 50/50	Booster charge Bursting charge	7,450	24,400	—	6.40	2.14×10^6
M1 dynamite	Demolition charge	6,100	20,000	0.92	—	—
Detonating cord	Priming, demolition charge	6,100 to 7,300	20,000 to 24,000	1.66	—	—
Sheet explosive	Cutting charge	7,300	24,000	1.14	—	—
Bangalore torpedo, M1A2	Demolition charge	7,800	25,600	1.17	—	—
Picratol	Bomb M103	6,972	22,875	—	—	—
Shaped charges M2A3, M2A4, and M3A1	Cutting charge	7,800	25,600	1.17	—	—
PTX-1	Shaped charges, bombs, demolition blocks, grenades, mines	7,376	24,200	—	—	—

Table 2-2 Characteristics of U.S. Explosives* (continued)						
		Detonation Velocity			Heat of Detonation	
Name	Applications	m/sec	m/sec	RE Factor	MJ/kg	ft-lb/lb
PTX-2	Shaped charge, main charge for fragmentation ammunition, booster	7,986	26,200	—	—	—
Binary mix, sodium perchlorate, and aluminum powder	FPE main charges	4,000	13,100	1.60	—	—

PETN–pentaerythritol tetranitrate
PTX–Picatinny Ternary eXplosive
RDX–Research Department eXplosive
TNT–trinitrotoluene
*Cooper, P.W. *Explosives Engineering*. Hoboken, New Jersey: John Wiley & Sons, Inc. 1996.
Department of Army. "Explosives and Demolitions." FM 3–34.214 (FM 5–250). Washington, DC: Department of Army. 2008. <http://info.publicintelligence.net/USArmy-Explosives.pdf> (April 16, 2013).
Department of Navy. "U. S. Explosive Ordnance." OP 1664. Washington, DC: Bureau of Ordnance Publication. May 28, 1947.

VBIEDs are a class of IED that uses a vehicle as the package, container, and means of delivery for the explosive. The VBIEDs come in all shapes and sizes, depending upon the type of vehicle used (e.g., compact sedans to semi-trailers) (U.S. National Counterterrorism Center, 2006).

For explosives, it is common to express the explosive energy as an equivalent weight of trinitrotoluene (TNT) for the detonating materials by relating the explosive energy of the "effective charge weight" of those materials to that of an equivalent weight of TNT (DOD, 2008). In addition to the energy output, other factors may affect the equivalency of material, such as shape, the number of explosive items, explosive confinement, and the pressure range being considered. The energy-equivalency-based equation could be obtained in various ways. A commonly used equation for unconfined detonation is given by (Cooper, 1996; DOD, 2008, 2002).

$$W_E = \frac{H_{EXP}}{H_{TNT}} W_{EXP} \quad (2\text{-}1)$$

where

W_E = effective charge weight
W_{EXP} = weight of the explosive in question
H_{EXP} = heat of detonation of explosive in question
H_{TNT} = heat of detonation of TNT

The energy output per unit weight of an explosive depends on the relative amount of oxygen present in that explosive (Cooper, 1996, Section 2.3). An explosive produces the maximum energy output per unit weight if it is exactly oxygen balanced in stoichiometric terms, neither rich nor lean. For example, the chemical composition of TNT is $CH_3N_3O_6$ and its overall reaction formula is $C_7H_5N_3O_6$, giving the TNT a negative oxygen balance of about 74 percent. This is

compared to cyclotrimethlenetrinitramine (RDX), which has a chemical composition of $C_3H_6N_6O_3$ with an overall reaction formula of $C_3H_6N_6O_6$, giving it a negative oxygen balance of about 22 percent (Cooper, 1996, Section 2.4). Because RDX has less negative oxygen balance than TNT, it has an effective charge weight, w_E, of about 1.60, (i.e., energy output per unit weight of RDX is 60 percent more than that of TNT). Table 2-2 provides detonation velocity and effective charge weight of a sample of U.S. explosives (Department of Army, 2008; Department of Navy, 1947; Cooper, 1996).

The U.S. National Counterterrorism Center has identified the TNT-equivalent explosive capacities for different vehicle sizes. The U.S. National Counterterrorism Center has a Bomb Threat Stand-Off Chart (U.S. National Counterterrorism Center, 2006), which is provided in Figure 2-1. This chart presents TNT-equivalent capacities based on the maximum weight of explosive material that could reasonably fit in a similarly sized container. Some of the containers identified in the table include a typical pipe bomb, briefcase/suitcase bomb, and six different vehicle types.

For the vehicles listed in Figure 2-1, the maximum TNT-equivalent explosives' holding capacities range from 227 to 27,215 kg [500 to 60,000 lb].

UNCLASSIFIED

Bomb Threat Stand-Off Distances

Threat Description		Explosives Capacity[1] (TNT Equivalent)	Building Evacuation Distance[2]	Outdoor Evacuation Distance[3]
	Pipe Bomb	5 LBS/ 2.3 KG	70 FT/ 21 M	850 FT/ 259 M
	Briefcase/ Suitcase Bomb	50 LBS/ 23 KG	150 FT/ 46 M	1,850 FT/ 564 M
	Compact Sedan	500 LBS/ 227 KG	320 FT/ 98 M	1,500 FT/ 457 M
	Sedan	1,000 LBS/ 454 KG	400 FT/ 122 M	1,750 FT/ 533 M
	Passenger/ Cargo Van	4,000 LBS/ 1,814 KG	600 FT/ 183 M	2,750 FT/ 838 M
	Small Moving Van/ Delivery Truck	10,000 LBS/ 4,536 KG	860 FT/ 262 M	3,750 FT/ 1,143 M
	Moving Van/ Water Truck	30,000 LBS/ 13,608 KG	1,240 FT/ 378 M	6,500 FT/ 1,981 M
	Semi-Trailer	60,000 LBS/ 27,216 KG	1,500 FT/ 457 M	7,000 FT/ 2,134 M

This table is for general emergency planning only. A given building's vulnerability to explosions depends on its construction and composition. The data in these tables may not accurately reflect these variables. Some risk will remain for any persons closer than the Outdoor Evacuation Distance.

Figure 2-1 U.S. National Counterterrorism Center Bomb Threat Stand-Off Chart (U.S. National Counterterrorism Center, 2006)

The type of vehicle used for VBIED detonation determines the height at which explosives detonate above the ground, making it an important parameter for explosive effects on underground and surface structures. For compact cars, the aboveground heights of vehicles vary from 56.5 to 58.1 cm [22.2 to 22.9 in] depending on the vehicle make and model. The vehicle height for sedans varies from 55.9 to 58.9 cm [22.0 to 23.2 in], and passenger vans may range from 67.4 to 96.1 cm [26.5 to 37.8 in]. The floor heights of vehicles are not readily available; however, they can be easily measured. With the vehicle height and floor height known, aboveground blast height may be approximated.

2.2 Dynamics of Explosion Propagation in Air and Underground Media

VBIED detonation in air near the ground or at the ground surface, and transmission of explosion waves through air and underground media are evaluated to estimate the pressures generated. This evaluation includes the phenomena of blast overpressure in air and the hemispherical shock front that reflects from the ground and refracts into the ground.

Two hypothetical case examples are considered here to the dynamics of a VBIED explosion. The first case is where the explosive is surrounded by open air. The second case is when the explosive is encased in a structure, providing a measure of confinement.

In the first case, if the detonating explosive is surrounded by open air, the hydrodynamic expansion of the explosive device generates debris and heated air produces a strong shock wave, expanding the surrounding air. The detonation wave propagates out onto the surrounding air as an intensive shock or blast wave and is driven by the expanding hot gases, which were the explosive material. As the blast wave expands, it decays in strength, lengthens in duration, and slows down, both because of spherical divergence and because the chemical reaction is over, except for afterburning, as the hot explosion products mix with the surrounding air.

If the explosive is encased and the explosive energy is greater than the mechanical integrity of the casing material, it will drive the casing material outward at high velocity until the casing falls into fragments. The high pressure gases then vent out past the casing fragments and again drive a strong blast wave into the surrounding atmosphere.

The single most important parameter for determining air blast wave characteristics of explosives is the total heat of detonation, which is directly proportional to the total weight or mass of the explosive. Each explosive has a specific heat of detonation per unit weight or mass.

An air blast produces overpressure in the air as shown in Figure 2-2. An overpressure is defined as the difference between the transient pressure and the ambient pressure (surrounding atmospheric). The maximum pressure that occurs at a location is defined as the peak overpressure and is one of the values used to evaluate the response of a structure to an explosive event (Baker, 1973). As the blast wave arrives at a given point, the overpressure rapidly increases from zero to the peak overpressure. The main characteristics of the pressure wave or pulse in Figure 2-2 are

- Arrival time t_a: time taken by the pulse to reach the location under consideration
- Peak pressure p_{max}: maximum pressure of the pulse which is reached with extremely fast rise time and then decreases until it reaches the atmospheric pressure, p_0 (also called side-on pressure)

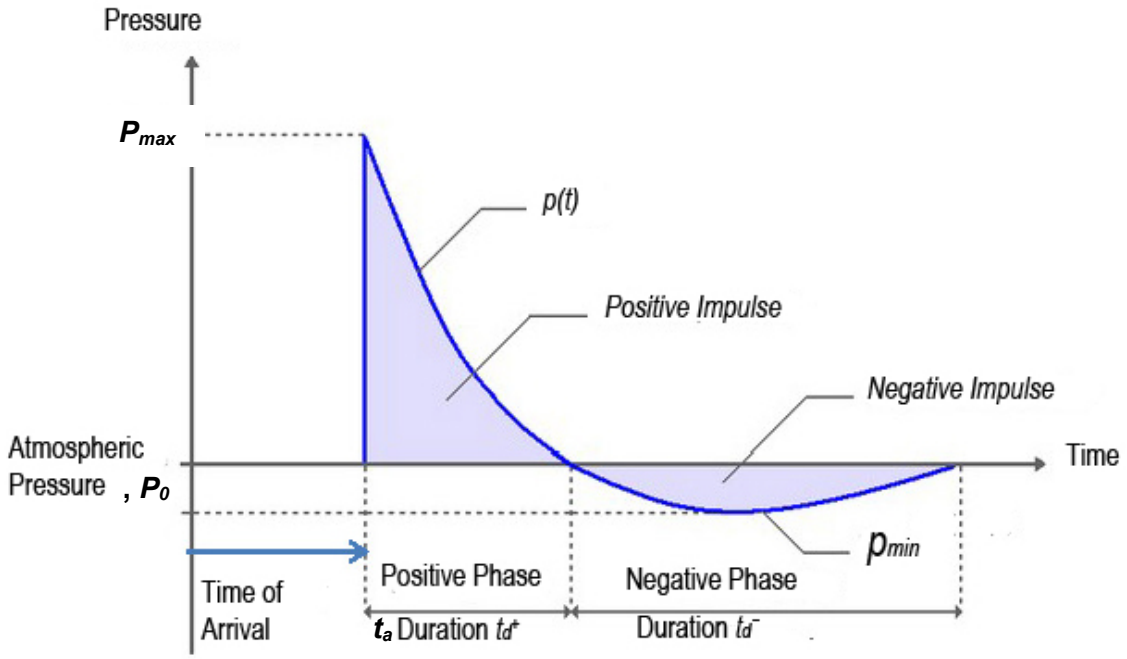

Figure 2-2 Variation of Air Burst Overpressure at a Given Location in Air With Time

- Positive phase duration t_d^+: time when the pressure is above atmospheric pressure
- Negative phase duration t_d^-: time when the pressure is below the atmospheric pressure
- Impulse i: time integral of pressure, normally limited to the positive phase of the pressure

As an air burst progresses, the surrounding air is compressed and accelerated away from the point of detonation. The time of arrival of the blast front at a given location in air depends primarily upon the explosive yield and the distance from the point of burst (ASCE, 1985). The duration of the blast wave at that location in the air is characterized by two distinct phases: the positive and the negative phases, as shown qualitatively in Figure 2-2. During the duration of the positive phase, the blast wave overpressure rises very rapidly from ambient to peak value, subsides more slowly to ambient pressure, and further subsides to the negative phase.

During the negative phase, a partial vacuum is created, sucking the air toward the initial source of the explosion [i.e., the flow is directed toward the point of detonation (ASCE, 1985)]. As in the case of peak overpressure, underpressure peak values also decrease with distance from the explosion, but at a slower rate. The peak values of underpressure are usually much smaller than during the positive phase, but may be important for the design of some structural components. A more detailed quantitative discussion of blast wave propagation in air appears in Section 2.4.

Although it is important to understand the phenomenology of explosive effects propagating through air, their progression into the soil surrounding an underground structure is more complex and more important as a potential threat. When an incident air blast wave encounters denser medium, it is reflected partially back into the air, as shown in Figure 2-3 (Glasstone and

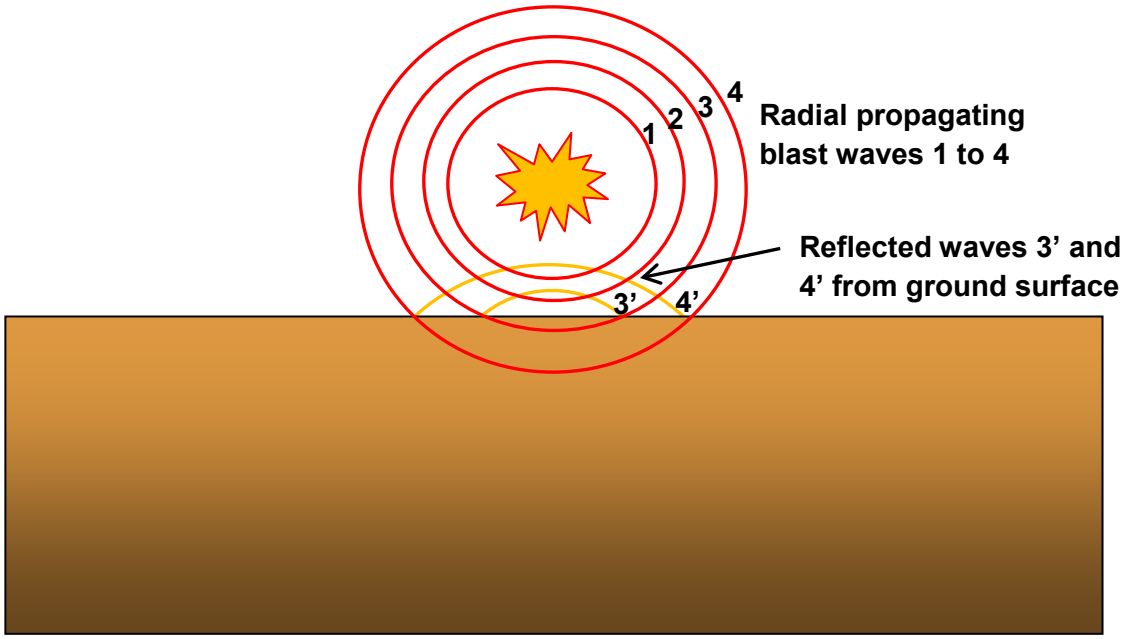

Figure 2-3 Reflection of Wave at the Earth's Surface in an Air Blast; t1 to t4 Represent Successive Times

Dolan, 1977), and refracted partially into the ground. Figure 2-3 shows four stages of the outward motion of the spherical blast wave originating from an air burst. In the first and second stages, the wave front has not reached the ground, and in the third and fourth stages, the pressure wave has interacted with the ground, producing a reflected wave, indicated by the dashed lines. The reflected blast wave would produce an instantaneous overpressure at the surface more than twice the peak overpressure of the incident wave for an ideal surface. This reflected overpressure decreases rapidly with time, as do the associated blast effects and ground responses.

The portion of the wave refracted into the ground produces Body and Raleigh waves that travel into the medium. Depending on overpressure conditions, proximity to the surface, and properties of the medium, the refracted wave could also create a crater. The mechanism of crater formation and potential effects on the underground medium are briefly reviewed as a foundation for identifying important parameters affecting the distribution of underground stresses, which in turn affect the potential for damage to an underground structure.

When an explosion occurs at or near the ground surface, the ground shock is transmitted through the Earth downward and outward. Depending on material properties and strength of the explosion, this may create a crater (ASCE, 1985). For bursts near (above) the surface, ground shock waves can be produced in two primary ways. The first mechanism is by direct coupling of explosive energy to the ground in the vicinity of the crater, causing shock waves to contribute to the crater formation and the plastic zones immediately around the crater. The second mechanism is by pressure of the air blast wave as it radiates outward along the ground surface. For air bursts (where the explosive is not embedded or emplaced in the underlying medium), the air blast pressure is the source of most of the stress on the underground medium beyond the crater area (DOD and ERDA, 1977).

Formation of a depression crater is a result of overpressure forces (Figure 2-4). Surface material can be removed by being pushed, thrown, and scoured out by the pressure wave developed by the air. Some of this material may fall back into the crater, but most of it is deposited around the edges to form the lip of the crater or is scattered beyond the crater. The primary variables that affect the size and shape of the crater include the yield of the explosive, the height or depth of burst, and the underlying medium and its properties (ASCE, 1985).

The shock wave generated by a near-surface blast produces body waves traveling into the medium, assuming an elastic half-space, with hemispherical wave fronts and Raleigh waves propagating radially outward. These body and surface waves are attenuated by two basic mechanisms. The geometric effect (Smith and Hetherington, 1994) occurs because as the waves propagate away from the source, the energy is distributed over a large area, reducing its effect. The hysteresis effect (Smith and Hetherington, 1994) results from the energy being dissipated as a result of plastic deformation of the geologic media. The underground wave propagation is discussed quantitatively in Section 2.4.

U.S. Department of Defense (DOD, 1986) notes that the propagation of ground shock in a soil medium is a complex function of the dynamic constitutive properties of the soil, the detonation products, and the geometry of the explosion. No single soil index, or combination of indices, can adequately describe the process in a simple way for all cases (DOD, 1986). For example, the water content of the soil significantly influences the propagation of shock waves in cohesive soils, particularly if the degree of soil saturation is 95 percent or more. This is because water that is typically bound within the skeletal structures of cohesive soils provides a significant contribution to the overall stiffness and strength of the soil structure. Wang, et al. (2004) found that, with 4 percent air content by volume, the peak pressure (PP) in the soil could be more than one order of magnitude smaller than that in water-saturated soils and the peak particle velocity

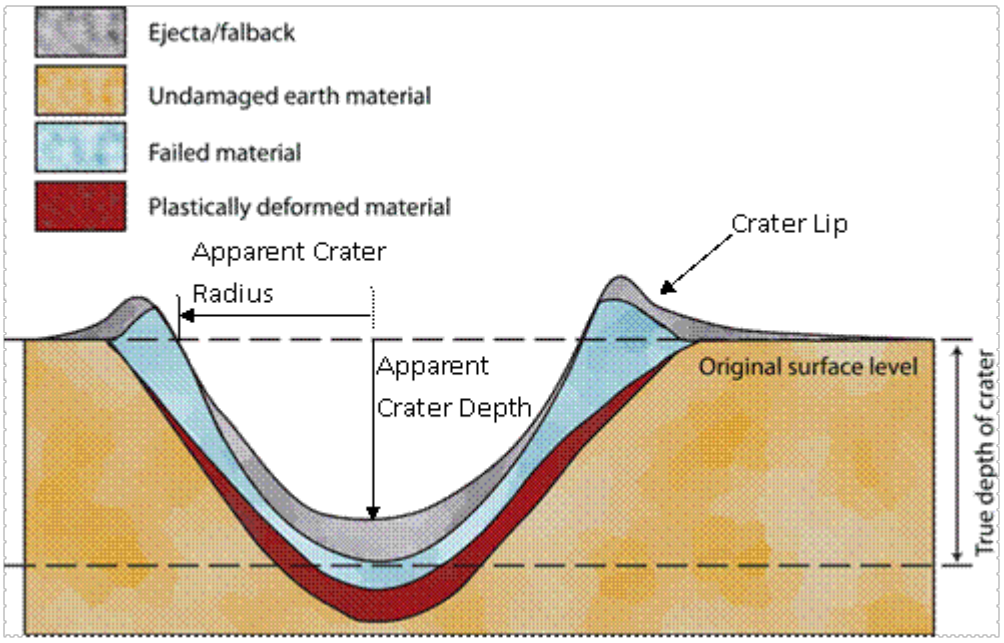

Figure 2-4 Air-Burst Generated Crater

reduces by two to six times. They also found that at relatively high air content in the soil, the attenuation relations show a noticeable nonlinear trend for soils. The variation in PPs indicates the need to understand soil properties in order to characterize an explosive event. DOD (1986) also stated that as soil saturation approached 100 percent, peak stresses and accelerations increased significantly in wet clays, clay shales, and sandy clays. Seismic surveys generally show a sharp jump in the soil seismic velocity, to more than 1,524 mps [5,000 fps], at the depth of a saturated zone.

DOD (1986) pointed out that granular soils with high relative density are generally not as strongly influenced by water saturation as are the cohesive soils discussed earlier. This is because the stiffness in granular soil is provided by the grain-to-grain contacts in the skeleton with only a small contribution by the free water. This has been demonstrated by controlled laboratory and field experiments in dense, nearly saturated sands that showed no large influence of the pore water on shock wave propagation in granular soils. In contrast, the effects of water in sands with low relative densities can produce effects similar to those seen in cohesive soils. In sands with low relative densities, the soil skeleton can collapse, and the loss of grain-to-grain contacts results in high pore pressures as the sand liquefies.

The shock load on an underground structure caused by detonation of high explosives also is affected by engineered site-specific conditions, such as the presence of a surface building floor slab, a rock barrier, or an explosive protection slab some distance above the underground structure (Figure 2-5). The protection slab, building floor slab, or rock barrier will reflect the explosion wave propagating through the air, thereby reducing effects on the underground structures. These barriers also could prevent an aboveground launched weapon planned for underground detonation from penetrating the soil and detonating adjacent to the structure. To be effective, barriers should extend beyond the edge of an underground structure to form at least a 45 degree angle with the bottom edge of the underground structure (DOD, 2008). To mitigate the effects of an underground detonation adjacent to a buried structure due to a weapon penetrating the soil at an angle less than 45 degrees (Figure 2-5), the protection slab or rock barrier may have to be extended further.

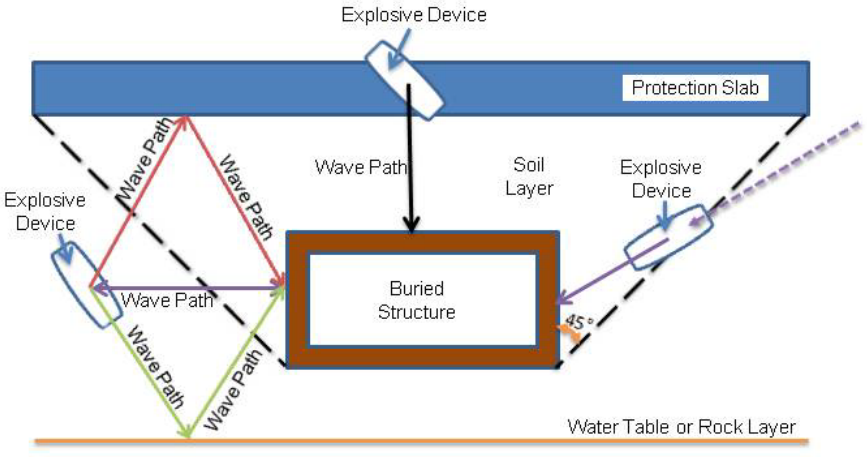

Figure 2-5 Engineered Site-Specific Barriers Above an Underground Structure

In summary, the attenuation of ground shock in soil is controlled by the irreversible crushing of the void volume within a soil matrix by the passage of a stress wave. The volume of the air-filled voids is considered as the index for the attenuation of ground motions in cohesive soils, whereas in granular soils, relative density is considered as the index for attenuation. Based on the previous discussions, soils with high relative density or a low volume of air voids will attenuate the ground shock less than low relative density or high-air-void soils.

2.3 Blast Consequences

This section briefly discusses how a surface blast may affect the structure, personnel, and equipment within an underground structure. The amount of damage to the structure will be a function of the depth of the structure and the explosive charge size. Because the structure is buried, injury to humans due to direct exposure to the air blast pressure wave would occur if there is perforation of the structure; however, blast-induced fragmentation (spallation) is also a potential hazard to humans. For an underground structure that is directly connected to the surface by a tunnel, shaft, stack, or other conduit, some of the air blast pressure and shock wave may propagate into the structure. Furthermore, equipment contained within the underground structure and attached to either walls or the floor could be affected by ground shock depending on the magnitude of the ground shock and the resulting structural vibration.

2.3.1 Effects on the Structure

From the standpoint of the structure, the most important quantity is the magnitude of the stresses that are generated by the ground shock wave (Slawson, et al., 1986). The factors that determine the strength of the ground shock are discussed in Section 2.4. Blast-induced effects that are important include fire, temperature increase, fragmentation due to spallation, and dust (fine particulate blast debris) pose a hazard to personnel.

Ground shock is particularly important for close-in blasts in which an explosive charge is located on the surface directly above a buried structure. In this case, the pressure loading is distributed over a localized area. The degree of localization depends on the depth of the structure. As will be shown in Section 3 of this report, depending on the size of the explosive charge, substantial cratering can develop, which could partially exhume or expose the underground structure. The localized dynamic pressure loading can cause different concrete failure modes: (i) scabbing, which is loss of material from the back face of the wall; (ii) spalling, which is the loss of material from the wall front face directly exposed to the blast wave; (iii) penetration, which is the formation of a crater in wall front face; and (iv) perforation, which is complete penetration through the wall forming a hole. Attempting to quantify or predict these modes of damage by analytical methods is extremely difficult (Bangash, 2001). McVay (1988) compiled an extensive theoretical and experimental study on spall damage to concrete structures subjected to air blast from bare and cased explosive charges. The empirical and experimental data were used to estimate whether local damage would occur. McVay (1988) found, however, that the small-scale test damage results were difficult to scale up to actual damage states observed in full-scale tests. In addition, damage predictions based on empirical equations did not always predict small-scale test observations well (McVay, 1988). Therefore, from a structural analysis perspective, close-in blasts with localized loading are the most challenging to solve. Appropriate analytical techniques for evaluating the structural response of a buried structure are further discussed in Section 4.2 of this report.

The shock wave also results in an impulse force, which may have a large magnitude over a very short duration. This impulse force, coupled with soil–structure interaction effects, can cause significant vibration in the structure.

2.3.2 Effects on Equipment

Blast-induced pressures, motion (vibration), and shock may affect internal equipment. The equipment can potentially be subjected to blast pressures due leakage into the structure through openings. If the opening is sufficiently small, "jetting" may occur, which results in an increased blast pressure and may cause the equipment to fall or tip over (DOD, 2008). However, if the equipment is sufficiently attached to the structure, it is typically not affected by the increased pressure. Equipment damage can be classified as either temporary or permanent failure. Temporary failure typically results only in the disruption of operation of the affected equipment for a period of time. Permanent failure is either the actual destruction of equipment or a failure that prevents the equipment from performing its intended function over an unacceptably long period of time (DOD, 2008). The degree of damage a piece of equipment can withstand is typically referred to as its fragility level, which is the amount of acceleration (shock) that the equipment can withstand and still perform its intended function. The fragility level depends on the piece of equipment and how it is attached to the structure. In addition to acceleration, equipment vibration is important especially if the vibration frequency results in resonance. However, whether continued vibration of the structure occurs depends on the amount of structural damping due to soil-structure-interaction effects. Therefore, to determine the equipment fragility level, the natural frequency and damping characteristics of the equipment supports/mounting need to be evaluated also (DOD, 2008). The equipment fragility level is determined by testing. Testing has found that most commercial mechanical equipment can withstand an acceleration level of 3 g {1 g is the gravitational acceleration constant of 9.80665 m/s^2 [32.174 ft/s^2]}. Electronic components are considerably more fragile and can withstand acceleration levels of approximately 1.5 g. DOD (2008, Table 1-4) provides a list of peak acceleration levels for typical equipment (e.g., light fixtures and pumps). The peak acceleration levels range from 10 to 70 g (DOD, 2008). Note that for equipment to withstand these acceleration levels, it must be sufficiently attached to the structure and should employ dampers at the supports to provide some form of shock isolation to protect the equipment (DOD, 2008).

2.3.3 Effects on Humans

For personnel not directly exposed to an unabated air blast shock wave, human tolerance of blast effects can be considered relatively high. Air blast effects on humans can be classified as primary, secondary, and tertiary (Richmond and White, 1966). Primary effects are from direct exposure to the blast-induced pressure wave. Secondary effects are from being struck by debris generated from the blast. Tertiary effects occur when the body is thrown by the blast wave and the body subsequently impacts other objects (e.g., floor or wall) (Richmond and White, 1966). The extent of injury is dependent on the weight and position of the person relative to the blast wave and the orientation of the person (i.e., standing, sitting, or prone) (DOD, 2008). Other effects are fire and the inhalation of high concentrations of dust (White, 1961).

A critical factor is the duration of the blast pressure increase (i.e., fast rise with short duration, "fast-fill" rooms versus slow rise with long duration "slow-fill" rooms) (Richmond and White, 1966). Humans can tolerate higher pressures for short durations, but injury can occur at much lower pressures for long duration pressure increases (DOD, 2008).

Hirsch (1966) stated that when comparing different types of blast-induced trauma, injury to ears is of secondary importance when compared to the potential trauma that can occur in the lungs and other organs which have air emboli (gas bubbles) in their vascular elements. This air embolism occurs when a damaged lung allows the air bubbles to pass into the circulatory system and then pass to the brain or heart, resulting in death (Richmond and White, 1966). However, for lung damage to occur, the air blast must strike the chest directly, and the damage is caused by the pressure acting on the chest wall and not the pressure entering the lungs through the respiratory passage (Richmond and White, 1966). Data presented in DOD (2008, Table 1-1) show that lung damage can occur for short duration (3 to 5 ms) pressures between 207 and 552 kPa [30 and 80 psi]. Death can occur at a threshold pressure of 689 kPa [100 psi], and certain death occurs for pressures of 1,379 kPa [200 psi]. By comparison, for long duration blast loads, petechial hemorrhaging, which is a mild form of hemorrhaging due to rupture of blood vessels in the skin resulting in red or purple spots can occur at pressures of as low as 69 to 103 kPa [10 to 15 psi]. Thus for long duration loads injury is due to a prolonged "squeezing" effect.

Damage to hearing can be quantified in terms of eardrum rupture and temporary hearing loss. As shown in DOD (2008, Table 1-1), the threshold for eardrum rupture to occur is 34 kPa [5 psi]; at a pressure of 103 kPa [15 psi], eardrum rupture will occur for 50 percent of people exposed to this pressure. It is also noted that temporary hearing loss can occur at pressure levels lower than 34 kPa [5 psi] depending on whether the blast wave occurs in a normal direction to the eardrum (DOD, 2008; DOE, 1981).

Being struck by flying debris is considered a secondary blast effect. The debris is typically either fragments of the explosive charge casing or fragments of the structure. For an underground structure subjected only to a surface charge, there is a low likelihood that any blast-induced fragments could injure personnel. However, if the explosion results in perforation of a structural component [e.g., ceiling slab or substantial damage that results in spalling (fragmentation) of the concrete], flying debris could be generated.

As mentioned previously, a tertiary effect of blast is the body being thrown about the structure. DOD (2008) states that an acceleration of 0.5 g is tolerable for personnel who are standing, sitting, or prone. If the body is thrown, an impact velocity of 3 m/s [10 ft/s] is considered tolerable (DOD, 2008).

2.4 Surface Blast Effects and Ground Shock

Air burst and surface explosions are dynamic events which result in the generation of ground shock, which travels on the surface and through the subsurface. The severity of the ground shock highly depends on the amount of coupling between the explosive charge and the ground (Smith and Hetherington, 1994). Figure 2-6 shows the different forms of explosions and the resulting severity of ground shock. Air bursts, with the exception of nuclear explosions, generate moderate to low amounts of ground shock because of limited coupling with the ground. Surface bursts have a high severity of ground shock due to the potential for a significant amount of coupling between the explosive charge and ground. Buried charges can generate the most severe amounts of ground shock. Charges that are "tightly" buried, (i.e., fully confined with no surrounding void space), are the most severe, while charges surrounded by void, (e.g., in a tunnel), generate a lesser amount of ground shock. Subsurface effects from buried charges are not within the scope of this report.

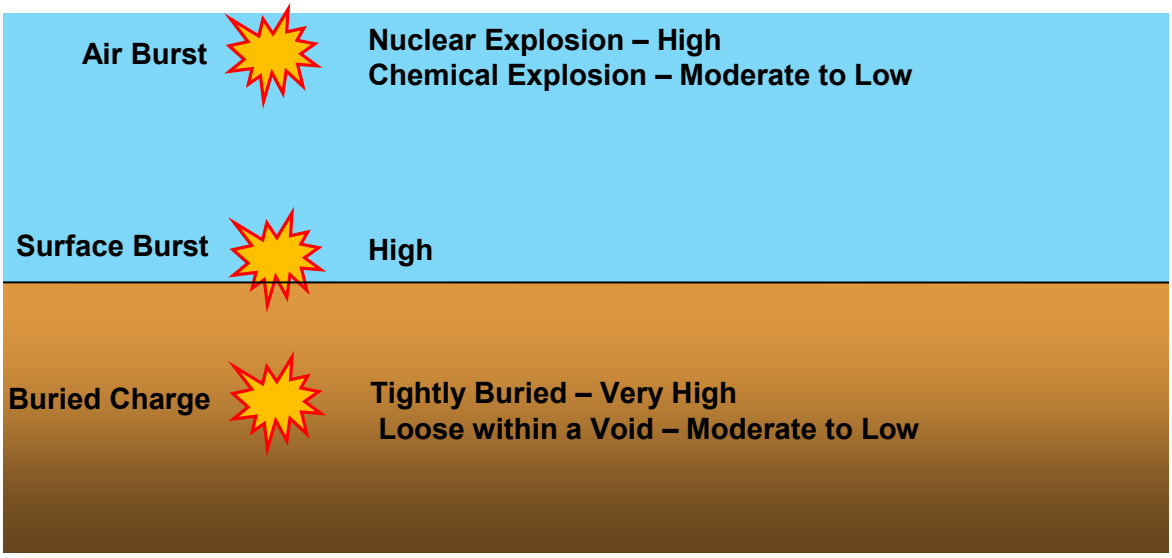

Figure 2-6 Different Forms of Explosions and Severity of Ground Shock Effects

The primary interest in ground shock is to determine its effects on a buried structure in the form of structural loads. Ground shock loading on a buried structure is a function of the following variables: (i) explosive charge size, (ii) degree of coupling between the charge and the ground, (iii) properties of the geologic media, and (iv) the distance from the explosive charge to the structure (Smith and Hetherington, 1994).

For an air burst, the amount of energy transmitted as ground shock highly depends on the degree of coupling between the explosive charge and the ground and is determined by the location of the charge relative to the soil surface; this is referred to as height-of-burst (HOB). In empirical expressions, HOB is usually expressed as a function of the radius of an assumed spherically-shaped charge.

Finally, it needs to be noted that a high water content, or a high water table, can potentially lead to liquefaction in low-cohesion and cohesionless soils when subject to blast-induced ground shock (Bretz, 1990). If liquefaction develops, there is the potential for structural instability to occur. Numerical studies have investigated instability of surface structures due to blast-induced liquefaction using finite element analysis in Wang, et al. (2008). It is well established that liquefaction can cause buried structures to displace upward towards the surface.

2.4.1 Analytical Methods for Evaluating Blast-Induced Ground Effects

Analytical methods are available for calculating blast-induced effects in the air, on the ground surface, below the ground surface, and underwater. These analytical methods provide a means to calculate important quantities affecting underground structures, such as blast wave arrival time, time duration of the blast wave, peak free-field pressure, and particle (e.g., soil, displacement, velocity, acceleration, and specific impulse force). Most empirical equations are based on the assumption of a spherically shaped explosive charge. However, limited empirical equations are also available for non-spherical explosive charges (e.g., cylinders, cubes, and cones). If an explosive charge with a nonspherical shape is detonated, the shock wave resulting from the entire charge surface will not enter the surrounding air simultaneously;

consequently, the blast waves will not be spherical. The shape and magnitude of the shock wave will be functions of the charge geometry and relative location of initiation of the detonation process (DOE, 1981). Therefore, the blast parameters will depend on azimuth and, possibly, the elevation, as well as the radial distance. Experimental observations from detonation of nonspherical but regular-shaped (e.g., cylinders, cubes, cones) explosive charges show that the largest blast pressure wave was generated from the charge face which had the largest surface area (DOE, 1981). Furthermore, multiple peaks occur in the positive overpressure phase (DOE, 1981). However, U.S. Department of Energy (DOE, 1981) notes that as the stand-off distance increases, the blast wave becomes more spherical.

The following discussion focuses on spherical charges because the numerical studies presented in Section 3 use pressure-time histories based on this geometry. Empirical relationships presented in this section are compared with the numerical results in Section 3.

2.4.1.1 Blast Wavefront Parameters

Three characteristic parameters of the blast wavefront are the blast wavefront velocity, U_s; the air density, ρ_s, behind the wavefront; and the dynamic pressure, q_s. These three parameters can be calculated from the following expressions given in Smith and Hetherington (1994)

$$U_s = \sqrt{\frac{6P_s + 7P_0}{7P_0}}\, a_0 \tag{2-2}$$

$$\rho_s = \frac{6P_s + 7P_0}{P_s + 7P_0}\, \rho_0 \tag{2-3}$$

$$q_s = \frac{5P_s^2}{2(P_s+7P_0)} \tag{2-4}$$

where P_0 is the ambient air pressure, P_s is the peak side-on overpressure, ρ_0 is the air density at ambient pressure, and a_0 is the speed of sound at ambient air pressure.

It is not feasible to categorize all of the different geologic media and know the *in-situ* state of the geologic media without site-specific assessment. Therefore, dimensional analysis is commonly used to obtain a first-order quantification of the effects of explosives (Cooper, 1996). Dimensional analysis typically takes the form of so-called "cube-root scaling." The empirical relationships presented in this section for PP, particle velocity, and acceleration are typically scaled by $W^{1/3}$ such that the scaled distance, Z, becomes

$$Z = \frac{R}{W^{1/3}} \tag{2-5}$$

where R is the distance from the charge center and W is the TNT-equivalent charge weight. The use of scaling allows test data using different explosive types, geologic media, and *in-situ* states to be combined. However, Cooper (1996) states that even with cube-root scaling, a

significant amount of scatter is observed in empirically derived constants, which can lead to significant uncertainty in results calculated from empirical relationships.

Kinney and Graham (1985) give the side-on overpressure distance relation as

$$\frac{P_s}{P_0} = \frac{808\left[1+\left(\frac{Z}{4.5}\right)^2\right]}{\sqrt{1+\left(\frac{Z}{0.048}\right)^2}\sqrt{1+\left(\frac{Z}{0.32}\right)^2}\sqrt{1+\left(\frac{Z}{1.35}\right)^2}} \tag{2-6}$$

Alternatively, Brode (1954) developed overpressure relationships and given by Smith and Hetherington (1994)

$$P_s = \frac{6.7}{Z^3} + 1 \quad (\text{for } P_s > 0.1 \text{ MPa})$$
$$P_s = \frac{0.975}{Z} + \frac{1.455}{Z^2} + \frac{5.85}{Z^3} - 0.019 \quad (\text{for } 0.1 < P_s < 1 \text{ MPa}) \tag{2-7}$$

In these expressions, the peak side-on overpressure is considered in the near field when greater than 1 MPa [145 psi] and when less than 1 MPa [145 psi], the peak static overpressure is considered in the medium and far field.

The complete air blast pressure-time history curve, Figure 2-2, can be determined using the modified Friedlander equation as given by Baker (1973)

$$P(t) = P_0 + P_s\left[1-\frac{t}{t_d^+}\right]e^{-\frac{b\,t}{t_d^+}} \tag{2-8}$$

where the parameter, b [sometimes referred to as the “waveform parameter” (Smith and Hetherington, 1994)], relates to pressure decay and is a function of the peak side-on overpressure P_s (Smith and Hetherington, 1994), and t_d^+ is the time duration of the positive overpressure phase. The specific impulse, i_s, is calculated by integrating the area under the positive part of the air blast pressure-time history curve

$$i_s = \int_{t_a}^{t_a + t_d^+} P(t)\,dt \tag{2-9}$$

Kinney and Graham (1985) and Larcher (2007) give the following equation to estimate the specific impulse (Pa·s)

$$i_s = 100 \cdot \frac{0.067\sqrt{1+\left(\frac{Z}{0.23}\right)^4}}{Z^2 \cdot \sqrt[3]{1+\left(\frac{Z}{1.55}\right)^3}} \cdot \sqrt[3]{W} \qquad (2\text{-}10)$$

Positive Air Blast Pressure t_d^+

Duration of the air blast pressure wave is one important parameter associated with the damage of a structure. Because the positive pressure phase is generally measured more precisely and is typically the more damaging phase, the positive air blast pressure phase t_d^+ is taken as the index of the air blast duration (Kinney and Graham, 1985; Larcher, 2007). Kinney and Graham (1985) give the following equation for estimating the duration, t_d^+, for chemical explosions

$$\frac{t_d^+}{W^{1/3}} = \frac{980\left[1+\left(\frac{Z}{0.54}\right)^{10}\right]}{\left[1+\left(\frac{Z}{0.02}\right)^3\right]\left[1+\left(\frac{Z}{0.74}\right)^6\right]\sqrt{1+\left(\frac{Z}{6.9}\right)^2}} \qquad (2\text{-}11)$$

where $t_d^+/W^{1/3}$ is the duration of the positive phase in milliseconds for 1 kg [2.2 lb] of TNT explosion and Z is the scaled distance in meters scaled to 1 kg [2.2 lb] of TNT.

Negative Air Blast Pressure P_{min} and Duration t_d^-

The air blast pressure in the negative phase drops below the atmospheric pressure. Although for most structural evaluations the positive phase of the air blast pressure is the most important, for structural panels (e.g., glass and composite), negative pressures can lead to additional failure modes (Krauthammer and Altenberg, 2000). Thus, depending on the structure subjected to the air blast, the negative phase may have considerable influence on the structural response (Krauthammer and Altenberg, 2000). For example, at scaled distances Z larger than 50, Krauthammer and Altenberg (2000) showed that the positive and negative air blast pressures can be similar in magnitude. Thus, the negative air blast pressure cannot always be neglected.

The negative air blast overpressure P_{min} and its duration t_d^- are given by Larcher (2007)

$$P_{min} = \begin{cases} \dfrac{3.5 \times 10^4}{Z} & \text{for } Z > 3.5 \\ 10^4 & \text{for } Z < 3.5 \end{cases} \qquad (2\text{-}12)$$

and

$$t_d^- = \begin{cases} 0.0101 \cdot W^{1/3} & \text{for } Z < 0.3 \\ (0.003125 \cdot \log Z + 0.01201) \cdot W^{1/3} & \text{for } 0.3 \geq Z \leq 1.9 \\ 0.0139 \cdot W^{1/3} & \text{for } Z > 1.9 \end{cases} \qquad (2\text{-}13)$$

2.4.1.2 Blast-Induced Ground Motions

Murphy (1981) investigated the near-field ground motion from surface explosions and determined that the low-frequency components of the ground motions are Rayleigh waves induced by the air blast acting on the ground surface. The amplitude of the Rayleigh wave is directly proportional to the cube-root of yield of the explosion and is independent of surface geology. In the following discussion, expressions are given to describe the motion of a particle both on the ground surface and below the surface.

Surface Ground Motion

Energy from an explosion that occurs near or on the ground surface can result in two forms of ground shock effects: air-induced ground motion and direct-induced ground motion (DOD, 2008). Air-induced ground shock is caused when the shock wave developed from the detonation compresses the ground, generating a stress pulse propagating downward. The maximum amplitude of this pulse occurs at the ground surface and attenuates with depth unless a strata interface, water table at shallow depth, or other discontinuities are present (DOD, 2008). Direct-induced ground shock is caused by the explosive energy that is directly transmitted through the ground. Direct-induced ground motion has a longer duration than air-induced ground motion. Expressions to estimate the surface ground motion are presented next.

Air-induced Ground Motion

DOD (2008) describes the motion of the ground surface in terms of one-dimensional wave propagation theory. Here, the peak vertical velocity, V_V, on the ground surface is given by

$$V_V = \frac{P_{max}}{\rho\, C_p} \tag{2-14}$$

where ρ is the mass density of the soil, C_p is the soil compressive wave propagation velocity in ft/s, and P_{max} is the peak positive air blast pressure in psi. The peak vertical ground surface displacement, D_V, is given by

$$D_V = \frac{i_s^+}{1000\, \rho\, C_p} \tag{2-15}$$

where i_s^+ is specific impulse calculated from the positive pressure phase of the air blast pressure-time history. Assuming a linear velocity increase during the pulse rise time (taken as 1 millisecond), the following formula to estimate the peak vertical ground surface acceleration, A_V, is given by

$$A_V = \frac{100\, P_{max}}{\rho\, C_p\, g} \tag{2-16}$$

where g is the gravitational constant. In Eqs. (2-14) to (2-16), the moisture content of the soil is accounted for via the soil density, ρ. However, DOD (2008) notes that Eq. (2-15) is only directly applicable to dry soils; for saturated soils and rock, it is recommended that the calculated acceleration value from Eq. (2-16) be doubled (DOD, 2008).

The peak horizontal ground surface motions can be estimated using

$$D_H = D_V \tan\left[\sin^{-1}\left({}^{C_p}/_{12000\ U}\right)\right] \tag{2-17}$$

$$V_H = V_V \tan\left[\sin^{-1}\left({}^{C_p}/_{12000\ U}\right)\right] \tag{2-18}$$

$$A_H = A_V \tan\left[\sin^{-1}\left({}^{C_p}/_{12000\ U}\right)\right] \tag{2-19}$$

where U is the velocity of propagation of the shock front (ft/s).

Direct-Induced Ground Motion

The direct-induced ground surface motion also can be estimated using empirical relationships given in DOD (2008). The peak vertical ground surface displacement, D_V, and peak horizontal ground surface displacement, D_H, for rock medium is

$$D_V = \frac{0.025 \cdot R^{1/3} \cdot W^{1/3}}{Z^{1/3}} \tag{2-20}$$

$$D_H = 0.5\, D_V \tag{2-21}$$

where R is the distance on the ground from the charge center, W is the TNT-equivalent charge weight, and Z is the cube-root scaling factor, $Z = R/W^{1/3}$. For soils, both dry and saturated, D_V and D_H are estimated using

$$D_V = \frac{0.17 \cdot R^{1/3} \cdot W^{1/3}}{Z^{2.3}} \tag{2-22}$$

$$D_H = D_V \tag{2-23}$$

The peak vertical ground surface velocity, V_V, and horizontal ground surface velocity, V_H for all types of soil and rock are

$$V_V = \frac{150}{Z^{1.5}} \tag{2-24}$$

$$V_H = V_V \tag{2-25}$$

Similarly, the peak vertical ground surface acceleration, A_V, for all cases is

$$A_V = \frac{10000}{W^{1/3} \cdot Z^2} \tag{2-26}$$

The peak horizontal ground surface acceleration, A_H, is

$$A_H = 0.5\ A_V \qquad \text{for rock} \qquad (2\text{-}27)$$

$$A_H = A_V \qquad \text{for soil} \qquad (2\text{-}28)$$

Subsurface Ground Motion

As discussed in DOD (1986), the time history for shock stress and particle velocity are typically expressed in an exponential form. That is, the magnitude of the free-field shock stress, P(t), at a given time t, is

$$P(t) = P_0 e^{-\alpha\left(\frac{t}{t_a}\right)} \qquad (2\text{-}29)$$

and the particle velocity, V(t), at a given time t, is

$$V(t) = V_0[1 - \beta(t/t_a)]e^{-\beta\left(\frac{t}{t_a}\right)} \qquad (2\text{-}30)$$

In Eqs. (2-29) and (2-30), α and β are constants that typically depend on the specific site (geologic media); however, DOD (1986) provides values of 1.0 and 0.4 for α and β, respectively. Also in Eqs. (2-29) and (2-30), the quantity t_a is the arrival time of the shock wave at a specified location. This arrival time can be calculated based on the seismic velocity, c, of the geologic media and the distance, R, from the explosion source

$$t_a = \frac{R}{c} \qquad (2\text{-}31)$$

Finally, the quantities P_0 and V_0 are the peak free-field shock stress and velocity, respectively. Empirical expressions for both these quantities as well as other ground motion quantities are given by DOD (1986) as follows

peak free-field pressure (psi)

$$P_0 = f \cdot (\rho c) \cdot 160 \cdot \left(\frac{R}{W^{1/3}}\right)^{-n} \qquad (2\text{-}32)$$

peak particle velocity (ft/s)

$$V_0 = f \cdot 160 \cdot \left(\frac{R}{W^{1/3}}\right)^{-n} \qquad (2\text{-}33)$$

peak acceleration (gs)

$$a_0\, W^{1/3} = f \cdot 50 \cdot c \cdot \left(\frac{R}{W^{1/3}}\right)^{(-n-1)} \qquad (2\text{-}34)$$

peak displacement (ft)

$$\frac{d_0}{W^{1/3}} = f \cdot 500 \cdot \left(\frac{1}{c}\right)\left(\frac{R}{W^{1/3}}\right)^{(-n+1)} \quad (2\text{-}35)$$

impulse (lb-s^2/in^2)

$$\frac{i_0}{W^{1/3}} = f \cdot \rho_0 \cdot 1.1 \cdot \left(\frac{R}{W^{1/3}}\right)^{(-n+1)} \quad (2\text{-}36)$$

In Eqs. (2-32) to (2-36), f is a coupling factor, (ρc) is the acoustic impedance [psi/(ft/s)], n is an attenuation coefficient, c is the seismic velocity (ft/s), and ρ_0 is mass density (lb-s^2/ft^4). The acoustic impedance, seismic velocity, and mass density are for a specific geologic media. Typical values are given in DOD (1986, Tables 5-1 and 5-2). The coupling factor is used to account for the location of the explosive charge in relation to the ground surface; higher amounts of coupling occur for charges that are in contact or buried below the ground surface. For example, the coupling factor for an air burst has a constant value of 0.14, while a surface charge has a coupling factor of 0.4 for soil (DOD, 1986, Figure 5-3); the coupling factor increases to a limiting value of 1.0 as the charge depth increases.

With the parameters defined in Eqs. (2-32) to (2-36), the response of a buried structure can then be determined using idealized single-degree-of-freedom (SDOF) or multiple-degree-of-freedom (MDOF) analyses, as well as more general dynamic finite element analyses. The theoretical basis and numerical algorithms for performing SDOF and MDOF analyses for structural response analyses are detailed in Section 4.

2.4.2 Calculation of Subsurface Pressure

Nagy, et al. (2010) provide an expression based on the empirical relations for ground shock, as presented in DOD (1986), for the free-field PP

$$PP = c\left(\frac{R}{W^{1/3}}\right)^{-n} \quad (2\text{-}37)$$

where R is the distance from the charge center (Figure 2-7), W is the TNT-equivalent charge weight, and c and n are empirical constants that are dependent on the soil type. Because of the inherent uncertainty in soil parameters, both upper and lower limits are given for c and n (Table 2-3) and will be used in the following calculations.

Figure 2-8 shows the calculated PP as a function of distance using Eq. (2-35) from the surface explosion for explosive charge weights from 45.3 to 4,530 kg [100 to 10,000 lb]. Figure 2-8 includes the peak pressure upper and lower limits corresponding to the values of c and n given in Table 2-3. Upper and lower limits are given because of the inherent uncertainty in the soil parameters, making bounding calculations the most appropriate approach. For a 45.3-kg [100 lb] charge, the pressure is calculated to dissipate to zero at a depth of approximately 20 m [66 ft], and for the 4,530-kg [10,000-lb] charge, the pressure is calculated to dissipate to zero at a depth of approximately 90 m [295 ft].

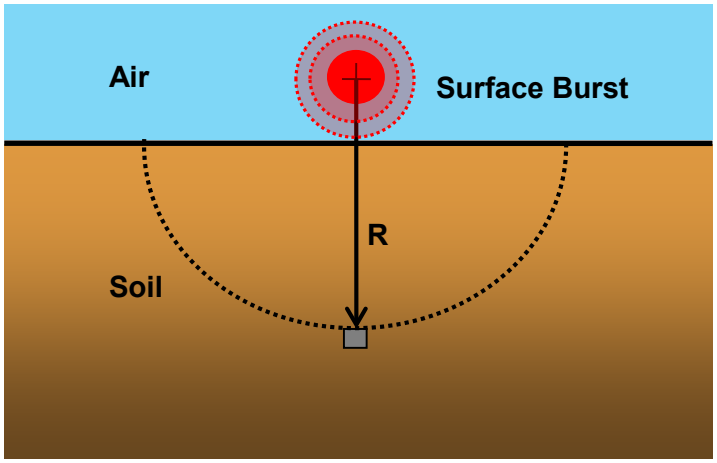

Figure 2-7 Description of Surface Burst

Table 2-3 Constants for Free Field Peak Pressure*		
	c	n
Upper Empirical Limit	1.12	2.75
Lower Empirical Limit	0.65	2.5
*Values taken from Nagy, N., M. Mohamed, and J.C. Boot. "Nonlinear Numerical Modelling for the Effects of Surface Explosions on Buried Reinforced Concrete Structures." *Geomechanics and Engineering*. Vol. 2. pp. 1–18. 2010.		

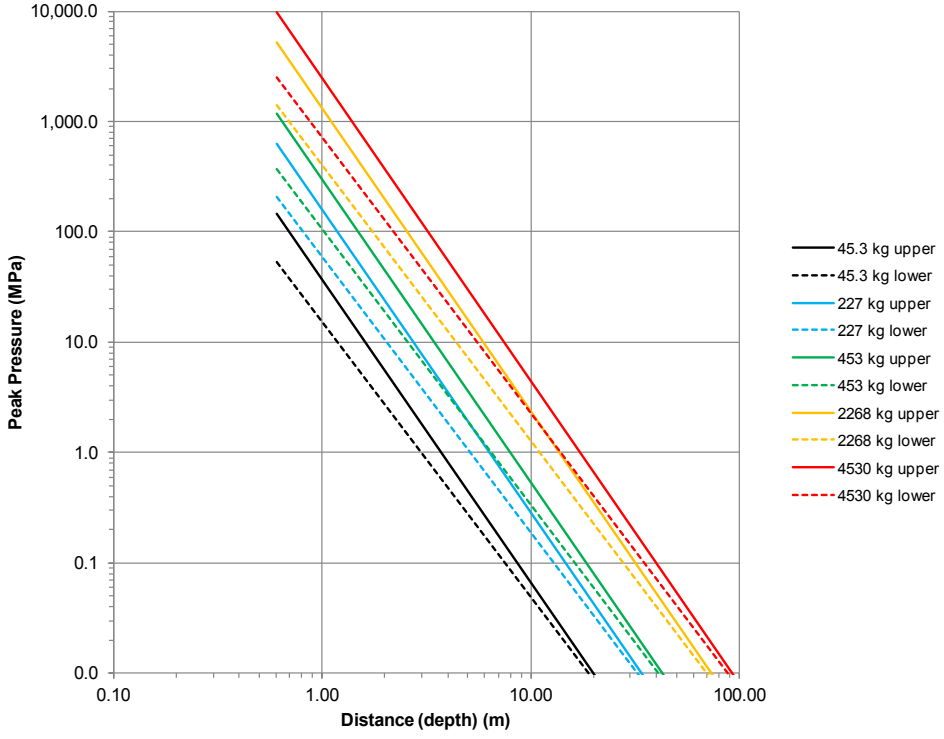

Figure 2-8 Empirical Relationship of Peak Pressure Versus Depth for Different Charge Weights. Explosive Charge Located on the Soil Surface.

2.4.3 Calculation of Crater Dimensions

As in ground shock, crater size is primarily influenced by the explosive charge weight, height of burst, the type of geologic media (e.g., soil or rock), and the water content in the geologic media (Gould, 1981). As a blast wave contacts the ground surface, the ground surface is scoured and detonation gases penetrate the surface. The expanding gases cause the formation of ejecta, which is thrown into the air. Further propagation of the blast wave causes compaction and plastic flow in the soil. A rarefaction wave with a reversed particle velocity develops and produces spalling and more ejecta (Cooper, 1996). The pressure wave in the ground results in the development of a plastic slip zone around the crater causing an upheaval of the geologic media and formation of a "lip" around the crater.

Gould (1981) notes that crater size can vary widely from test to test even when the previously mentioned four variables appear identical in each test. The deformation response of different types of geologic media and the potential uncertainty in the *in-situ* state make it difficult to formulate empirical models for predicting crater formation. Similarly, determining the appropriate method to account for this variability in numerical models makes numerical prediction of crater size quite challenging.

The apparent crater radius, R_a, in feet, can be approximated using the empirical relationships given by Cooper (1996). For an explosive charge located on the ground surface

$$R_a = (0.46 + 0.027\ P_{CJ})(2E_{CR}W)^{1/3} \tag{2-38}$$

where P_{CJ} is the Chapman-Jouguet (CJ) pressure in GPa, E_{CR} is the cratering efficiency, and W is the weight of the explosive charge in pounds. The cratering efficiency for a sandy clay soil is given as 0.475 (Cooper, 1996, Table 29.1). The sandy clay soil listed in Cooper (1996) is assumed to be the closest match to the soil used in the finite element model in Section 3.2.

The Chapman-Jouguet pressure, P_{CJ}, is calculated from Cooper (1996)

$$P_{CJ} = \frac{\rho D^2}{4} \tag{2-39}$$

where ρ is the density of the unreacted explosive in g/cm^3 and D is the detonation velocity in km/s.

The apparent crater radius for an explosive charge located above the ground surface can be approximated by the empirical relation given by Cooper (1996)

$$R_a=(0.46 + 0.027\ P_{CJ})(2\ E_{CR}W\ e^{-1.457\cdot HOB})^{1/3} \tag{2-40}$$

where HOB is the ratio of the charge height above the surface to the charge radius. Cooper (1996) does not provide any relationships to calculate apparent crater volume or apparent crater depth.

The apparent crater dimensions can also be calculated using the empirical relationship given by Gould (1981). Gould (1981) gives an expression for the apparent crater volume, V_a,

$$V_a = V_0 W \, e^{(-5.2 \, H \, (V_0 W)^{-1/3})} \tag{2-41}$$

where V_0 is the cratering efficiency of the explosive in ft^3/ton when the height of the burst is zero, W is the TNT-equivalent charge weight in tons, and H is the height of the explosive above the surface in feet. Gould (1981) also gives empirical expressions for the apparent crater radius in feet, R_a, and apparent crater depth in feet, D_a, as

$$R_a = 1.2 \, V_a^{1/3} \tag{2-42}$$

$$D_a = 0.5 \, V_a^{1/3} \tag{2-43}$$

Because of the inherent uncertainty in the soil parameters associated with each empirical relationship, it cannot be determined which empirical relationship is most accurate. The empirical relationships of Cooper (1996) and Gould (1981) will be used to predict crater dimensions in Sections 3.4 and 3.5.

2.5 Underwater Detonations

An underwater explosion will develop two phases of behavior: a shock wave and a bubble pulse. These two phases of behavior result in a partition of energy. According to Smith and Hetherington (1994), approximately 53 percent of the energy is partitioned in the shock wave and 47 percent of the energy is partitioned in the bubble pulse.

The transient shock wave significantly increases fluid velocity. The PP of the shock wave is very high, compared to a shock wave generated by a surface explosion, and results in a large impulse loading; the duration of the shock wave, however, is very short. Smith and Hetherington (1994) provide approximate expressions for the maximum pressure at the shock front.

$$P_m = \frac{355}{Z} + \frac{115}{Z^2} - \frac{2.44}{Z^3} \qquad 0.05 \le Z \le 10$$

$$P_m = \frac{294}{Z} + \frac{1387}{Z^2} - \frac{1783}{Z^3} \qquad 10 \le Z < 50 \tag{2-44}$$

The pressure, P_m, in Eq. (2-44) is calculated in bar (1 bar = 1×10^5 Pa), and Z is in $m/kg^{1/3}$. Analysis and calculation of the shock wave pressure-time history follow a similar procedure as for the air blast, although there are physical and quantitative differences in the results due to the difference in the surrounding medium (i.e., water versus air).

The bubble pulse is the result of the expansion of the detonation products (i.e., gases) (Smith and Hetherington, 1994), with the size and shape of the bubble oscillating over time. At first, the bubble radius is larger than what would correspond to hydrostatic equilibrium due to the initial expansion and inertia of the hot compressed gases. Subsequently, the bubble pressure decreases and the bubble collapses in response to the hydrostatic pressure. As the collapse

progresses, it recompresses the detonation gas, which eventually leads to a reexpansion of the bubble. A series of expansions and contractions continues until eventually the energy is dissipated and the bubble rises to the surface or contacts an underwater object. During the oscillatory phase, the bubble can take a mushroom-like shape; during contraction, or in the extreme case, the bubble has a torus shape with a powerful water jet passing through the central hole in the torus (Geersb and Hunter, 2002).

Bubble size depends on weight and composition of the explosive, as well as the depth of explosion below the water surface. Smith and Hetherington (1994) give an approximate expression for the initial maximum bubble radius, a_{max}

$$a_{max} = \frac{J_{ex} W^{1/3}}{(H + H_0)^{1/3}} \tag{2-45}$$

where J_{ex} is an empirical constant that depends on the explosive type. For example, for TNT J_{ex} is 3.5 $m^{4/3}/kg^{1/3}$ [13.1 $ft^{4/3}/lb^{1/3}$]. H is the charge depth in meters, H_0 is atmospheric head in meters, and W is charge weight in kg. The duration of the bubble pulse is at least two orders of magnitude longer than the shock wave (Geersb and Hunter, 2002); thus, damage to an underwater structure from the longer duration bubble pulse can be significant (Smith and Hetherington, 1994).

The most important aspect of an underwater detonation is its effect on a surface or underwater structure. In general, underwater explosions have three potential damaging mechanisms: high pressure, a so-called “whipping” effect, and water jet impact (Klaseboer, et al., 2005). High pressure is produced by the transient shock wave and can cause damage when it strikes the structure. The whipping effect can occur if the frequency of the bubble pulse (expansion and contraction) matches the eigen-frequency of the structure that the bubble contacts (Klaseboer, et al., 2005). Finally, the third damaging mechanism occurs when the bubble moves toward the structure and a high-speed water jet forms. If the water jet is in the direction of the structure, damage to the structure can occur. As Riley (2010a,b) discussed, damage severity is a function of the stand-off distance at which the explosion occurs relative to the structure. For example, if the bubble collapses after impinging on a structure, at close-in distances, it can impart a load more severe than the shock wave (Riley, 2010a,b). This severity may be caused by bubbles repeatedly reforming and pulsating against the structure causing several loading cycles (Riley, 2010a,b). Formation of the water jet at a close-in distance would also result in potentially severe loading.

3. NUMERICAL EVALUATION OF SURFACE AND SUBSURFACE EFFECTS DUE TO AIR AND SURFACE BURSTS

Numerical analyses using the finite element method were conducted assuming a spherical-shaped explosive charge and associated pressure-time histories, consistent with the empirical formulae presented in Section 2.4. This approach permits direct comparisons between the empirical and numerical results and also provides confidence that the numerical results are consistent with similar previous research in this topical area.

3.1 Finite Element Lagrangian Model

The finite element analyses used a Lagrangian representation of a soil block, which is loaded by a time-dependent surface pressure. Because the analyses focus on soil behavior, particularly soil stresses and crater formation, including air in the computational domain was considered unnecessary. However, this approach does have a limitation with respect to crater formation. Dynamic air blast pressure results in the production of soil ejecta during crater formation. Using the Lagrangian approach does not permit capturing this particular soil deformation mechanism. As will be shown in Sections 3.4 and 3.5, because the soil remains as a continuum, the ejecta is included as part of the "lip" that forms around the crater. Although a Lagrangian approach such as the mesh-free smoothed particle hydrodynamics (SPH) could be used to account for ejecta by modeling the soil as discrete particles (Liu and Liu, 2003), doing so was beyond the scope of this report. However, future analyses could utilize this approach to further refine the crater formation predictions using Lagrangian finite elements.

The finite element model in Figure 3-1 shows a block of soil modeled using Lagrangian three-dimensional solid continuum elements. The soil block represents a 100 × 100 × 50-m [328 × 328 × 164-ft] domain. The dimensions were selected based on previous experience [e.g., Wilt, et al. (2012)] so that the soil domain was sufficiently large, thereby preventing artificial pressure wave reflection from the domain boundaries.

A sufficiently fine mesh was constructed to allow a reasonable fidelity of the soil pressure distribution and crater formation without excessive computation time. The mesh shown in Figure 3-1 contains approximately a half-million elements. To capture complex near-field phenomena, the mesh was constructed with the finest discretization directly beneath the explosive charge.

3.2 Modeling of Soil Behavior

The deformation behavior of the soil was modeled using the Drucker-Prager Cap model available in ABAQUS/Explicit (Dassault Systèmes Simulia Corp., 2012a). The Drucker-Prager model is appropriate for soil behavior because it accounts for stress path dependence, accounts for volume dilatancy, and provides both hardening and softening behavior (Huang and Chen, 1990).

Figure 3-2 shows the yield surface for the Drucker-Prager Cap model. The cap surface controls both hardening and softening behavior and is a function of volumetric plastic strain. The cap surface limits the yield surface under hydrostatic compression by inelastic hardening, which represents plastic compaction of the soil. The cap surface also limits volume dilatancy by introducing softening when the soil yields on the shear failure surface. Two key material model parameters are β, which is the friction angle, and d, which measures cohesion; both define

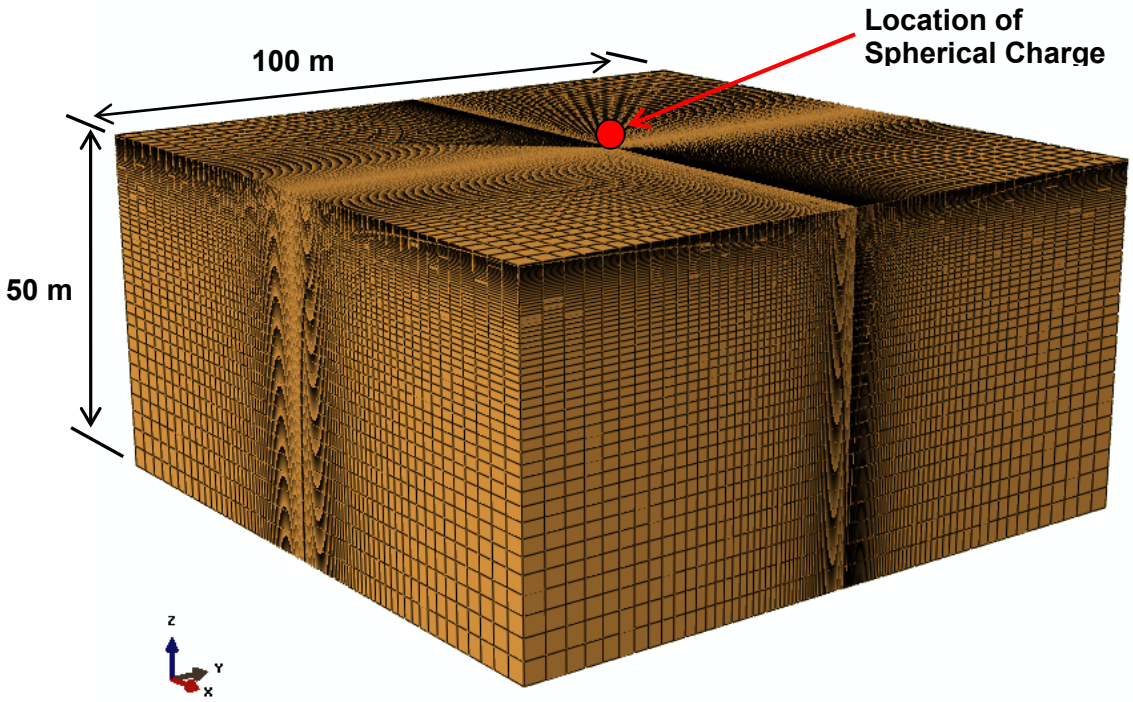

Figure 3-1 Three-Dimensional Finite Element Model of Soil

hydrostatic pressure-dependent shear failure. Huang and Chen (1990) offer additional discussion on determining the Drucker-Prager Cap model material parameters.

A literature search identified suitable material parameters to use in this particular Drucker-Prager Cap model. The material parameters for a silty clay soil were identified in Nagy, et al. (2010) and are provided in Table 3-1. This particular set of material parameters was chosen from Nagy, et al. (2010) because it is consistent with the empirical expressions also given in Nagy, et al. (2010) and will allow direct comparison between the empirical and finite element results.

3.3 Blast Pressure Loading

The dynamic, time-dependent air-blast loading was calculated using the CONWEP algorithm available in ABAQUS/Explicit (Dassault Systèmes Simulia Corp., 2012b). The CONWEP algorithm implemented in ABAQUS/Explicit is based on a program the U.S. Army developed to calculate conventional weapons effects. The equations used in the CONWEP algorithm are based on the Friedlander equation (see Section 2.4). Because CONWEP is an empirical method, there is a specific range of validity. The minimum valid distance is equal to the explosive charge radius. Therefore, for the parametric study presented in Section 3.5, some limitations on the height of burst as a function of the explosive charge weight are imposed and will be further discussed in that section.

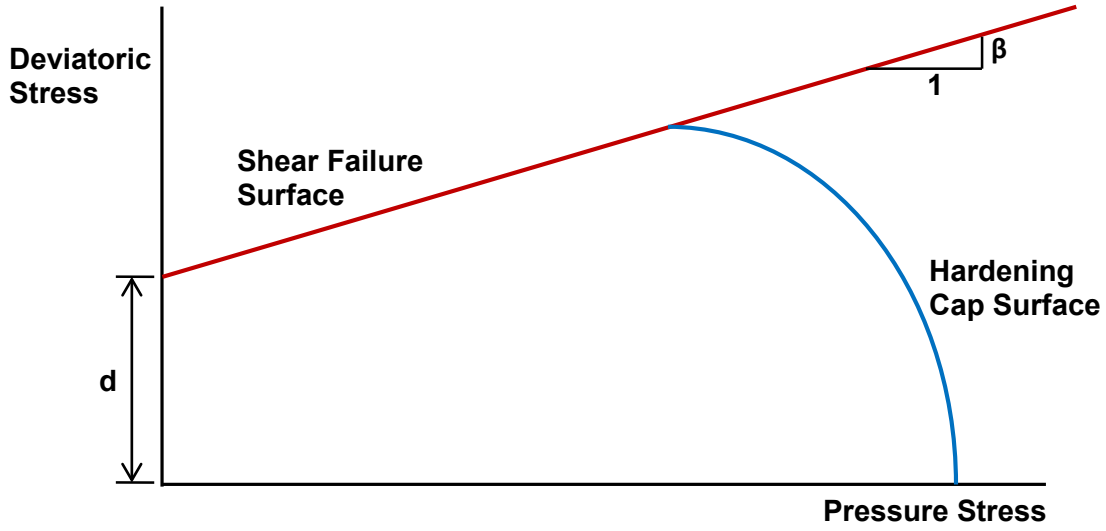

Figure 3-2 Drucker-Prager Cap Model Yield Surface

Table 3-1 Drucker-Prager Cap Model Parameters for Silty Clay*	
Parameter	**Value**
Young's modulus (E)	51.7 MPa [7.5 ksi]
Poisson's ratio (ν)	0.45
Density (ρ)	1920 kg/m^3 [120 lb/ft^3]
Material cohesion (d)	0.036 MPa [5 × 10^{-3} ksi]
Material angle of friction (β)	24 degrees
Cap eccentricity (R)	0.3
Initial cap yield surface position (ε_v)	0.02
Transition surface radius (α)	0.0
Cap hardening behavior (stress vs. plastic strain)	2.75 MPa [0.4 ksi], 0.00
	4.83 MPa [0.7 ksi], 0.02
	5.15 MPa [0.75 ksi], 0.04
	6.20 MPa [0.9 ksi], 0.08
* Values taken from Nagy, N., M. Mohamed, and J.C. Boot. "Nonlinear Numerical Modeling for the Effects of Surface Explosions on Buried Reinforced Concrete Structures." *Geomechanics and Engineering*. Vol. 2. pp. 1–88. 2010.	

Because the analyses in this report focus on the soil behavior (i.e., soil pressures and crater formation), the CONWEP algorithm was chosen to generate the air blast, which eliminated the need to model the explosive charge and surrounding air environment. This approach substantially reduces the computational cost of the analyses.

The input required for the ABAQUS/Explicit CONWEP algorithm is the trinitrotoluene (TNT)-equivalent explosive charge weight, the location of the charge, and the target surface area to which the air-blast load will be applied.

3.4 Empirical and Numerical Analyses for a 100-kg [220-lb] TNT Explosive Charge—Soil Pressures and Crater Formation

A case was considered with a 100-kg [220-lb] TNT explosive charge located 0.5 m [20 in] above the soil surface. Soil pressure calculations using empirical expressions and the finite element results are compared. Predicted crater dimensions using empirical expressions and the crater produced in the finite element analysis are also discussed.

Comparing the finite element results to the empirical results also provides a method to establish the validity and accuracy of the finite element modeling. This same finite element model is used later in a parametric study of charge height, height of burst, and charge weight.

3.4.1 Evaluation of Soil Pressures

In this problem, the soil peak pressure (PP) was calculated using Eq. (2-37) and the data given previously in Table 2-3. The PP as function of soil depth is plotted in Figure 3-3. Note that the peak soil pressure is calculated to dissipate to zero at an approximate depth of 25 m [984 ft].

In the analyses reported by Nagy, et al. (2010), the center of the 100-kg [220-lb] TNT spherical charge was in direct contact with the soil surface; thus the bottom hemisphere of the spherical charge was buried in the soil. Embedded in the constant c is a coupling factor which adjusts the amount of energy that is transferred from the explosive charge to the soil. This coupling factor is discussed in DOD (1986). For the case of Nagy, et al. (2010), the coupling factor would be 0.40. However, in the present analysis, in order to use the CONWEP option, the center of the charge must be located at a distance above the soil surface such that no portion of the charge is located below the surface. Therefore, the coupling factor should be reduced to 0.14 as given in DOD (1986). Figure 3-4 shows values of PP now scaled by the factor (0.14/0.40) to account for the center of the explosive charge being located above the surface. Thus, because the explosive charge is now elevated above the surface, the peak soil pressure is predicted to dissipate to zero at a depth of approximately 15 m [590 ft].

An ABAQUS/Explicit analysis was run using the finite element model discussed in Section 3.1 to determine how the PP in the soil at different locations compared with the empirical predictions given in Figure 3-4. The comparison of the empirical and finite element results is shown in Figure 3-5. Two finite element analyses were performed: an elastic–plastic analysis (FE Plastic) using the Drucker-Prager Cap model, discussed in Section 3.2, and a simple elastic analysis (FE Elastic). Interestingly, the elastic analysis peak soil pressures match more closely with the empirically calculated upper limit. As compared to the elastic–plastic analysis, the elastic analysis produces a higher peak soil pressure at depths less than 2 m [6.6 ft] and lower soil pressure at depths greater than 3 m [9.8 ft]. At shallower depths, the formation of plasticity (plastic dissipation) in the soil does not permit the soil pressure to reach the magnitude predicted by the elastic analysis. At depths greater than 3 m [9.8 ft], however, the peak soil pressure from the elastic–plastic analysis is higher than the elastic analysis. This may be due to the permanent plastic deformation (crater), which constrains the soil displacement and does not allow the soil pressure (stress) to redistribute and relax at these depths.

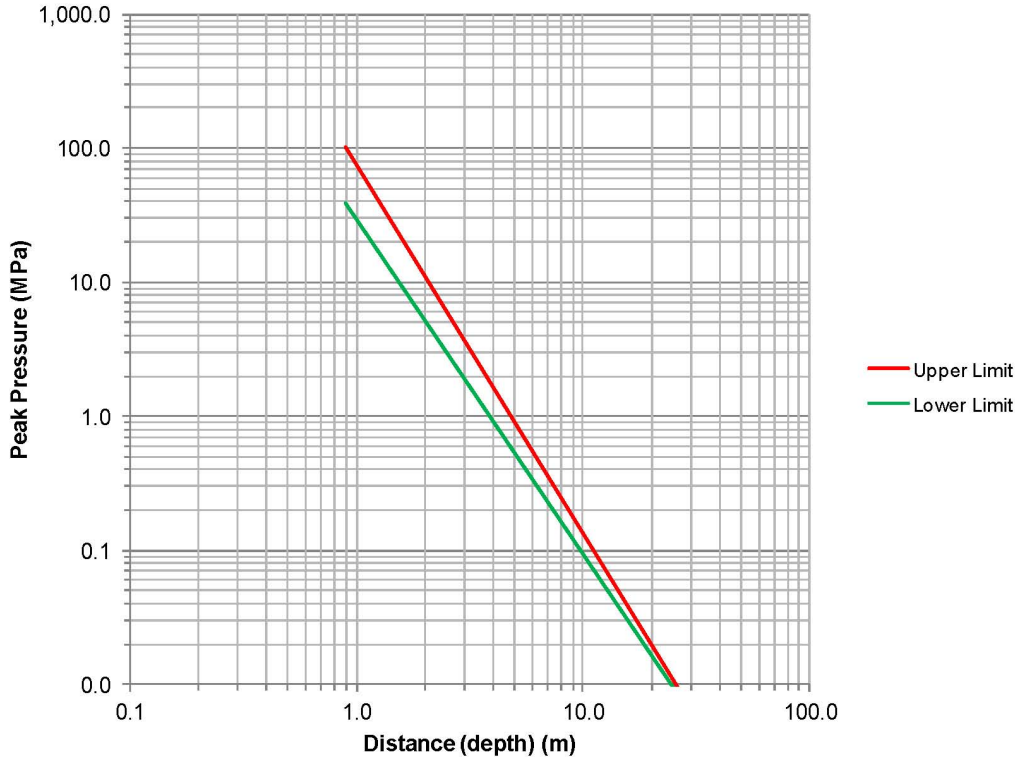

Figure 3-3 Range of Peak Pressure from Nagy, et al. (2010)
{100-kg [220-lb]-TNT Charge}

Figure 3-6 shows the pressure-time history in the soil at selected depth locations of 1.115, 2.175, 3.132, and 5.105 m [3.6, 7.1, 10.3, and 16.7 ft]. These depths correspond to locations of element centroids, where pressure values can be obtained directly without interpolation. The ABAQUS/Explicit analysis terminated at a time of 0.03 seconds. Figure 3-6 shows that at 0.03 seconds, the soil pressure at all locations has decreased below 0.5 MPa [72.5 psi], indicating that significant reduction in the soil pressure occurs rapidly.

Finally, Figure 3-7(a and b) show the pressure distribution in the soil (units are in Pa). For clarity, a half cross section of the soil block is shown. Figure 3-7(a) shows the extent of the pressure propagation throughout the soil block and that the pressure is localized around the crater. At no time did the pressure interact with the soil block boundary resulting in artificial reflection.

3.4.2 Evaluation of Predicted Crater Dimensions

Empirical and numerical crater dimension predictions are compared next. The empirical methods of Cooper (1996) and Gould (1981) are used to calculate apparent crater dimensions.

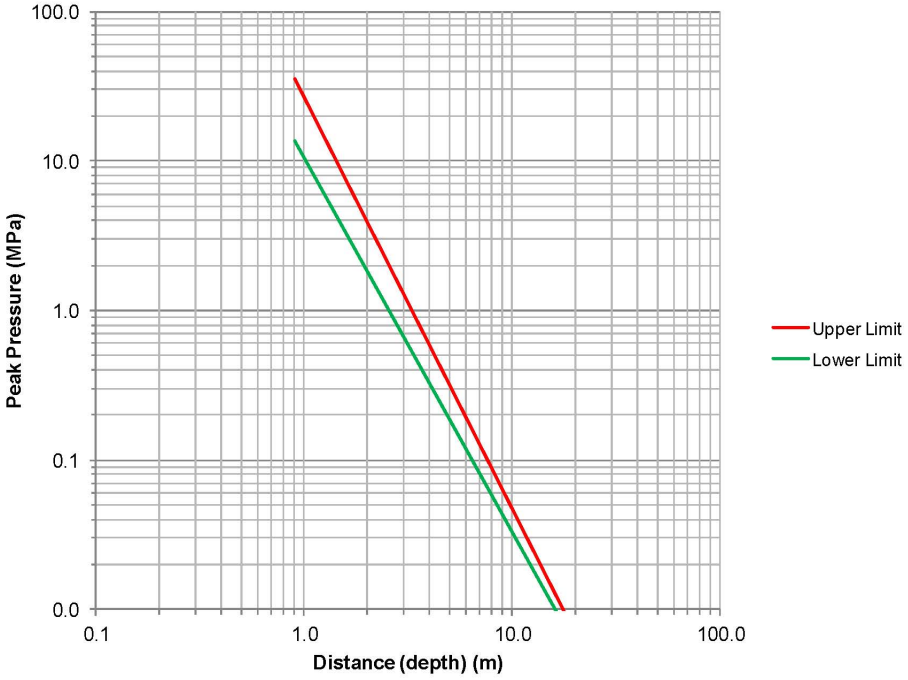

Figure 3-4 Range of Peak Pressure Scaled for Above Surface Blast {100-kg [220-lb]-TNT Charge}

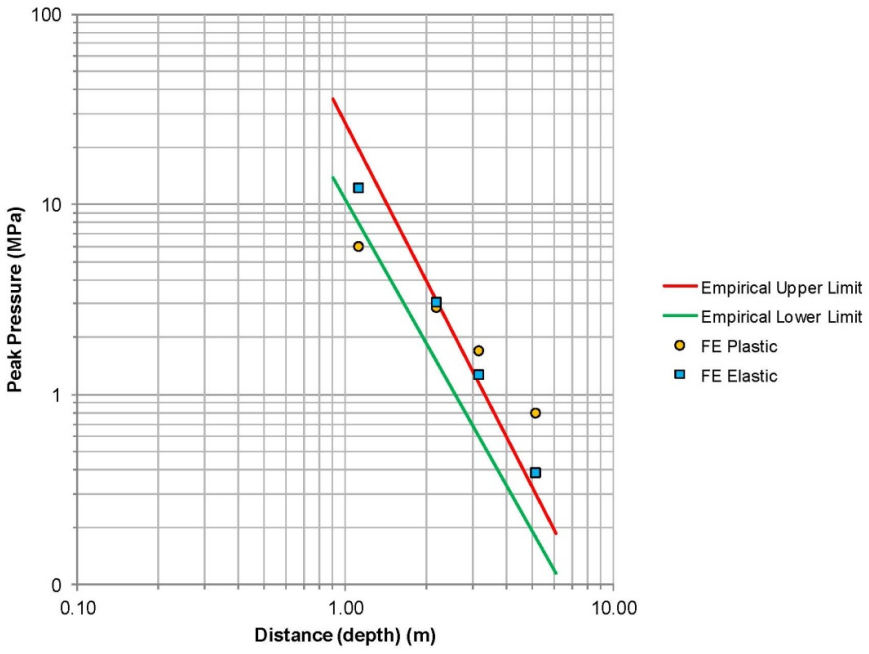

Figure 3-5 Comparison of Empirical Peak Pressure With Finite Element Predictions {100-kg [220-lb]-TNT Charge}

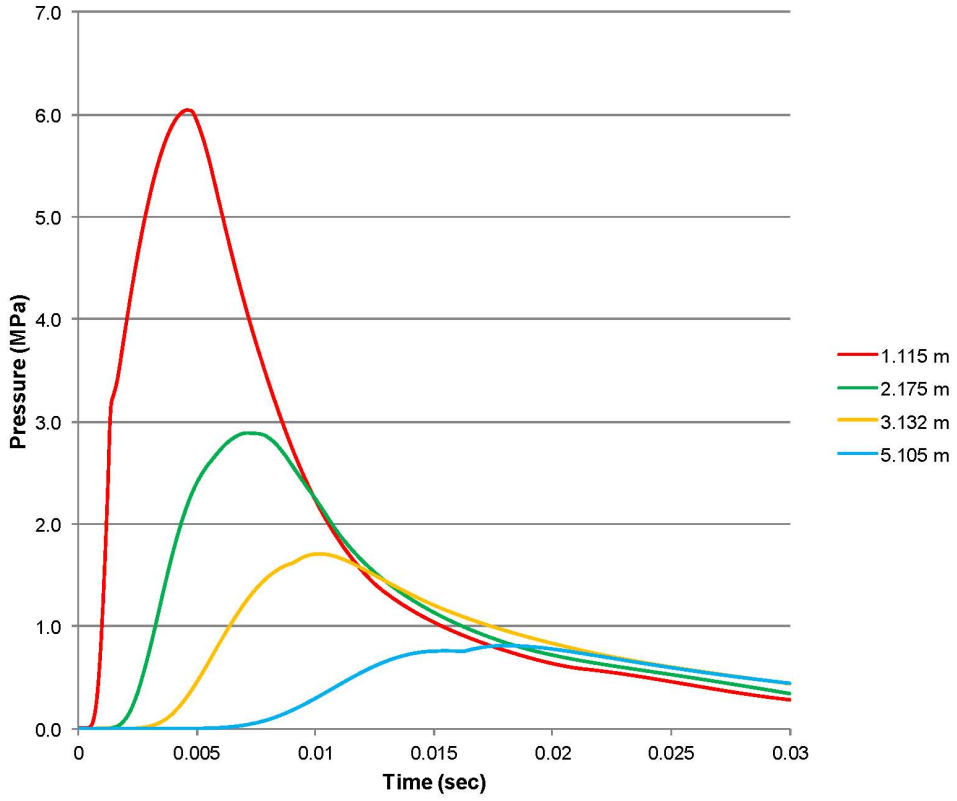

Figure 3-6 Pressure-Time Histories at Different Depths {100-kg [220-lb]-TNT Charge}

The empirical method of Cooper (1996), Eqs. (2-38) to (2-39), requires the detonation velocity, D; the Chapman-Jouguet pressure, P_{CJ}; the cratering efficiency, E_{CR}; and the explosive charge weight, W. From Cooper (1996), D for TNT is approximately 6.97 km/s [15,591 mi/hr] (Cooper, 1996, Table 5.1) with a density of 1.630 g/cm^3 [0.0598 lb/in^3]. For the 100-kg [220-lb] TNT charge, P_{CJ} is calculated to be 20.1 GPa [2,915 ksi]. Using these values for P_{CJ}, E_{CR}, and W, the apparent crater radius, R_a, is approximately 1.8 m [5.9 ft].

The empirical method of Gould (1981) requires the cratering efficiency of the explosive, V_0; the charge weight, W; and the height of the explosive above the surface, H. From Gould (1981), values of V_0 = 312 m^3/tonne [10,000 ft^3/ton] and V_0 = 47 m^3/tonne [1,500 ft^3/ton] for wet and dry clay, respectively, were chosen because the precise moisture content of the soil represented in the finite element model is not known. Recall that the soil of Nagy, et al. (2010) was described as “silty clay”; therefore, the value of V_0 = 34 m^3/tonne [1,100 ft^3/ton] corresponding to dry alluvium was also selected as a lower bound. Gould (1981) does not give data for a wet alluvium.

For the 100-kg [0.11-ton]-TNT-equivalent charge at 0.5 m [1.7 ft] above the surface, using Eqs. (2-41) to (2-43), the apparent crater volume, radius, and depth are given in Table 3-2. Thus, the apparent crater radius ranges from 2.85 to 1.01 m [9.35 to 3.31 ft] and the apparent crater depth ranges from 1.19 to 0.42 m [3.9 to 1.38 ft].

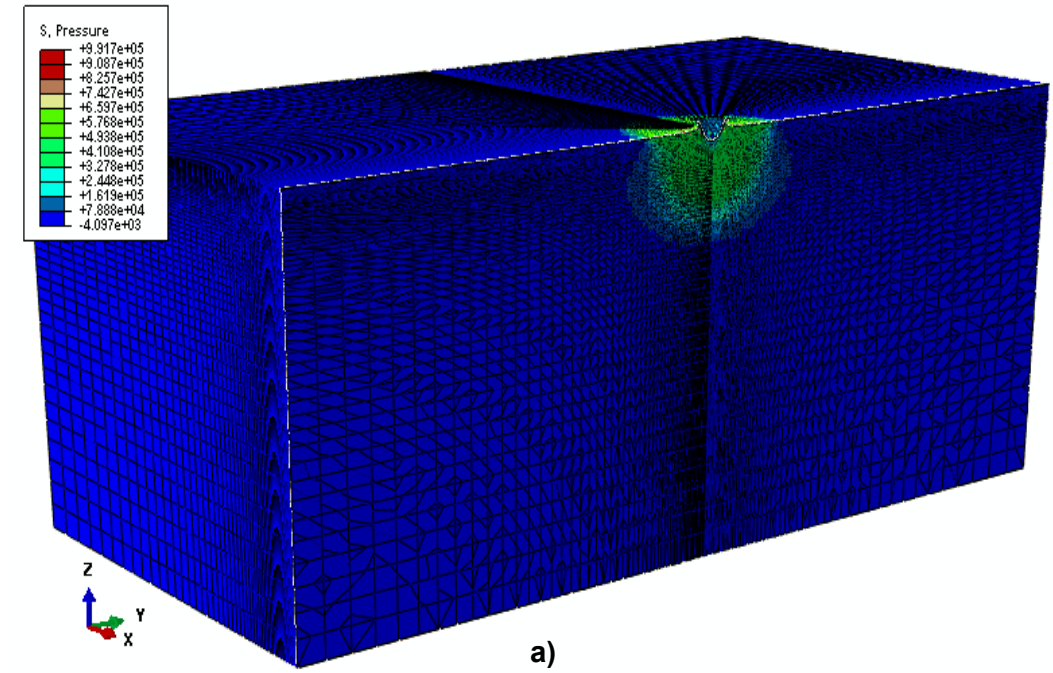

a)

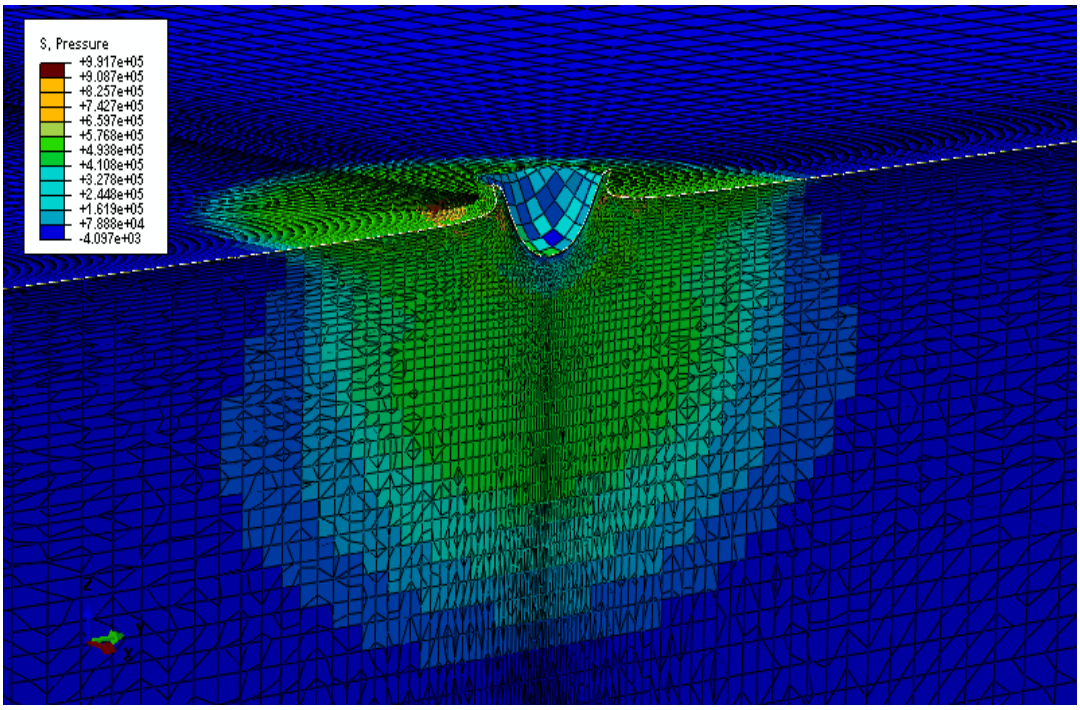

b)

Figure 3-7 Soil Pressure Distribution (Pa) at Time = 0.03 sec {100-kg [220-lb]-TNT Charge}

Table 3-2 Apparent Crater Dimensions using Gould (1981)*		
Soil Type	**Apparent Crater Radius (m)**	**Apparent Crater Depth (m)**
Wet Clay	2.85	1.19
Dry Clay	1.18	0.49
Dry Alluvium	1.01	0.42
*Based on Gould, K.E. "High-Explosive Field Tests: Explosion Phenomena and Environmental Impacts." DNA 6187F. Washington, DC: Defense Nuclear Agency. October 1981.		

In the finite element analysis, the crater dimensions were measured at 0.03 seconds after detonation because it was determined that the center node displacement had reached steady-state at that time (Figure 3-8). Figure 3-9 shows the apparent crater radius and depth, which is measured relative to the original surface shown by the dashed line.

The finite element analysis predicts an apparent crater radius, R_a, of 1.37 m [4.49 ft] and an apparent crater depth, D_a, of 1.2 m [3.9 ft]. A comparison of the apparent crater dimensions calculated from Cooper (1996), Gould (1981), and finite element results are given in Table 3-3. Both of these predicted crater dimensions lie within the range of the empirically calculated values. This provides a degree of confidence that the current Lagrangian finite element model produces a reasonably consistent prediction of crater formation compared to the empirical data.

Figures 3-10 and 3-11 show the progression of the plastic strain distribution in the soil around the crater as a function of time. The quantity D_p has been introduced here, which quantifies the depth of the plastic strain. Note the nonspherical plastic strain zone that forms in the soil around the crater boundary.

Figure 3-12 shows plots of the soil displacement vectors at selected times in the analysis. The red vectors signify the largest displacements. Initially at time 0.0006 seconds, the primary movement of the soil is downward; however, as time proceeds, the soil begins an upward movement (upheaval) forming the "lip" around the crater. This upward movement also indicates the development of ejecta. However, as discussed in Section 3.1, actual formation of ejecta is not possible using the current Lagrangian continuum approach. A Lagrangian finite element analysis incorporating mesh-free SPH in conjunction with an appropriate failure criterion would be required to attempt to simulate the formation of ejecta.

3.5 Finite Element Parametric Study on Different TNT-Equivalent Charge Weights and Above-Surface Heights

Based on the discussion in Section 2.1, a small moving van is chosen as the representative vehicle. The maximum payload is approximately 4,536 kg [10,000 lb] (GM, 2012a). For a 2008 full-size cutaway van produced by General Motors (GM), the dimension from the ground to the top of rear load floor ranges from 57 to 64 cm [22.3 to 25.1 in] (GM, 2012b). The explosive charge sizes used in the analyses are 45.3, 227, 453, 2,268, and 4,536 kg [100, 500, 1,000, 5,000, and 10,000 lb].

The finite element results are presented in the form of soil pressure distributions throughout the soil. Plots of pressure stress contours in the soil are used to determine the location of shock wave attenuation. Finite element results showing the predicted crater in the soil surface are also shown.

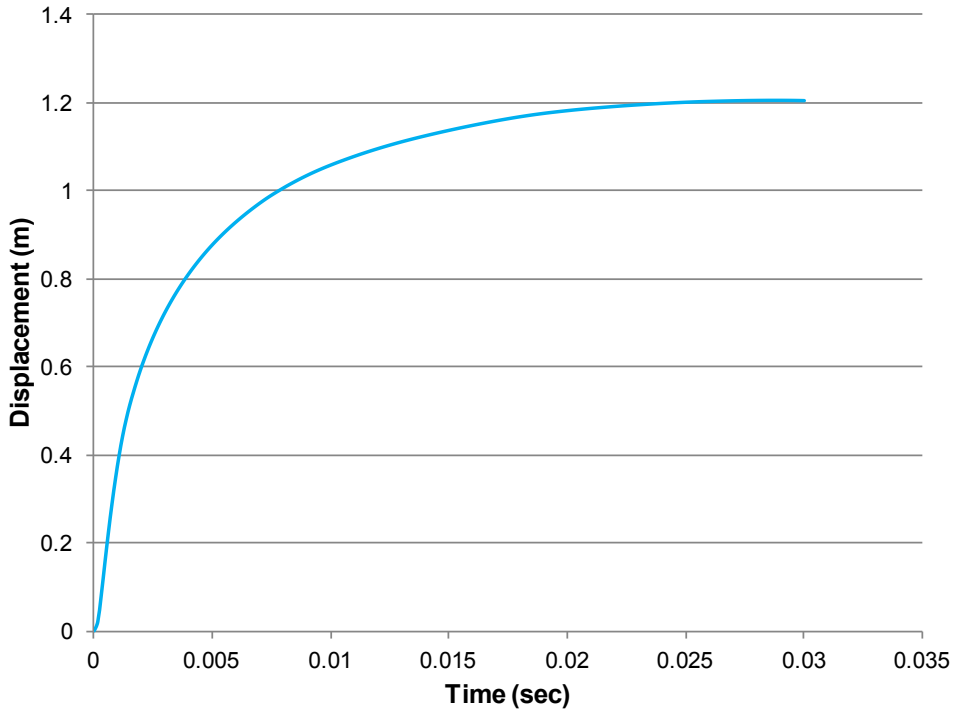

Figure 3-8 Time History of Center Displacement Showing Development of Crater Depth {100-kg [220-lb]-TNT Charge}

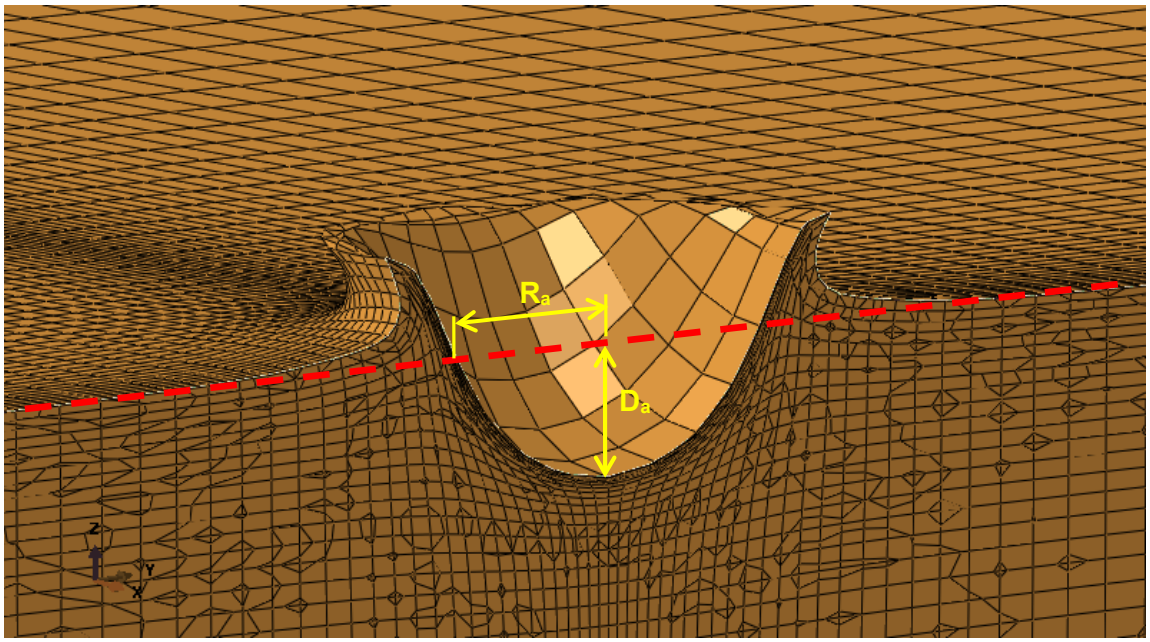

Figure 3-9 Apparent Crater Diameter and Depth Predicted by Finite Element Analysis {100-kg [220-lb]-TNT Charge}

Table 3-3 Comparison of Apparent Crater Dimensions for a 100-kg [220-lb] TNT Charge Located at a Height of 0.50 m [20 in]		
Results	**Apparent Crater Radius m [ft]**	**Apparent Crater Depth m [ft]**
Cooper*	1.8 [5.9]	-
Gould†	2.85–1.01 [9.35–3.31]	1.19–0.42 [3.90–1.38]
Finite Element	1.37 [4.49]	1.2 [3.9]
* Cooper, P.W. *Explosives Engineering*. Hoboken, New Jersey: John Wiley & Sons, Inc. 1996. †Gould, K.E. "High-Explosive Field Tests: Explosion Phenomena and Environmental Impacts." DNA 6187F. Washington, DC: Defense Nuclear Agency. October 1981.		

Time = 0.0006 sec

D_p = 0.6 m

Time = 0.0048 sec

D_p = 1.9 m

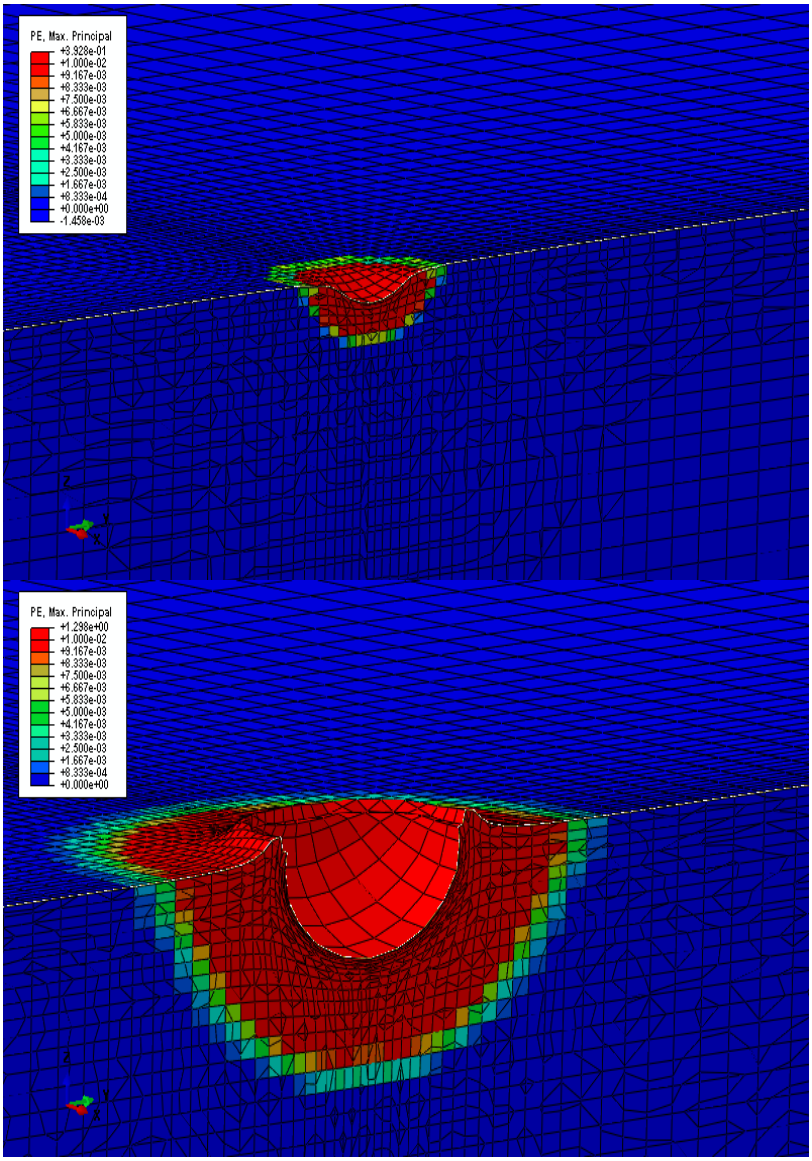

Figure 3-10 Plastic Strain Distribution (D_p = Plastic Strain Depth) {100-kg [220-lb]-TNT Charge}

Time = 0.01 sec

D_p = 3.3 m

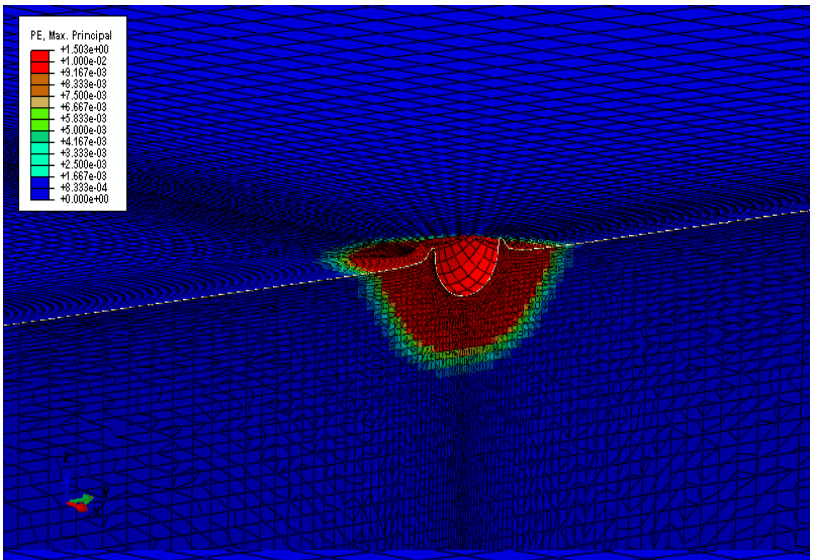

Time = 0.02 sec

D_p = 5.7 m

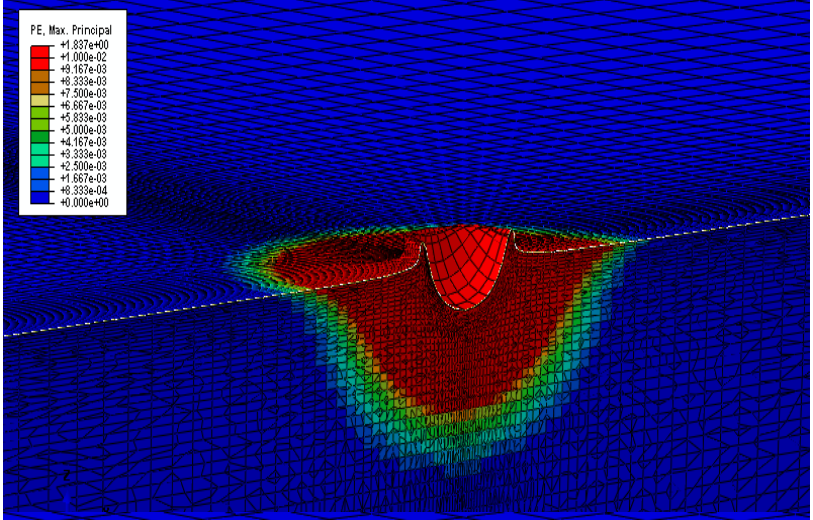

Time = 0.03 sec

D_p = 7.7 m

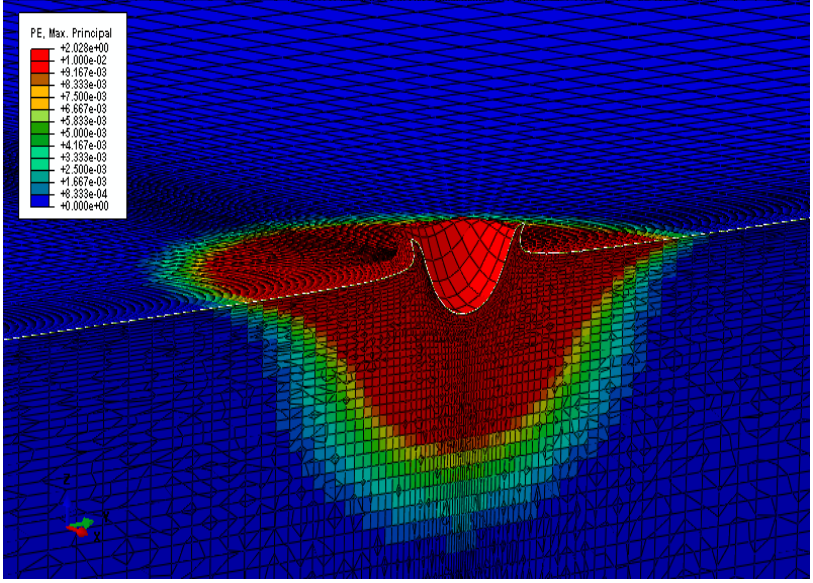

Figure 3-11 Plastic Strain Distribution Continued (D_p = Plastic Strain Depth) {100-kg [220-lb]-TNT Charge}

Time = 0.0006 sec

Time = 0.0048 sec

Time = 0.02 sec

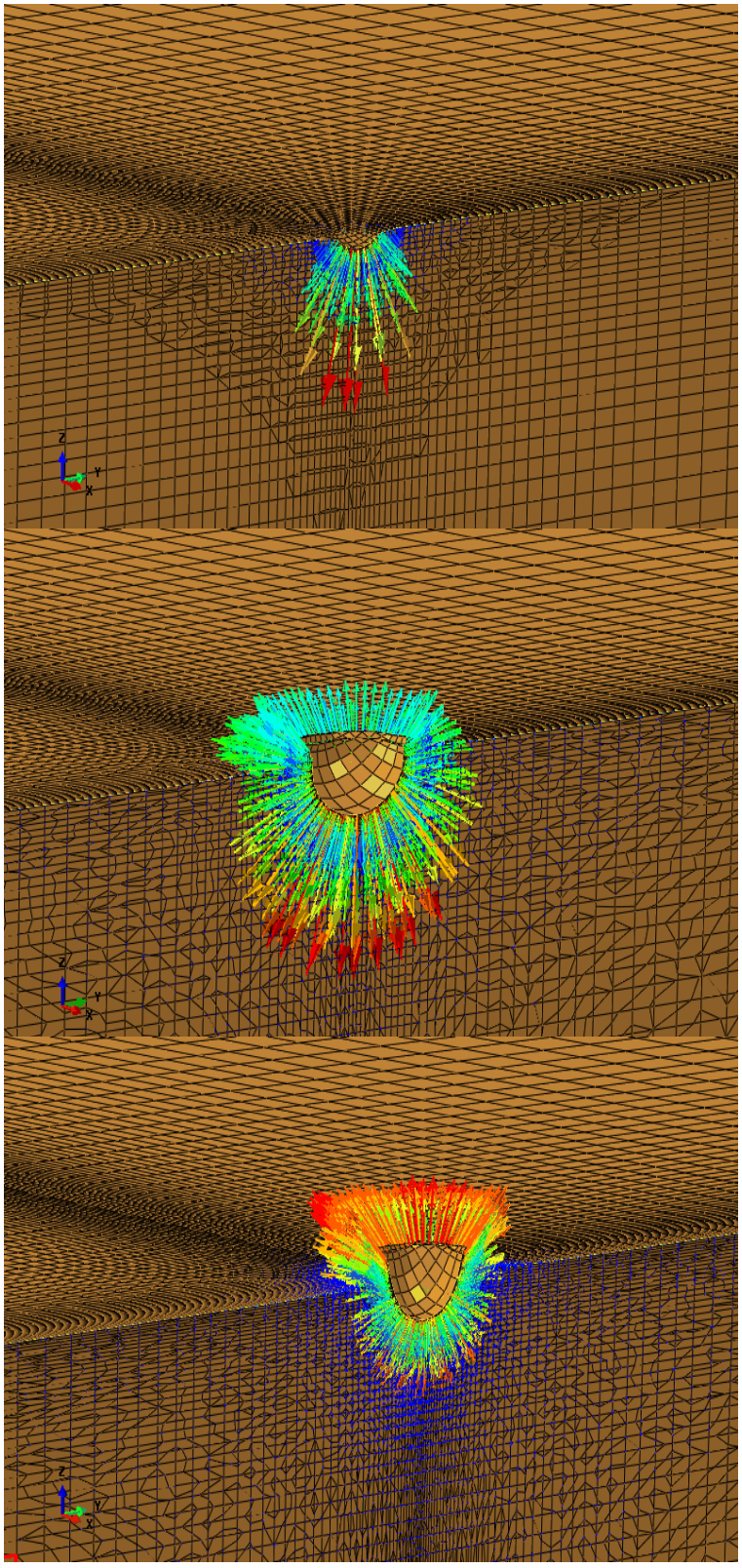

Figure 3-12 Displacement Vectors Indicating Direction of Soil Movement {100-kg [220-lb]-TNT Charge}

For the weight range between 2,268 and 4,535.9 kg [5,000 and 10,000 lb] TNT, the CONWEP algorithm cannot be used for charge heights less than the charge radius. This is because the corresponding dimensions would cause part of the spherical charge to be buried in the soil, a geometry for which the CONWEP algorithm is not valid. Table 3-4 shows the spherical charge radii for each charge weight. Thus, ABAQUS/Explicit analyses were not performed for those cases where the spherical charge would have been partially buried in the soil.

Tables 3-5 to 3-8 show the empirically calculated and finite element predicted apparent crater dimensions for different charge weights located at different heights. The empirical values were calculated using Eqs. (2-37) to (2-39) (Gould, 1981). Figure 3-13 shows the craters predicted by the finite element analyses for charge weights of 45.4, 226.8, and 453.6 kg [100, 500, 1,000 lb].

Table 3-4 Spherical Charge Dimensions

Charge Weight W_{TNT} kg [lb]	Charge Volume m^3 [ft^3]	Charge Radius m [ft]
45.4 [100]	0.028 [0.989]	0.19 [0.62]
226.8 [50]	0.139 [4.91]	0.32 [1.05]
453.6 [1,000]	0.278 [9.82]	0.41 [1.34]
2268.0 [5,000]	1.391 [49.12]	0.69 [2.26]
4535.9 [10,000]	2.783 [98.28]	0.87 [2.85]

For TNT: density = 1,630 kg/m^3

volume = weight/density = $\frac{4}{3}\pi r^3$ where r is radius

Table 3-5 Apparent Crater Dimensions* for an Above-Surface Charge Located at a Height of 0.5588 m [22 in]

Charge Weight W_{TNT} kg [lb]	Empirical		Finite Element	
	R_a m [ft]	D_a m [ft]	R_a m [ft]	D_a m [ft]
45.4 [100]	1.94–0.60 [6.36–1.97]	0.81–0.25 [2.66–0.82]	0.78 [2.56]	0.18 [0.59]
226.8 [500]	3.92–1.46 [12.9–4.79]	1.63–0.61 [5.35–2.00]	1.26 [4.13]	1.06 [3.48]
453.6 [1,000]	5.18–2.03 [17.0–6.66]	2.16–0.85 [7.09–2.79]	1.63 [5.35]	1.41 [4.62]
2268.0 [5,000]	9.56–4.07 [31.4–13.3]	3.98–1.70 [13.1–5.58]	–	–
4535.9 [10,000]	12.31–5.38 [40.39–17.65]	5.13–2.24 [16.83–7.35]	–	–

*Based on Gould, K.E. "High-Explosive Field Tests: Explosion Phenomena and Environmental Impacts." DNA 6187F. Washington, DC: Defense Nuclear Agency. October 1981.

– Indicates that charge height is less than charge radius, making the CONWEP algorithm invalid.

Table 3-6 Apparent Crater Dimensions* for an Above-Surface Charge Located at a Height of 0.6096 m [24 in]

Charge Weight W_{TNT} kg [lb]	Empirical		Finite Element	
	R_a m [ft]	D_a m [ft]	R_a m [ft]	D_a m [ft]
45.4 [100]	1.87–0.56 [6.14–1.84]	0.78–0.23 [2.56–0.75]	0.52 [1.71]	0.15 [0.49]
226.8 [500]	3.83–1.39 [12.56–4.56]	1.60–0.58 [5.25–1.90]	1.21 [3.97]	1.04 [3.41]
453.6 [1,000]	5.09–1.96 [16.70–6.43]	2.12–0.82 [6.96–2.69]	1.57 [5.15]	1.38 [4.53]
2268.0 [5,000]	9.46–3.99 [31.03–13.09]	3.94–1.66 [12.93–5.45]	–	–
4535.9 [10,000]	12.22–5.29 [40.09–7.36]	5.09–2.20 [16.70–7.22]	–	–

*Based on Gould, K.E. "High-Explosive Field Tests: Explosion Phenomena and Environmental Impacts." DNA 6187F. Washington, DC: Defense Nuclear Agency. October 1981.

– Indicates that charge height is less than charge radius, making the CONWEP algorithm invalid.

Table 3-7 Apparent Crater Dimensions* for an Above-Surface Charge Located at a Height of 0.6604 m [26 in]				
Charge Weight W_{TNT} kg [lb]	**Empirical**		**Finite Element**	
	R_a m [ft]	**D_a m [ft]**	**R_a m [ft]**	**D_a m [ft]**
45.4 [100]	1.80–0.52 [5.91–1.71]	0.75–0.22 [.46–0.72]	0.67 [2.20]	0.12 [0.39]
226.8 [500]	3.75–1.33 [12.30–4.36]	1.56–0.55 [5.12–1.80]	1.09 [3.58]	0.96 [3.15]
453.6 [1,000)	5.00–1.89 [16.4–6.20]	2.09–0.79 [6.86–2.59]	1.49 [4.89]	1.37 [4.49]
2268.0 [5,000]	9.37–3.91 [30.75–12.83]	3.90–1.63 [12.80–5.35]	–	–
4535.9 [10,000]	12.12–5.20 [39.76–17.06]	5.05–2.17 [16.57–7.12]	–	–
*Based on Gould, K.E. "High-Explosive Field Tests: Explosion Phenomena and Environmental Impacts." DNA 6187F. Washington, DC: Defense Nuclear Agency. October 1981. – Indicates that charge height is less than charge radius, making the CONWEP algorithm invalid.				

Table 3-8 Apparent Crater Dimensions* for an Above-Surface Charge Located at a Height of 0.7112 m [28 in]				
Charge Weight W_{TNT} kg [lb]	**Empirical**		**Finite Element**	
	R_a m [ft]	**D_a m [ft]**	**R_a m [ft]**	**D_a m [ft]**
45.4 [100]	1.74–0.48 [5.71–1.57]	0.72–0.20 [2.36–0.66]	0.70 [2.30]	0.10 [0.33]
226.8 [500]	3.67–1.27 [12.04–4.17]	1.53–0.53 [5.02–1.74]	1.10 [3.61]	0.86 [2.82]
453.6 [1,000]	4.92–1.82 [16.14–5.97]	2.05–0.76 [6.73–2.49]	1.43 [4.69]	1.21 [3.97]
2268.0 [5,000]	9.28–3.83 [30.45–12.57]	3.87–1.59 [12.70–5.22]	2.72 [8.92]	2.50 [8.20]
4535.9 [10,000]	12.03–5.12 [39.47–16.80]	5.01–2.13 [16.44–6.99]	–	–
*Based on Gould, K.E. "High-Explosive Field Tests: Explosion Phenomena and Environmental Impacts." DNA 6187F. Washington, DC: Defense Nuclear Agency. October 1981. – Indicates that charge height is less than charge radius, making the CONWEP algorithm invalid.				

Tables 3-5 to 3-8 show that the crater radius (depth) from the finite element analyses is consistently smaller than the empirical calculations. One possible explanation is that there is uncertainty in whether the soil parameters used in the empirical relationships are consistent with the soil parameters used in the Drucker-Prager Cap model. This demonstrates the difficulty in using empirical constants obtained from tables (from a variety of sources) because there is typically wide variability in data and the data are not always complete. However, considering that in Section 3.4.1 the finite element analysis soil pressures were comparable to those Nagy, et al. (2010) calculated, the differences in crater radius is most likely due to discrepancies between the empirical and Drucker-Prager Cap model soil parameters.

3.5.1 Predicting Crater Formation Using Element Deletion and Continuum-To-Particle Conversion

The formation of a crater in soil also was predicted using the element deletion approach available in ABAQUS/Explicit. A soil failure criterion was used to determine when an element would be deleted from the finite element mesh. Calculating failure utilizes effective strain, $\bar{\varepsilon}$, which is based on a von Mises form

$$\bar{\varepsilon} = \left[(\varepsilon_1 - \varepsilon_2)^2 + (\varepsilon_2 - \varepsilon_3)^2 + (\varepsilon_3 - \varepsilon_1)^2\right]^{1/2} \quad (3\text{-}1)$$

Charge Weight = 45.4 kg [100 lb]

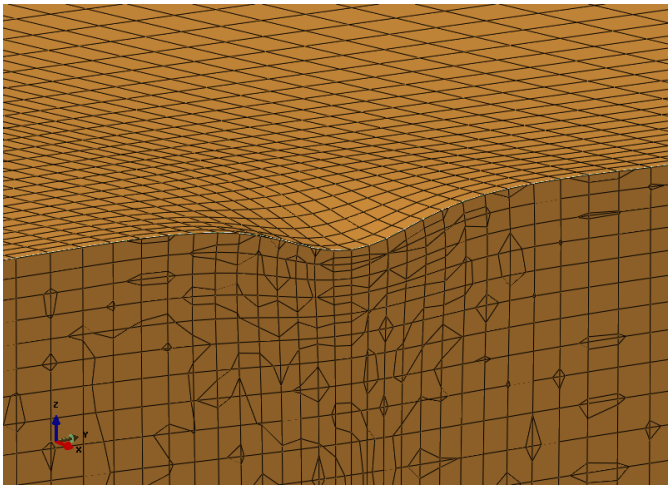

Charge Weight = 226.8 kg [500 lb]

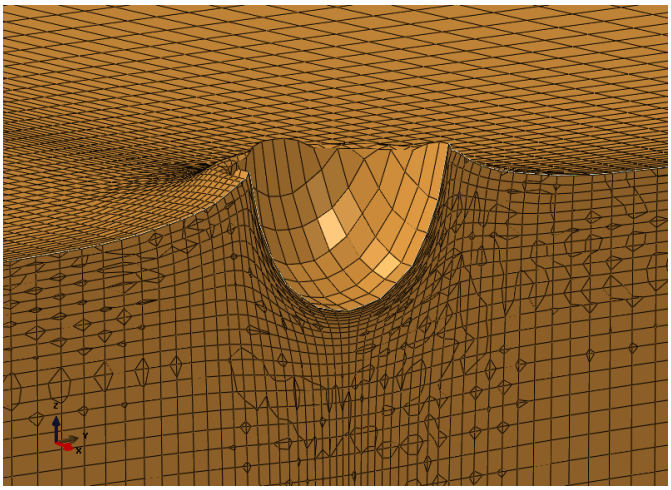

Charge Weight = 453.6 kg [1,000 lb]

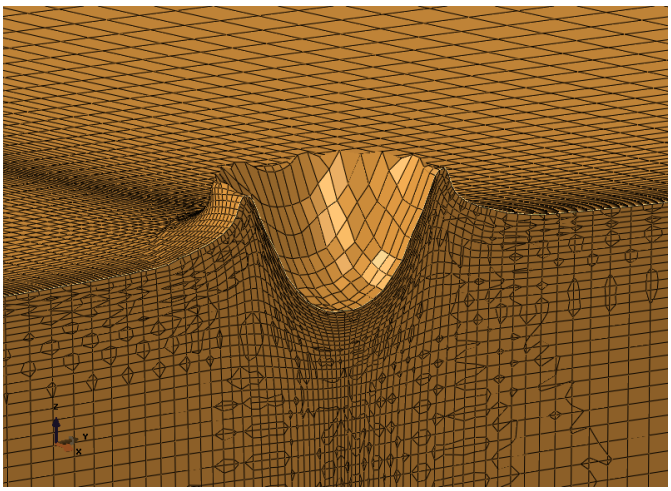

Figure 3-13 Predicted Crater Sizes for Above-Surface Charge Located at a Height of 0.6096 m [24 in]

where the quantities ε_1, ε_2, ε_3 are principal strains. This expression was implemented using the ABAQUS/Explicit user utility subroutine VUSDFLD (Dassault Systèmes Simulia Corp., 2012a). The failure criterion used principal plastic strains in the effective strain calculation [Eq. (3-1)]. For the analyses in this report, a failure criterion of 15 percent effective plastic strain was used.

3.5.1.1 Element Deletion

A 454-kg [1,000-lb] TNT-equivalent charge located at a height of 0.6096 m [24 in] was analyzed. Figure 3-14 shows the predicted crater size using the element deletion technique. The predicted apparent crater radius, R_a, is approximately 2.41 m [7.91 ft] which is within the range of 5.09 to 1.96 m [16.7 to 6.4 ft] as previously given in Table 3-6. The apparent crater depth, D_a, is approximately 1.89 m [6.2 ft] which is within the range of 2.12 to 0.82 m [6.96 to 2.69 ft], also previously given in Table 3-6.

Additional analyses were performed for other TNT-equivalent charge sizes of 4,536; 9,072; 18,144; and 27,216 kg [10,000; 20,000; 40,000; and 60,000 lb]. Table 3-9 shows the location of the center of the spherical charge, which is equal to the radius of the spherical charge. These charge heights result in the charge just touching the ground surface. Table 3-10 shows both the empirical and finite element predictions of the apparent crater dimensions for each charge size. For each charge size, the finite element predicted apparent crater depth falls within the range given by the empirical expressions of Gould (1981), but the predicted apparent crater radius is

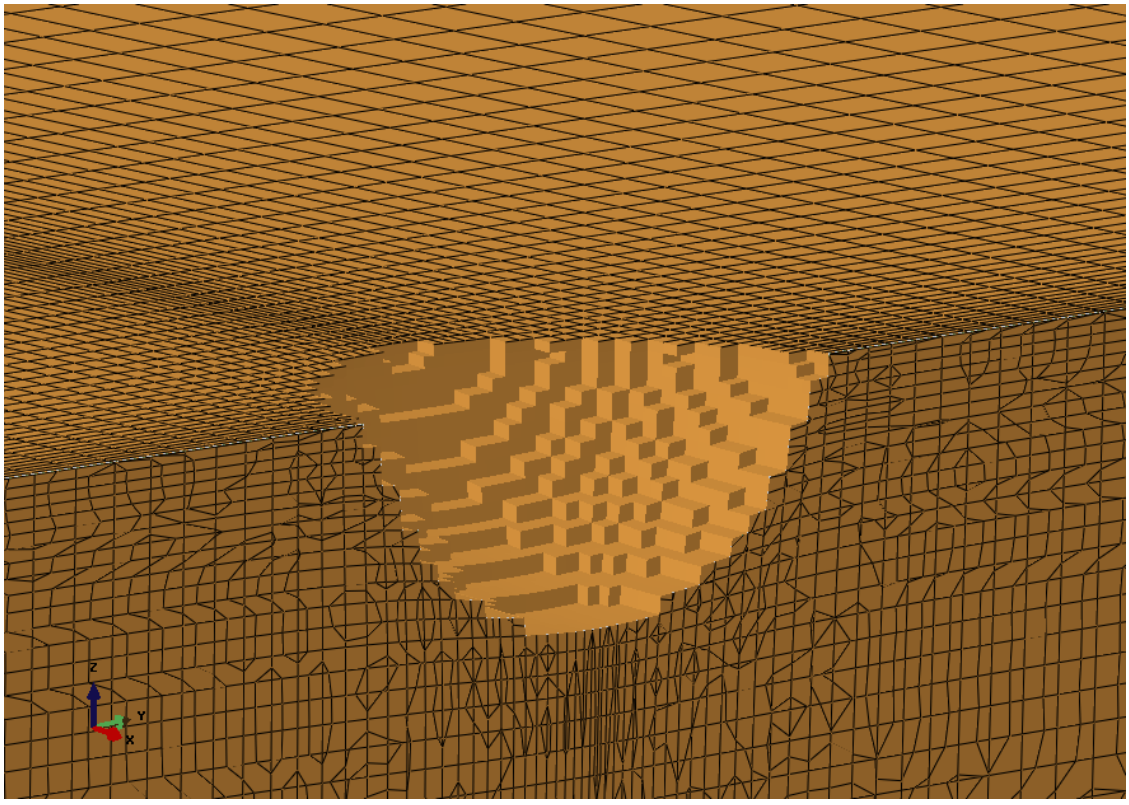

Figure 3-14 Predicted Crater for 454-kg [1,000-lb]-TNT-Equivalent Charge Located at a Height of 0.6096 m [24 in]

Table 3-9 Height of Above-Surface Charge		
Charge Weight W_{TNT} kg [lb]	Radius of Spherical Charge m [ft]	Height of Charge Center Above Surface m [ft]
4,536 [10,000]	0.87 [2.85]	0.9 [2.95]
9,072 [20,000]	1.10 [3.61]	1.1 [3.64]
18,144 [40,000]	1.39 [4.56]	1.4 [4.59]
27,216 [60,000]	1.59 [5.22]	1.6 [5.25]

Table 3-10 Apparent Crater Dimensions* for Above-Surface Charges				
Charge Weight WTNT kg [lb]	Empirical		Finite Element	
	Ra m [ft]	Da m [ft]	Ra m [ft]	Da m [ft]
4,536 [10,000]	11.68–4.82 [38.32–15.82]	4.87–2.01 [15.98–6.59]	3.46 [11.35]	2.79 [9.15]
9,072 [20,000]	14.76–6.10 [48.42–20.01]	6.15–2.54 [20.18–8.33]	5.99 [19.65]	3.88 [12.73]
18,144 [40,000]	18.59–7.68 [60.99–25.20]	7.74–3.20 [25.39–10.50]	7.50 [24.61]	5.91 [19.39]
27,216 [60,000]	21.27–8.80 [69.78–28.87]	8.86–3.67 [29.07–12.04]	8.67 [28.44]	6.87 [22.54]
* Based on Gould, K.E. "High-Explosive Field Tests: Explosion Phenomena and Environmental Impacts." DNA 6187F. Washington, DC: Defense Nuclear Agency. October 1981. – Indicates that charge height is less than charge radius, making the CONWEP algorithm invalid.				

just below the lower limit. For the 454-kg [1,000-lb] charge, the predicted apparent crater radius was also within the limits of Gould (1981). At this point, there is not a clear explanation other than the selected failure criterion for the discrepancy at the larger charge weights (Table 3-10). In this study, a soil failure criterion of 15 percent equivalent plastic strain was chosen based on a range of values found in the literature. However, because of the variability in soil parameter values reported in the literature it is recommended that additional failure criterion values be investigated to determine their effect on apparent crater dimensions. In addition, alternative failure criteria, such as equivalent total strain and maximum principal tensile strain, also have been used. Further investigation of these alternative failure criteria may prove useful.

Figures 3-15 and 3-16 show the finite element predicted soil pressure distributions. The times given correspond to when the finite element model maximum energy occurred and when the kinetic energy reached steady state.

3.5.1.2 Continuum-to-Particle Conversion

A third approach for predicting crater formation was investigated using the "continuum-to-particle" conversion option in which the solid continuum elements are converted to SPH particles once a specified failure criterion is satisfied. As in the element deletion approach, an effective plastic strain failure criterion of 15 percent was used. Figure 3-17 shows results where the failed continuum elements have been converted to SPH particles.

Figure 3-17 shows that SPH particles penetrate the contact surface that represents the crater wall; this is not physically realistic. Dassault Systèmes Simulia Corp. user support was contacted regarding this observation and it was confirmed that ABAQUS/Explicit has a "bug" that allows SPH particles to penetrate contact surfaces. Dassault Systèmes Simulia Corp. stated their intent to correct this error, possibly in the release of ABAQUS/Explicit Version 6.14 in May 2014. The continuum-to-particle conversion technique in ABAQUS/Explicit cannot be used until this error is corrected by the software vendor.

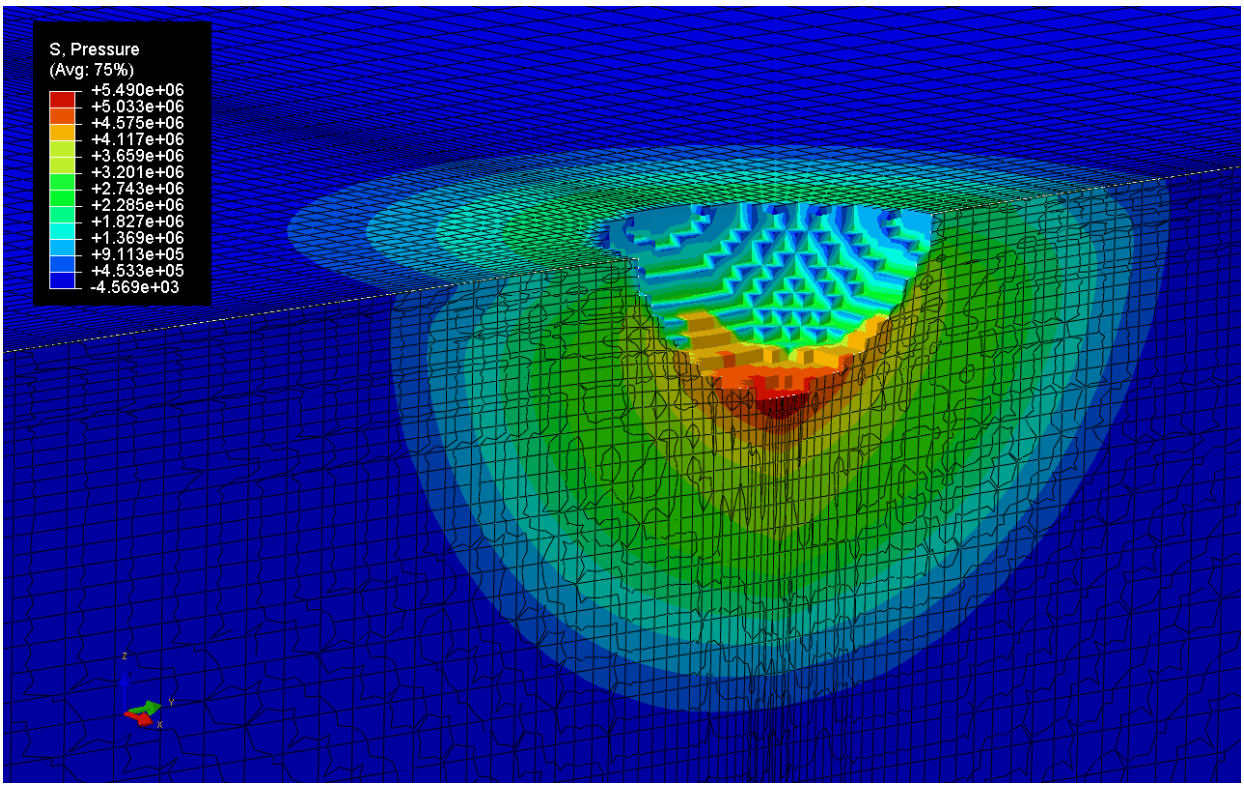

4,536 kg [10,000 lb] Charge at Time = 2.4 ms

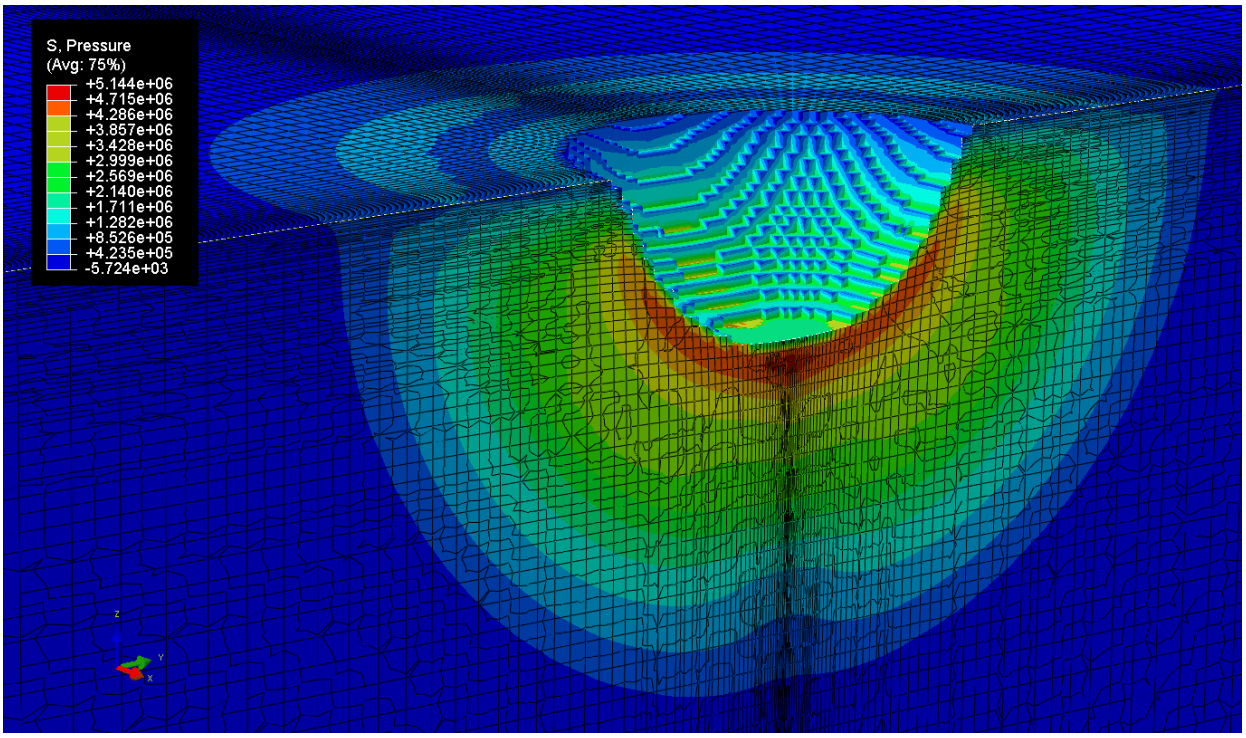

9,072 kg [20,000 lb] Charge at Time = 5.3 ms

Figure 3-15 Soil Pressure Distributions for 4,536 and 9,072 kg [10,000 and 20,000 lb] Charges. Pressure Is in Pa.

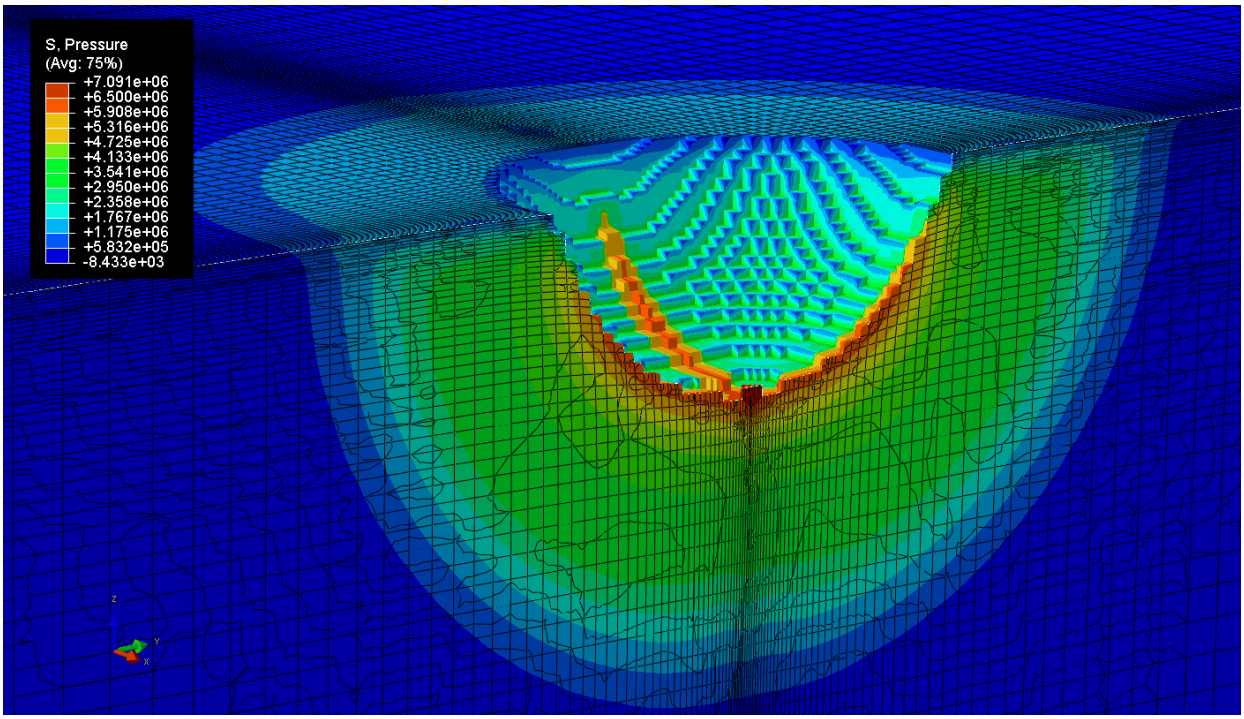

18,144 kg [40,000 lb] Charge at Time = 6.6 ms

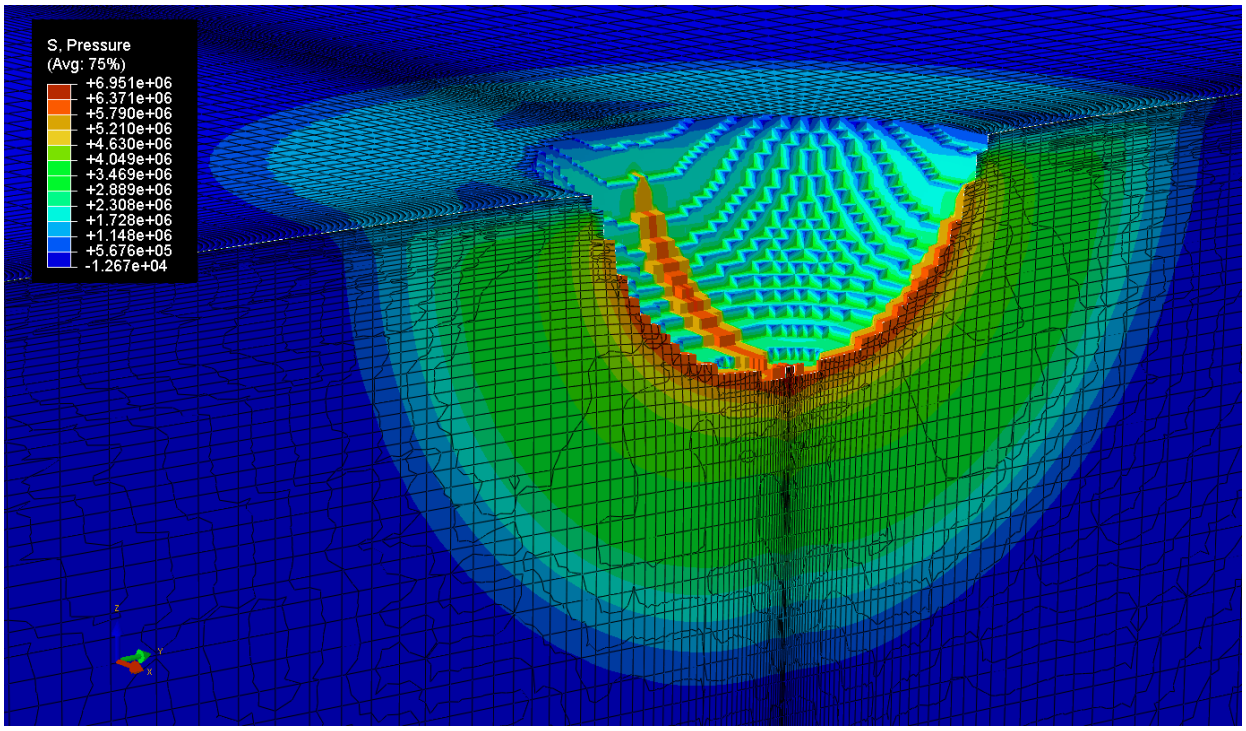

27,216 kg [60,000 lb] Charge at Time = 7.8 ms

Figure 3-16 Soil Pressure Distributions for 18,144 and 27,216 kg [40,000 and 60,000 lb] Charges. Pressure Is in Pa.

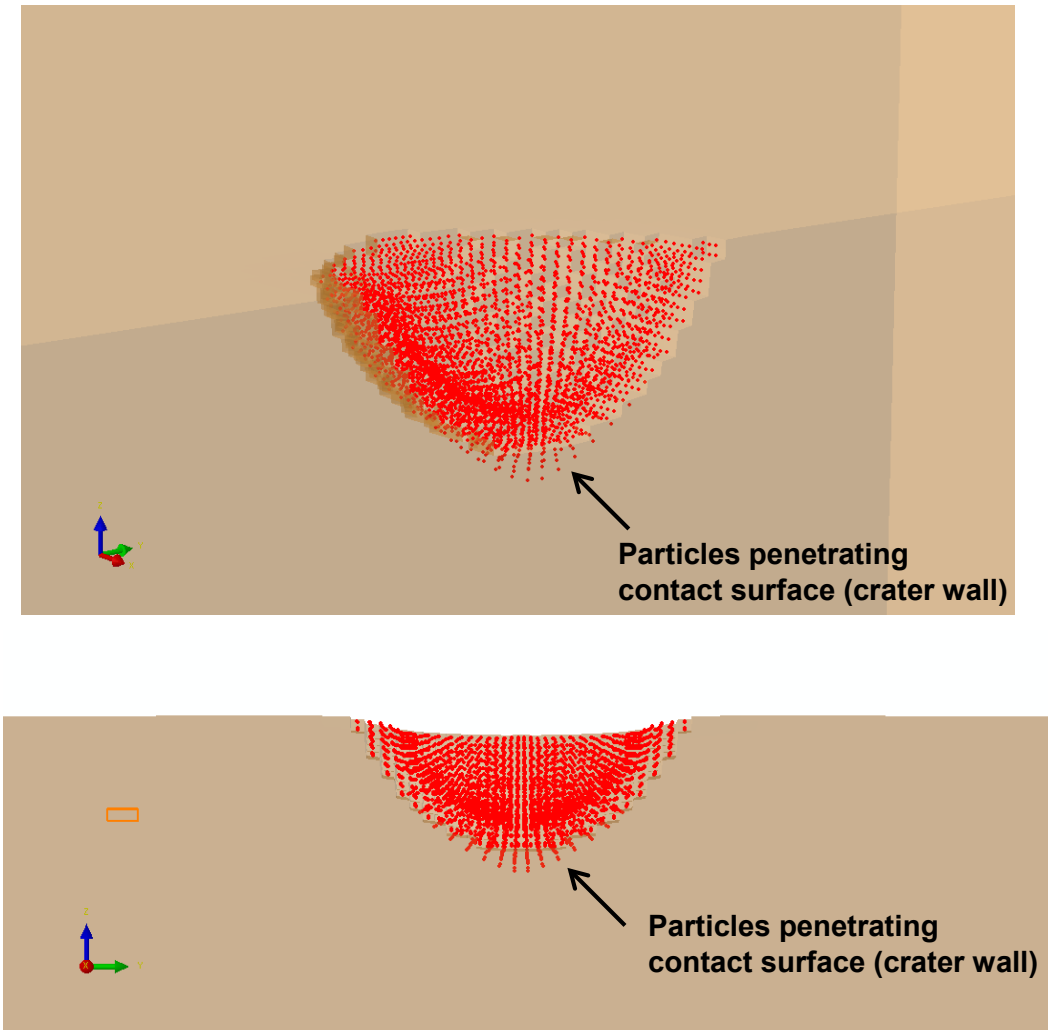

Figure 3-17 ABAQUS/Explicit Smoothed Particle Hydrodynamics Results for a 454-kg [1,000-lb]-TNT-Equivalent Charge Located at a Height of 0.6096 m [24 in]

3.6 Eulerian Finite Element Analysis

As an alternative to the Lagrangian approach with CONWEP generated blast pressures (Sections 3.4 and 3.5), a multi-material Eulerian approach was investigated. This approach involved constructing an Eulerian mesh containing all the materials in the solution domain: air, explosive charge, and soil, Figure 3-18. Although Figure 3-18 does not show the mesh, approximately 1.5 million elements were used to provide sufficient mesh density. Air was modeled using the ideal gas equation-of-state (EOS) (Dassault Systèmes Simulia Corp., 2012b)

and the necessary parameters are given in Table 3-11. A spherically shaped explosive charge having a weight of 454 kg [1,000 lb] was modeled and its detonation behavior modeled using the Jones-Wilkens-Lee (JWL) EOS (Dassault Systèmes Simulia Corp., 2012b). The JWL EOS parameters are given in Table 3-12 and are the same as those given in Nagy, et al. (2010). The soil was represented by the same Drucker-Prager Cap model and soil parameters as described in Section 3.2 of this report.

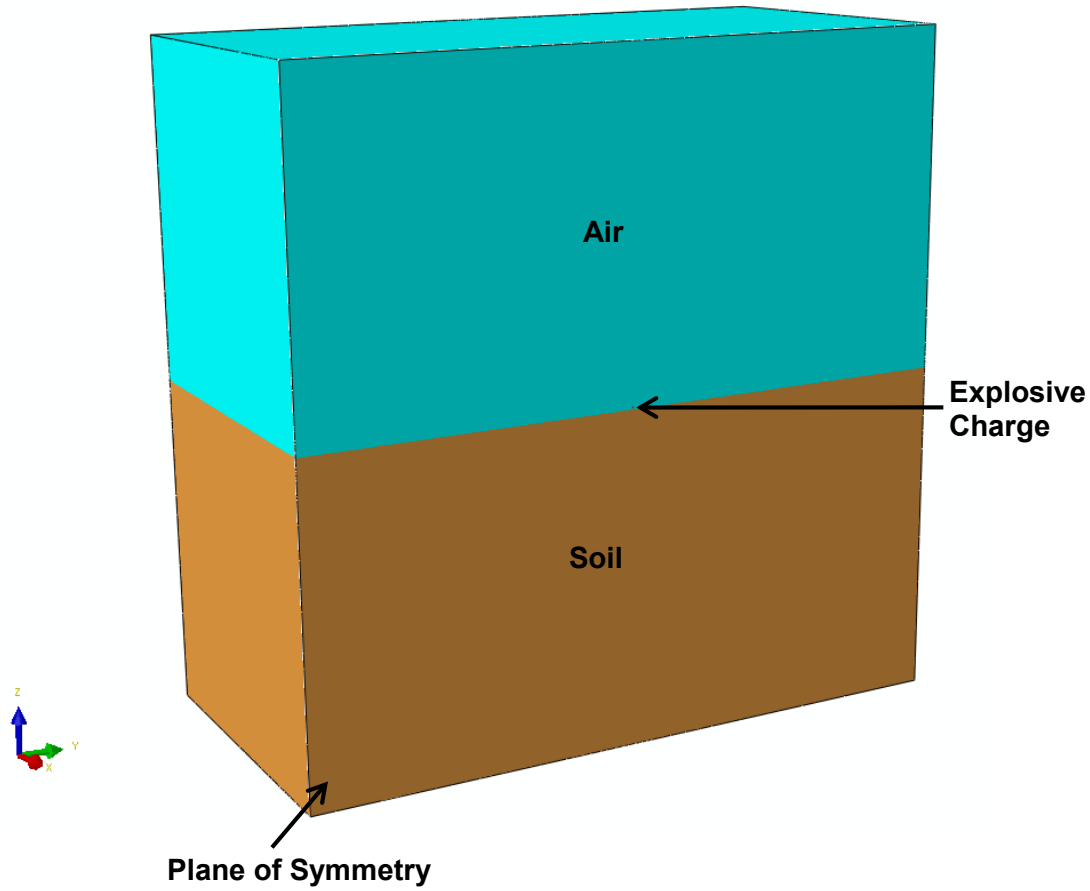

Figure 3-18 Multi-Material Eulerian Analysis Model (One Half of the Solution Domain Is Shown)

Table 3-11 Ideal Gas Parameters	
Parameter	**Value**
Reference Density (ρ_a)	1.225 kg/m^3 [0.0765 lb/ft^3]
Gas constant for air (R_{air})	286.9 J/kg·K [1716 ft·lb/slug·R]
Specific heat capacity (c_v)	717.3 J/kg·K [0.1714 BTU/lbm·F]
Reference temperature (T_0)	288.2° K [59.4° F]

Figure 3-19 shows results of the Eulerian analysis and the predicted shape of the crater at 6.24 ms. The yellow line denotes the original ground surface. The apparent crater depth is 0.9 m [2.95 ft]. The Lagrangian analysis predicted an apparent crater depth of 1.37 m [4.49 ft],

a difference of approximately 34 percent. Interestingly, the value of 0.9 m [2.95 ft] falls within the empirically predicted range of 2.09–0.79 m [6.86–2.59 ft] given in Table 3-7. There are a number of possible reasons for the difference between the Eulerian and Lagrangian results. The primary reason may be insufficient mesh refinement of the air domain surrounding the explosive charge. If the elements are too large, inaccuracy in the propagation of the air blast shock wave may result, which would in turn under-predict the ground surface blast pressure loading compared to the loading calculated by the CONWEP algorithm used in the Lagrangian

Table 3-12 Jones-Wilkens-Lee Equation of State Parameters

Parameter	Value
Detonation wave speed (C_d)	6,930 m/s [22,736 ft/s]*
A	373.8 GPa [54,215 ksi]*
B	3.747 GPa [543 ksi]*
R_1	4.15*
R_2	0.9*
ω	0.35*
Density of explosive (ρ_0)	1,630 kg/m^3 (102 lb/ft^3)*
Initial specific energy (E_{m0})	4.56 MJ/kg (1961.8 Btu/lb)†

*Values taken from Nagy, N., M. Mohamed, and J.C. Boot. "Nonlinear Numerical Modelling for the Effects of Surface Explosions on Buried Reinforced Concrete Structures." *Geomechanics and Engineering*. Vol. 2. pp. 1–18. 2010.
†Value taken from Smith, P.D. and J.G. Hetherington. *Blast and Ballistic Loading of Structures*. Oxford, England: Butterworth-Heinemann. 1994.

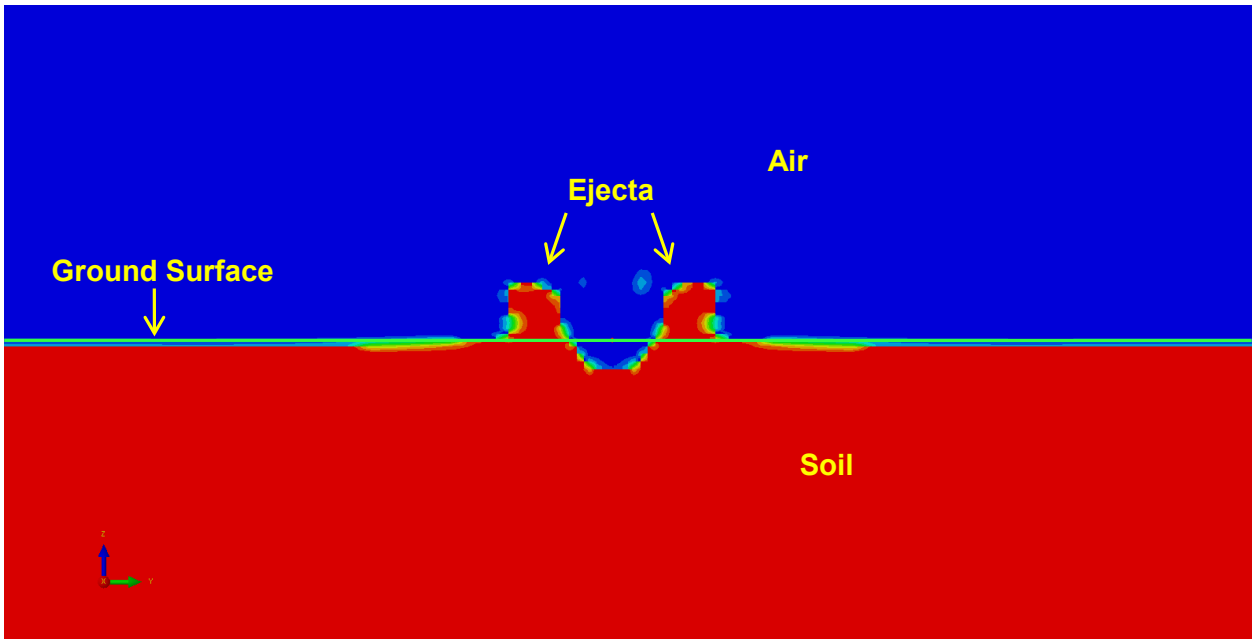

Figure 3-19 Eulerian-Analysis-Predicted Apparent Crater Size

analyses. It is recommended that a finer mesh be used in modeling the air domain to investigate the accuracy of the ground surface blast loading pressure.

3.7 Alternative Analysis Codes Reviewed

This section briefly discusses alternative codes that can be used to model blast-induced shock waves and their effects on underground structures. Open literature sources provide examples of both commercially available and restricted use codes that are commonly used for blast analyses will be discussed. The rationale for using ABAQUS/Explicit for the analyses in this report was to utilize commercially available software that does not have access restrictions. Analyses conducted by nuclear power plant licensees may not qualify for access to specialized codes, which typically have use restrictions. Nevertheless, it is recognized that these highly specialized codes are useful when performing blast analyses.

Commercial Codes

Both Autodyn (ANSYS, 2013) and LS-DYNA (LSTC, 2013) have wide acceptance for performing explicit dynamic analyses. Both of these codes are capable of multi-material Eulerian, Lagrangian, Arbitrary Lagrangian-Eulerian analysis, and SPH modeling capabilities. LS-DYNA also has an element free Galerkin (EFG) analysis capability which is useful for crack propagation analysis. Both codes have a large number of material models for applicable to large deformation, high strain rate behavior and EOS for solids, fluids, and gases. There are no restrictions on the use of either Autodyn or LS-DYNA.

Restricted Codes

The shock physics code CTH (Sandia, 2013) is well-known and widely used to calculate blast-induced pressures produced by explosive charges. CTH is an Eulerian code capable of modeling shock waves and large deformations of materials. The JWL EOS used in the ABAQUS/Explicit analyses is also available in CTH for modeling the explosive charge. A common approach is to use CTH to calculate the blast-induced pressure distributions, which are then input as time-dependent pressure loads in a separate Lagrangian finite element structural analysis. Access to CTH is restricted to use by the U.S. government or its contractors working for the U.S. government.

Another software tool is the code EPIC (Elastic-Plastic Impact Computations) (Gerlach and Johnson, 2009). This code was developed for the purpose of understanding the effects of Improvised Explosive Devices (IEDs) buried in soil. EPIC is a Lagrangian code that uses a so-called hybrid particle-finite element approach involving both solid continuum elements and hybrid particles. Distribution of EPIC is limited to the U.S. Department of Defense and its contractors.

4. CHARACTERIZING STRUCTURE RESPONSE

4.1 Codes and Standards for Design of Underground Structures

This section briefly describes codes, specifications, and standards that could be used to design underground structures subjected to dynamic loads generated by detonation of high explosives in air, at the ground surface, and underground.

4.1.1 Design and Analysis of Hardened Structures to Conventional Weapons Effects and Structures to Resist the Effects of Accidental Explosions

The Unified Facilities Criteria (UFC) Joint Services Manuals (DOD, 2008, 2002) are regarded as the principal guidance documents for design of structures subjected to explosive loads. Although the design approach presented in these manuals is directed primarily toward structures subjected to the effects of a high explosive detonation, it is also applicable to the design of structures exposed to other explosive detonations. The design methods account for the close-in effects of an explosion on structures. These design methods also are applicable for intermediate and far-range effects on structures located away from the explosion. These guidance documents use concepts and provisions from other specific codes, standards, and design manuals commonly used in the design of reinforced concrete, prestressed concrete, masonry, and steel structures (e.g., ACI, 2011; AISC, 1994; PCI, 1978; J. Healey, et al., 1975). The design procedure is applicable to both surface and underground structures subjected to explosive loads.

4.1.2 Fundamentals of Protective Design for Conventional Weapons

This U.S. Army Manual (DOD, 1986) was originally published in 1949 as the first standard to provide design guidelines for structures subjected to explosive loads in a single document. This document used extensive structural damage data produced during World War II and was revised in 1986. This document provides guidance on the design of reinforced concrete structures under explosive loads. It uses concepts and provisions of the American Concrete Institute code to design reinforced concrete structures, with special consideration for the rate of loading effects on the strength properties of concrete and reinforcing steel. This manual is referenced in U.S. Department of Defense (DOD, 2008, 2002) and provides more detailed design guidelines for reinforced concrete underground structures.

4.2 Analytical Tools for Modeling Underground Structure Response

The effects of surface blast-induced ground shock on an underground structure are different than the effects of an air blast on a surface structure. The structural response of a freestanding surface structure is primarily from the air blast, with ground shock effects being secondary. For an underground structure, this is not the case, because the structure is surrounded by a medium (e.g., soil) that is closer in density to the material of the underground structure than to air, which facilitates stronger energy coupling. In the region where the crater forms, there is typically significant structural damage, but the depth at which the structure will remain undamaged is difficult to predict because it depends on the soil characteristics, which control pressure wave attenuation and ground motion. Therefore, the responses of the ground and the structure are closely related. The motion of the underground structure (i.e., displacement, velocity, and acceleration) is closely coupled with the motion and constraining effect of the ground (Glasstone and Dolan, 1977). Because of this coupling, commonly referred to as

soil-structure interaction (SSI), developing purely analytical methods to analyze underground structures is difficult.

Baylot (1992) investigated various parameters that affect the loading on buried structures when a conventional weapon (explosive) detonates near a buried structure. As Baylot (1992) states, the most difficult part of designing an underground structure is to accurately determine the blast-induced loading. The typical approach is to calculate the free-field stresses at a specific location that would be produced without the presence of the structure. These stresses are then modified to approximate the interface stresses that would occur on the structure (Baylot, 1992).

An approach provided in DOD (1986) uses semi-empirical methods to predict the free-field stresses, displacements, velocities, accelerations, and impulse forces. These expressions were presented in Section 2.4.1.2, Eqs. (2-32) to (2-36). To calculate the shock of the buried structure, the parameters R_1 and R_2 are the distance from the explosive charge to the front face and back face of the structure, respectively (Dove, 1992). The original expressions given in Eqs. (2-32) to (2-36) are then integrated over the range R_1 to R_2 to give uniform displacements, velocities, and accelerations (Dove, 1992)

$$\frac{d_{avg}}{W^{1/3}} = \frac{500\, f\, W^{\frac{(n-1)}{3}} (R_1^{-n+2} - R_2^{-n+2})}{c\,(n-2)\,(R_2 - R_1)} \tag{4-1}$$

$$V_{avg} = \frac{160\, f\, W^{\frac{n}{3}} (R_1^{-n+1} - R_2^{-n+1})}{(n-1)\,(R_2 - R_1)} \tag{4-2}$$

$$a_{avg} W^{1/3} = \frac{50\, f\, c\, W^{\frac{n+1}{3}} (R_1^{-n} - R_2^{-n})}{n\,(R_2 - R_1)} \tag{4-3}$$

Equations (4-1) to (4-3) give the average free-field motions, and the parameters f, c, n, and W are the same as described in Section 2.4.1.2. Finally, a reduction factor is applied, which is based on the geometry of the structure. Dove (1992) states that although this approach conservatively estimates structural response it has limited applicability because it uses a box-like structure. Baylot (1992) also states that this method significantly overpredicts the loading on the structure, which results in an overprediction of the structural response.

A second approach is the single-degree-of-freedom (SDOF) analysis, which reduces the problem to a simple spring, mass, and damper system, as shown in Figure 4-1.

Here, the spring represents the stiffness (K) of a structural component (e.g., wall, slab), and the mass (M) and damper (C) are calculated to give the same frequency and damping characteristics as the actual structure (Dove, 1992). The term F(t) is the time-dependent loading. Because the SDOF approach is very common, it is not discussed in this report. Instead the reader is referred to Paz and Leigh (2004) and Weidlinger and Hinman (1988), who present a thorough discussion on SDOF analysis, as well as multiple-degree-of-freedom (MDOF)

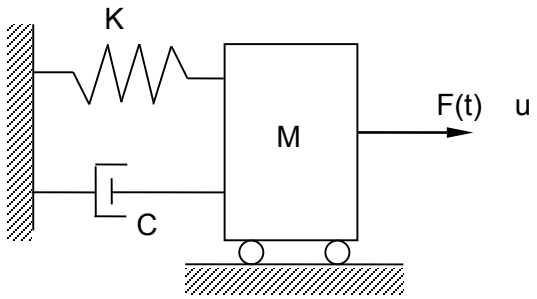

Figure 4-1 Single Degree of Freedom System

analysis. Dove (1992) states that SDOF analyses tend to be inconsistent because of the difficulty calculating the structural loading.

To accurately calculate loading of the structure, it is necessary to know the deformability of the structure relative to the surrounding soil (Glasstone and Dolan, 1977). Glasstone and Dolan (1977) state that if the structure is at least as deformable as the surrounding soil, then the free-field pressure can be applied to the structure and considered as an upper limit. If the structure is more deformable than the surrounding soil, then the pressure loading can be lower (Glasstone and Dolan, 1977). In this case the structure may deflect away from the soil, which creates the so-called “soil arching” effect. Soil arching will result in part of the pressure being transmitted around the structure. Chen, et al. (1990) state that for burial depths equal to or greater than approximately 20 percent of the span of the structure, accounting for soil arching is important. Dove (1992) and Baylot (1992) conclude that the complicating factor in the methods discussed previously is the inability to accurately account for SSI. Therefore, the overall conclusion is that to accurately analyze an underground structure subjected to a surface explosion, numerical methods such as the finite element method should be used. Despite the shortcomings of the empirical methods, the current design methodology for underground structures (DOD, 2008, 2002, 1986) makes significant use of the conservative empirical approach discussed in Chapter 6 of this report.

5. COMPARISON OF EXPLOSIVE LOADS AND SEISMIC LOADS IN UNDERGROUND MEDIUM

Three sources of dynamic waves that may propagate through an underground medium. These are (i) natural earthquakes, (ii) surface explosions, and (iii) underground explosions. Although this discussion focuses on conventional explosive loads and seismic loads, explosive loads from nuclear weapons are discussed herein to the extent applicable (ASCE, 1985). Differences between the characteristics of explosion-induced and earthquake-induced responses of the geological media are examined here to support analyses on the effects of these sources in Chapter 6 of this report.

Natural earthquakes primarily occur due to the sudden release of strain energy when the rock ruptures at plate boundaries or at faults. As the earthquake occurs at depth, dynamic waves radiate away from the source and travel rapidly through Earth's crust, as shown in Figure 5-1 (Gere and Shah, 1984). These waves are either body waves or surface waves (Kramer, 1996).

When an explosive is detonated in air near the surface, it produces overpressure in the air (Section 2.2, Figure 2-2), which interacts with the ground surface and, under certain circumstances may create a crater (Section 2.2, Figure 2-4, and Section 3.4.2). When an

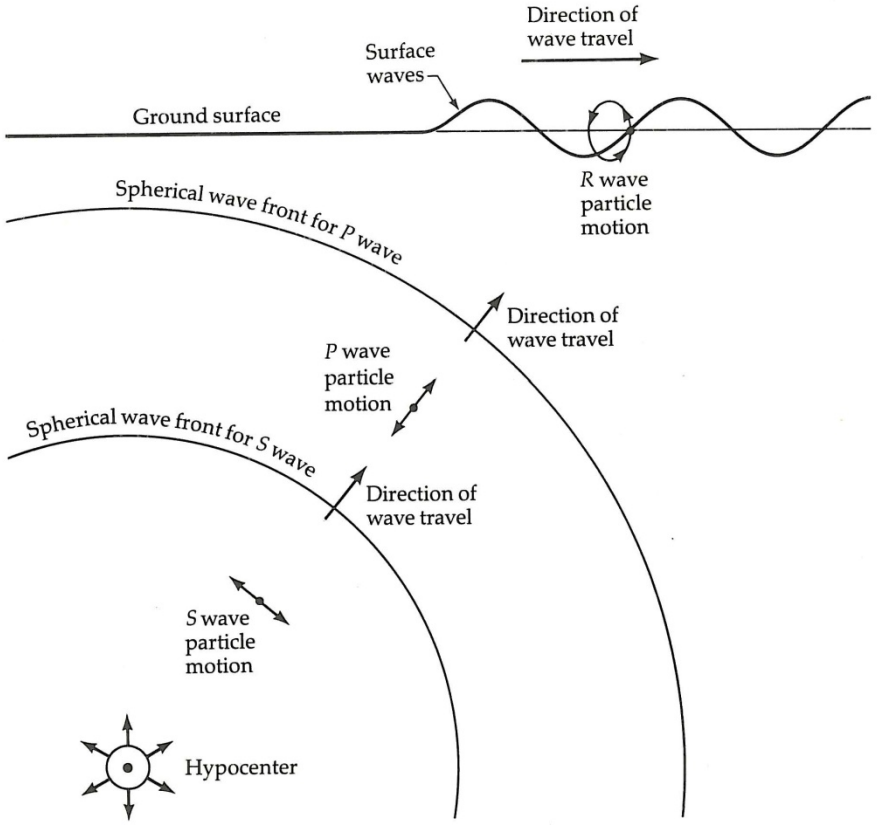

Figure 5-1 Seismic Waves (After Gere and Shah, 1984)

explosion occurs at the surface, it is more likely to produce a crater, because of the intense interaction associated with more direct coupling of the energy into the ground (Sections 2.2 and 3.4.2). The shock wave produces body waves and surface waves, as discussed in Sections 2.2 and 2.4.

Body waves are created by the energy released at relatively great depth by an earthquake and at shallow depths in the vicinity of a surface or near-surface explosion. Two types of body waves travel through the underground media: P-waves and S-waves. P-waves, also known as primary, compressional, or longitudinal waves, involve successive compression and rarefaction of the underground media through which they pass. The P-waves can travel through both solid and fluid media. Underground media are stiffest in compression, so P-waves travel faster than other seismic waves and are therefore the first to arrive at a particular site. S-waves, also known as secondary, shear, or transverse waves, produce shear deformations as they travel through a material. S-waves can travel only through solid media. S-waves are divided into two components: SV (vertical plane movement) and SH (horizontal plane movement). The speed at which body waves travel varies with the stiffness of the underground media. Figure 5-2 shows travel time of a seismic wave.

When body waves interact with either the surface or surficial layers of the Earth, surface waves result. The waves that travel along the Earth's surface have amplitudes that decrease roughly exponentially with depth. Surface waves are more prominent at lateral distances farther from

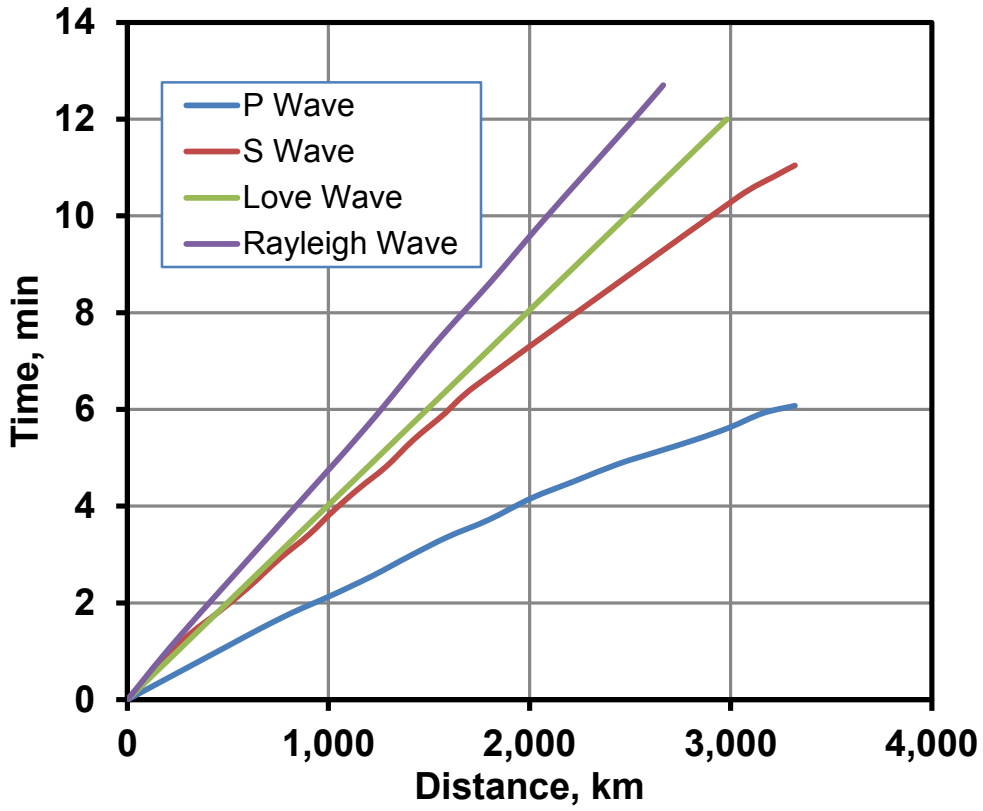

Figure 5-2 Example of a Seismic Wave's Travel Time

the source of an earthquake. This is because of the nature of the interactions that take place between the body waves and the surface and surficial layers of the Earth that produce them. For engineering purposes, Rayleigh waves and Love waves are the two most important surface waves. Raleigh waves have both vertical and horizontal particle motion, whereas Love waves have only horizontal particle motion.

There are differences between the waves generated by earthquakes and those of explosions. These may be due to differences in various parameters, such as source dimension, source time function, source mechanism and focal depth, or a combination of these parameters (Dahy and Hassib, 2009). Because explosions are primarily spherically symmetric disturbances, the explosions radiate p-waves efficiently. In contrast, earthquakes that result primarily from sliding or rupture along a buried fault surface, over a relatively large area for a longer time, excite the transverse motions of S-waves efficiently. Berry (1967) found that for earthquakes and underground nuclear tests with body waves of similar magnitude, the surface waves for the underground explosions are usually much smaller in amplitude than those for the earthquakes. Thus, all explosions will show stronger P-waves and weaker S-waves than observed for similar magnitude earthquakes (Figure 5-3) (University of California at Berkeley, 2009; Vortman, 1982, 1981; Walter, 2013; Walter, et al., 1998). Another reason for the relatively high amplitude P-waves and relatively lower amplitude surface waves for explosions is that these types of events release energy rapidly from a “point” source (Berry, 1967). However, despite these differences, seismic velocity is often used as a crude index of soil properties for ground shock prediction purposes.

To further distinguish the explosions from earthquakes, seismic waves for two cases have been studied in detail by Walter (2013). One way to quantify the difference between explosions and earthquakes is by determining the ratio of P-wave to S-wave (P/S) energy measured for both explosions and earthquakes. Explosions should result in higher P/S ratios than similarly located earthquakes. However, the frequency at which the best separation of explosion P/S ratio and earthquake P/S ratio occurs varies by conditions of geology of the region where explosions and earthquakes take place. Figure 5-4 shows the P/S ratio from a May 11, 1998, nuclear explosion test in India and for earthquakes in Asia (Figure 5-5). The measurements in Figure 5-4 were made at four different frequencies. The India test has a higher P/S ratio than the earthquakes, as expected. The other approach is to analyze the moment tensor of seismic data collected from various monitoring stations. The moment tensor solution should yield information on the source mechanism that triggers the ground shaking (Ford, et al., 2007; University of California at Berkeley, 2009).

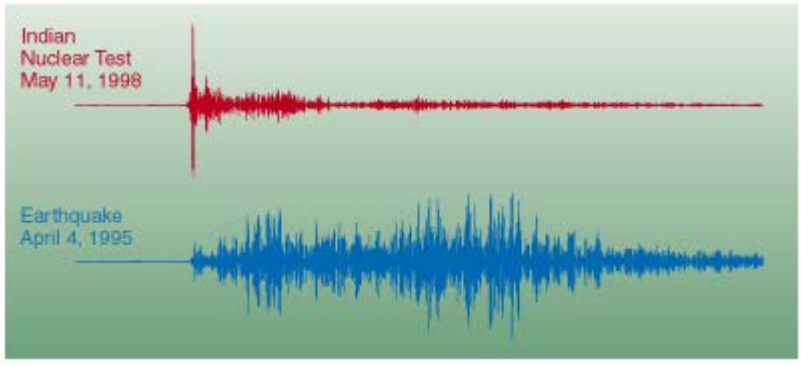

Figure 5-3 Comparison of Nuclear Explosion With an Earthquake Generated Wave Signals (After Walter, 2013)

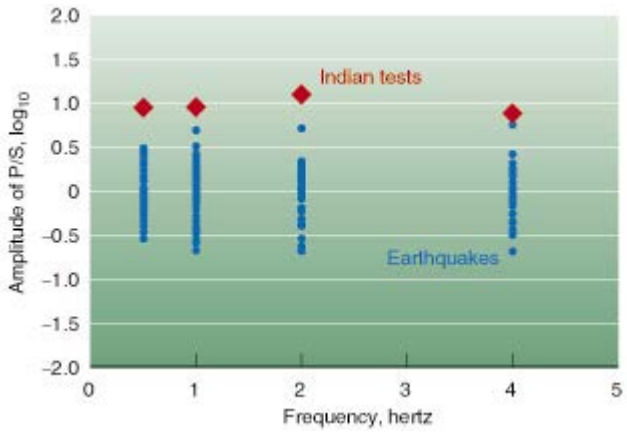

Figure 5-4 Comparison of P- to S-Wave Ratios of a Nuclear Explosion With Those of an Earthquake at Different Frequencies (After Walter, 2013)

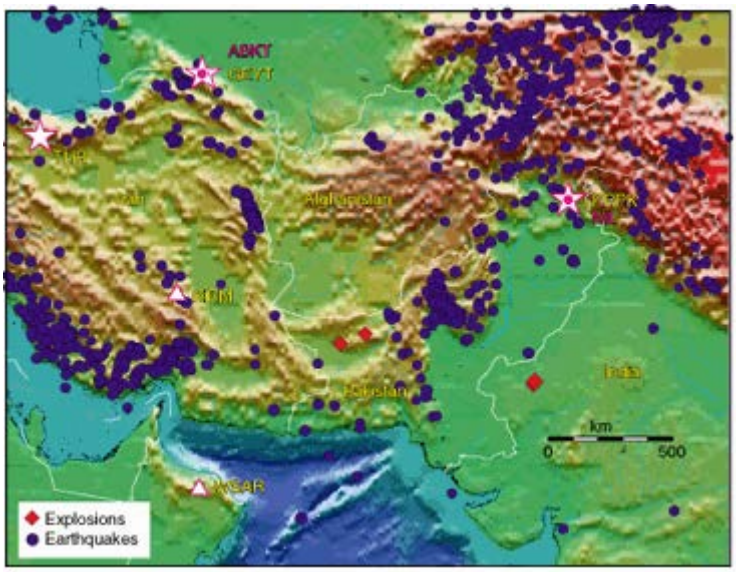

Figure 5-5 Topographic Map Showing Locations of Nuclear Test Locations (Diamonds), Earthquakes (Circles), Primary International Monitoring System (Stars), and Auxiliary International Monitoring System (Triangles) (After Walter, 2013)

The underground structures may be subjected to explosive and/or seismic loads, which have different characteristics, as shown in Figures 5-3 and 5-4. The differences in effects of these loads on underground structures are discussed qualitatively in Chapter 6 of this report.

6. DESIGN CONSIDERATIONS FOR PROTECTION OF UNDERGROUND STRUCTURES

The stress transients generated by high explosive detonations in air, near the surface, and underground can cause severe damage to underground structures. Underground structures that are designed to withstand detonation of high explosive charges mostly include sensitive military facilities, civil defense facilities, and, most recently, nuclear power plants [e.g., proposed small modular reactors (Braverman, et al., 1997)]. Military facilities include bunkers, missile silos, command and control facilities, and communication facilities. The shock exerted on an underground structure by detonation of high explosives will vary with the intensity of detonation force (Table 2-2), the distance of detonation from the underground structure (Figure 2-6), any barrier or protective system between the detonation point and the structure,(Figure 2-5), soil and rock types, and various drainage conditions of the underground media.

The pressure–time relationships of different components of underground structures, such as roof panels and exterior walls, depend not only on their distances from the location of detonation but also their geometric orientation with respect to detonation location. For example, an overhead burst produces the most critical loading for a roof panel, while a side burst produces the most critical loading for an exterior wall. Furthermore, the magnitude and distribution of the load acting on an underground structure component is greatly influenced by the deformability of the underground structure because of “soil arching” phenomena (Kiger, et al., 1984).

The effect of the soil is to modify the shock exerted on an underground structure as discussed in Section 2.2 of this report. The available capacity of the underground structure to resist blast load is reduced by the dead (or gravitational) load of the soil. At the same time, a portion of the soil surrounding the underground structure acts with the structural elements to increase the mass without proportional increase of stiffness, thereby increasing the natural period of vibration of the underground structure. A common approach is to treat the increase of mass approximately by assuming that the (i) mass of 0.61 m [2 ft] of soil acts with the mass of wall and (ii) entire mass of the soil supported by the roof or a depth of soil equal to one-quarter of the roof span (short span for a two-way panel), whichever is smaller, acts with the mass of the roof (DOD, 2008).

Underground structures should be designed so the dynamic response is limited to comparatively small deformations to prevent structural collapse due to Earth loads. Concrete underground structures should be designed so that the failure is caused by yielding of the reinforcing steel with sufficient ductility (DOD, 2008, 2002, 1986). The design of steel structures should use appropriate U.S. Department of Defense steel design codes and standards (DOD, 2008, 2002, 1986). To ensure any failure of underground structures is in the ductile regime, DOD (2008, 1986) suggests various ductility factors for different components of structures subjected to explosive loads.

An underground structure that may be subjected to both explosive and seismic loads should be designed to perform its intended function under both these loads. Although both of these dynamic loads require high energy-absorbing capacity of the underground structures, their energy spectra are very different. There are differences both in the spectral shape and in the magnitude of the spectral quantities. As a result, one spectrum will not reasonably envelope another spectrum. Furthermore, explosive and seismic loads can be assumed to occur independently of each other.

The combination of seismic load with other loads is well established in the design codes and standards (e.g., ACI, 2011, 2006; AISC, 2007, 1994). Although the design load combinations for reinforced concrete and steel nuclear structures in American Concrete Institute (2006) and American Institute of Steel Construction (2007), respectively, include missile impact load as an abnormal load, that impact load is generated internally by an operational accident, such as pipe whipping generated by or during the postulated accident. This is not relevant to the external explosive loads on underground structures addressed in this report. However, a similar approach for combining external explosive load with other loads will be reasonable for the design of underground structures.

7. OTHER PUBLICATIONS

The listed references are provided in this section for information only. They are not an NRC endorsement or acceptance of material content, methods, or approaches. Exceptions are Regulatory Guides, which provide methods or approaches acceptable for meeting NRC regulatory requirements.

Bailey, A. and S. Murray. *Explosives, Propellants, and Pyrotechnics.* London, United Kingdom: Brassey's. 1989.

Bowen, I.G., E.R. Fletcher, and D.R. Richmond. "Estimate of Man's Tolerance to the Direct Effects of Air Blast." Technical Report to Defense Atomic Support Agency, DASA 2113. Albuquerque, New Mexico: Lovelace Foundation for Medical Education and Research, AD 693105. October 1968.

GSA. "Window Glazing Analysis Response and Design (WINGARD)." Washington, DC: U.S. General Service Administration. 2013. Restricted.

Henry, G.A. "Blast Injuries to the Ear." *Laryngoscope*. Vol. 55. pp. 663–672. 1945.

Hirsch, F.G. "Effects of Overpressure on the Ear—A Review." *Annals New York Academy of Sciences*. Vol. 152, Art. 1. pp. 147–162. 1968.

Lees, F. *Loss Prevention in the Process Industries.* Oxford, United Kingdom: Butterworth-Heineman. 1996.

Malonee, D., S. Shariat, G. Stennies, R. Waxweiler, D. Hogan, and F. Jordan. "Physical Injuries and Fatalities Resulting From the Oklahoma City Bombing." *Journal of the American Medical Association.* Vol. 276, No. 5. pp. 382–387. 1996.

Merrifield, R. and J. MacKenzie. "Methodology for Estimating Explosive Yield of Incidents Involving Conventional or Improvised Explosives." Proceedings of the 8th International Symposium on the Interaction of the Effects of Munitions with Structures, McLean, Virginia, April 22–25, 1997.

NRC. Regulatory Guide 1.91, "Evaluation of Explosions Postulated to Occur at Nearby Facilities and on Transportation Routes Near Nuclear Power Plants." Rev. 2. ML12170A980. Washington, DC: U.S. Nuclear Regulatory Commission. 2011.

ORNL/NRC. "Guidance for Using Underwater Explosion (UNDEX) Data for Estimating Load on Submerged Target." Oakridge, Tennessee: Oak Ridge National Laboratory and Washington, DC: U.S. Nuclear Regulatory Commission. November 2003. Unclassified.

Ross, R., A. Coles, G. Garinther, D. Hodge, and C. Rice. "Criteria for Assessing Hearing Damage Risk from Impulse-Noise Exposure." Aberdeen Proving Ground, Maryland: Human Engineering Laboratory, AD 666 206. 1967.

Sartori, L. "The Effects of Nuclear Weapons." *Physics Today*. Vol. 36, Issue 3. pp. 32–41. 1983.

U.S. Army Corps of Engineers. “Single Degree Freedom Blast Design Spreadsheet (SBEDS).” *Version 5 Software and Methodology Manual*. Omaha, Nebraska: U.S. Army Corps of Engineers. March 2013. Unclassified.

U.S. Department of Army. *Structures to Resist the Effects of Accidental Explosions*. Army Manual TM 5-1300. Washington, DC: U.S. Department of Army. 1990.

U.S. Department of Defense. “Effects of Nuclear Weapons.” Washington, DC: Government Printing Office. 1977.

White, C.S. “The Scope of Blast and Shock Biology and Problem Areas in Relating Physical and Biological Parameters.” *Annals of the New York Academy of Sciences*. Vol. 152, Art. 1. pp. 89–102. 1968.

8. CONCLUSIONS

An underground structure may located with its upper elements at the ground surface or be deep underground. The physical positions of underground structures make them potentially vulnerable to terrorist attacks, though being located underground can provide a measure of protection. Explosive devices used in terrorist attacks are typically homemade, chemical-based explosive devices that could be fabricated from either military or commercial grade explosives, through theft or purchase, or from explosives that could be manufactured by combining publicly available common chemicals. An Improvised Explosive Device (IED) is the most prevalent form of explosive device that is used by terrorists. A Vehicle Borne Improvised Explosive Device (VBIED) is an IED in which a vehicle is used as a package and delivery means to conduct an attack. The energy released by an explosion is normally expressed as an equivalent weight of trinitrotoluene (TNT). The maximum TNT-equivalent explosive holding capacities of vehicles in the US range from about 227 to 27,215 kg [500 to 60,000 lb]. The type of vehicle used for a VBIED determines the height at which the VBIED detonates above the ground, making it an important parameter for explosion effects on surface and underground structures.

A detonation above the ground surface (often referred to as an air blast) produces a blast wave characterized by two distinct phases: the positive phase and the negative phase. During the positive phase, the blast wave overpressure rises very rapidly from zero (ambient) to peak value, subsides more slowly to zero (ambient), and further subsides to the negative phase. The peak value of negative pressure, which is called peak underpressure, is usually much smaller than the peak overpressure. The portion of the air-blast wave refracted into the ground and the underground wave generated by the blast at the ground surface are propagated through the underground media radially outward, potentially creating a crater and generating underground soil pressures that attenuate because of geometric and hysteresis effects. The underground soil pressure at a given location depends on the strength of the explosive, the properties of the media through which the blast waves propagate, and the distance from the explosion. This underground soil pressure affects the response of underground structures. Empirical equations are available for calculating important parameters that affect underground structures, such as explosion wave arrival time at the location of the structure; duration of the explosive wave; peak free-field pressure; impulse force; and particle displacement, velocity, and acceleration.

This report presents a parametric study on the subsurface effects caused by a surface burst. The size of the TNT-equivalent charge was varied and the resulting soil pressures and surface crater size were predicted. Charge weights varied from 45.3 kg [100 lb] to 4,536 kg [10,000 lb]. The finite element predicted crater dimensions were within the range of the empirically derived dimensions for all the TNT-equivalent charge sizes considered. For the case of a 100-kg [220-lb]-TNT-equivalent charge, the finite element soil pressures correlated well with the pressures calculated from empirical relationships. Additional analyses were conducted for TNT-equivalent charge sizes of 4,536; 9,072; 18144; and 27,216 kg [10,000; 20,000; 40,000; and 60,000 lb]. For the larger explosive charges, it was necessary to use the element deletion technique to eliminate excessive mesh distortion. Using this element deletion technique resulted in predicted apparent crater depths that were within the empirically calculated range; however, the predicted crater radii were slightly less than the empirically calculated lower limit. It is recommended that the equivalent plastic strain soil failure criterion value be further investigated, as well as alternative failure criteria, such as equivalent total strain and maximum principal tensile strain. Element-to-particle conversion techniques were considered; however, it was determined that element-to-particle techniques in ABAQUS/Explicit are currently not possible because of documented code errors that remain unresolved by the code vendor. An Eulerian analysis was performed for a 454-kg [1,000-lb] explosive charge, which predicted an

apparent crater depth within the range calculated using empirical equations of Gould (1981). Further investigation is recommended to evaluate the adequacy of mesh refinement in the air domain.

Design considerations are needed to protect underground structures subjected to dynamic forces generated by explosions in air, near the surface, and underground. These include special features associated with the behavior of underground structures (e.g., closely coupled motion of underground structures and surrounding soil and larger secondary effects due to lateral displacement of underground structures) and their analysis and design using specific design methodology.

In general, underground structures should be designed to withstand both explosive loads and seismic loads. Although explosive and seismic loads are similar in that they both produce P-waves, S-waves, and surface waves, explosions result in higher P/S ratios than similarly located earthquakes, making the energy spectra very different. In addition, there may be significant differences in the magnitude of spectral quantities. As a result, one spectrum will not reasonably envelope another spectrum. Nevertheless, an approach similar to that in American Concrete Institute (2011, 2006) and American Institute of Steel Construction (2007, 1994) of combining internal accidental missile load with other loads may be a reasonable approach for combining the external explosive load with other loads for the design of underground structures.

9. REFERENCES

ACI. "Building Code Requirements for Structural Concrete (ACI 318-11) and Commentary." ACI 318-11. Farmington Hills, Michigan: American Concrete Institute. 2011.

ACI. "Code Requirements for Nuclear Safety-Related Concrete Structures (ACI 349-06) and Commentary." Farmington Hills, Michigan: American Concrete Institute. 2006.

AISC. "Specification for Safety-Related Steel Structures for Nuclear Facilities." ANSI/AISC N690–06. Chicago, Illinois: American Institute of Steel Construction, Inc. 2007.

AISC. "Manual of Steel Construction—Load and Resistance Factor Design." 2nd Edition. Chicago, Illinois: American Institute of Steel Construction, Inc. 1994.

ANSYS. "Autodyn." Canonsburg, Pennsylvania: ANSYS Inc. <http://www.ansys.com> (March 11, 2013).

ASCE. "Manual 42, Design of Structures to Resist Nuclear Weapons Effects." New York City, New York: American Society of Civil Engineers. 1985.

Baker, W.E. *Explosions in Air*. Austin, Texas: University of Texas Press. 1973.

Bangash, M.Y.H. "*Manual of Numerical Methods in Concrete: Modeling and Applications Validated by Experimental and Site-Monitoring Data*." London, United Kingdom: Thomas Telford Publishing. 2001.

Baylot, J.T. "Parameters Affecting Loads on Buried Structures Subjected to Localized Blast Effects." Vicksburg, Mississippi: Department of the Army, Waterways Experiment Station, Corps of Engineers. 1992.

Berry, G. "Earthquakes or Explosion?" *Engineering and Science*. Pasadena, California: California Institute of Technology. 1967. <http://calteches.library.caltech.edu/265/1/berry.pdf> (February 1, 2013).

Braverman, J., R. Morante, and C. Hofmayer. NUREG/CR–6486, BNL–NUREG–52520, "Assessment of Modular Construction for Safety-Related Structures at Advanced Nuclear Power Plants." Washington, DC: U.S. Nuclear Regulatory Commission. March 1997.

Bretz, T.E. "Soil Liquefaction Resulting From Blast-Induced Spherical Stress Waves." Final Report. WL–TR–89–100. New Mexico: Kirtland Air Force Base, Weapons Laboratory, Air Force Systems Command. January 1990.

Brode, H.L. "Numerical Solutions of Spherical Blast Waves." RM–1363–AEC. Santa Monica, California: The Rand Corporation. September 1954.

Chen, H.L., S.P. Shah, and L.M. Keer. "Dynamic Response of Shallow-Buried Cylindrical Structures." *Journal of Engineering Mechanics*. Vol. 116, No. 1. pp. 152–171. 1990.

Cooper, P.W. *Explosives Engineering*. Hoboken, New Jersey: John Wiley & Sons, Inc. 1996.

Dahy, A.S. and H.G. Hassib. "Discriminating Nuclear Explosions From Earthquakes at Teleseismic Distances." *European Journal of Applied Sciences*. Vol. 1, No. 4. pp. 47–52. 2009.

Das, B.M. *Principles of Soil Dynamics.* Boston, Massachusetts: PWS-Kent Publishing Company. 1993.

Dassault Systèmes Simulia Corp. "ABAQUS Theory Manual, Version 6.12." Providence, Rhode Island: Dassault Systèmes Simulia Corp. 2012a.

Dassault Systèmes Simulia Corp. "ABAQUS Analysis User's Manual, Version 6.12." Providence, Rhode Island: Dassault Systèmes Simulia Corp. 2012b.

Department of Army. "Explosives and Demolitions." FM 3–34.214 (FM 5–250). Washington, DC: Department of the Army. 2008. <http://info.publicintelligence.net/USArmy-Explosives.pdf> (April 16, 2013).

Department of Navy. "U.S. Explosive Ordnance." OP 1664. Washington, DC: Bureau of Ordnance Publication. May 28, 1947.

DOD. "Structures To Resist the Effects of Accidental Explosions." Unified Facilities Criteria (UFC) 3–340–02. Arlington, Virginia: Department of Defense. December 2008.

DOD. "Design and Analysis of Hardened Structures to Conventional Weapons Effects." Unified Facilities Criteria (UFC) 3-340-01. Arlington, Virginia: Department of Defense. June 2002.

DOD. "Fundamentals of Protective Design for Conventional Weapons." TM 5–855–1. Arlington, Virginia: Department of Defense. 1986.

DOD and ERDA. "The Effects of Nuclear Weapons." Washington, DC: Department of Defense and Energy Research and Development Administration. 1977.

DOE. "A Manual for the Prediction of Blast and Fragment Loadings on Structures." DOE/TIC–11268. Amarillo, Texas: U.S. Department of Energy, Albuquerque Operations Office. August 1981.

Dove, R.C. "Evaluation of In-Structure Shock Prediction Techniques for Buried RC Structures." DNA–TR–91–89. Alexandria, Virginia: Defense Nuclear Agency, USAE Waterways Experiment Station. March 1992.

Ford, S.R., D.S. Dreger, and W.R. Walter. "Identifying Isotropic Events Using an Improved Regional Moment Tensor Inversion Technique." Proceedings of the 29th Monitoring Research Review: Ground-Based Nuclear Explosion Monitoring Technologies, Los Alamos, New Mexico, September 25–27, 2007. Los Alamos, New Mexico: National Nuclear Security Administration, Los Alamos National Laboratory and Brooks City Base, Texas: Air Force Research Laboratory. 2007. <http://www.osti.gov/bridge/servlets/purl/1027449/1027449.pdf> (February 1, 2013).

Geersb, T.L. and K.S. Hunter. "An Integrated Wave-Effects Model for an Underwater Explosion Bubble." *Journal of the Acoustical Society of America*. Vol. 111, No. 4. pp. 1,584–1,601. 2002.

Gere, J.M. and H.C. Shah. *Terra Non Firma: Understanding and Preparing for Earthquakes*. New York City, New York: W.H. Freeman and Company. 1984.

Gerlach, C.A. and G.R. Johnson. "Further Developments and Applications of Advanced Computational Approaches for Explosive-Soil-Air-Structure Interactions." Final Report. SwRI Report 18.14477. Minneapolis, Minnesota: Southwest Research Institute®. September, 2009.

Glasstone, S. and P.J. Dolan. "The Effects of Nuclear Weapons." 3rd Edition. Washington, DC: Department of Defense and Energy Research and Development Administration. 1977. <http://www.fourmilab.ch/etexts/www/effects/> (January 24, 2013).

GM. "2013 Chevrolet Express Cargo Specifications." Detroit, Michigan: General Motors Corporation. December 2012a. <http://media.gm.com/media/us/en/chevrolet/vehicles/express_cargo_van/2013.tab1.html> (December 13, 2012).

GM. "Vehicle and Frame Height Charts—2008: GM Upfitter Integration." Detroit, Michigan: General Motors Corporation. December 2012b. <http://www.gmupfitter.com/publicat/2008_BB/2008LD_FrameHgt_D1.pdf> (December 2012).

Gould, K.E. "High-Explosive Field Tests: Explosion Phenomena and Environmental Impacts." DNA 6187F. Washington, DC: Defense Nuclear Agency. October 1981.

Healey, J., G. Pecone, A. Ammar, S. Weissman, J. Vellozzi, and N. Dobbs. "Design of Steel Structures to Resist the Effects of HE Explosions." Technical Report 4837. New York City, New York: Ammann & Whitney Consulting Engineers. August 1975.

Hirsch, F.G. "Effects of Overpressure on the Ear—A Review." Washington, DC: Defense Atomic Support Agency. November 1966.

Huang, T.-K. and W.-F. Chen. "Simple Procedure for Determining Cap-Plasticity-Model Parameters." *Journal of Geotechnical Engineering*. Vol. 116, No. 3. pp. 492–513. 1990.

Kana, D.D., B.H.G. Brady, B.W. Vanzant, and P.K. Nair. NUREG/CR–5440, CNWRA/89-001, "Critical Assessment of Seismic and Geomechanics Literature Related to a High-Level Nuclear Waste Underground Repository." Washington, DC: U.S. Nuclear Regulatory Commission. 1991.

Kiger, S.A., T.R. Slawson, and D.W. Hyde. "Vulnerability of Shallow-Buried Flat-Roof Structures." Report 6, Technical Report SL–80–7. Vicksburg, Mississippi: U.S. Army Engineer Waterways Experiment Station. September 1984.

Kinney, G.F. and K.J. Graham. *Explosive Shocks in Air*. Berlin, Germany: Springer-Verlag. 1985.

Klaseboer, E., K.C. Hung, C. Wang, C.W. Wang, B.C. Khoo, P. Boyce, S. Debono, and H. Charlier. "Experimental and Numerical Investigation of the Dynamics of an Underwater Explosion Bubble Near a Resilient/Rigid Structure." *Journal of Fluid Mechanics*. Vol. 537. pp. 387–413. 2005.

Kramer, S.L. *Geotechnical Earthquake Engineering*. Upper Saddle River, New Jersey: Prentice-Hall, Inc. 1996.

Krauthammer, T. and A. Altenberg. "Negative Phase Blast Effects on Glass Panels." *International Journal of Impact Engineering*. Vol. 24. pp. 1–17. 2000.

Larcher, M. "Simulation of the Effects of an Air Blast Wave." JRC Technical Notes (JRC) 41337. Luxembourg: European Communities. 2007.

Liu, G.R. and M.B. Liu. *Smoothed Particle Hydrodynamics: A Meshfree Particle Method*. London, England: World Scientific Publishing Company. October 2003.

LSTC. "LS-DYNA." 2013. Livermore, California: Livermore Software Technology Corporation. <http://www.lstc.com/> (March 8, 2013).

McVay, M.K. "Spall Damage of Concrete Structures." Technical Report SL–88–22. Vicksburg, Mississippi: Department of the Army, Waterways Experiment Station, Corps of Engineers. June 1988.

Murphy, J.R. "Near-Field Rayleigh Waves From Surface Explosions." *Bulletin of the Seismological Society of America*. Vol. 71, No. 1. pp. 223–248. February 1981.

Nagy, N., M. Mohamed, and J.C. Boot. "Nonlinear Numerical Modelling for the Effects of Surface Explosions on Buried Reinforced Concrete Structures." *Geomechanics and Engineering*. Vol. 2. pp. 1–18. 2010.

Nardin, J. "Homemade Explosives." Laramie, Wyoming: Arista Tek, Inc. 2005.

Newmark, N.M. and E. Rosenblueth. *Fundamentals of Earthquake Engineering*. Englewood Cliffs, New Jersey: Prentice-Hall, Inc. 1971.

Paz, M. and W. Leigh. *Structural Dynamics: Theory and Computation*. 5th Edition. Norwell, Massachusetts: Kluwer Academic Publishers. 2004.

PCI. *Design Handbook Precast Prestressed Concrete*. Chicago, Illinois: Prestressed Concrete Institute. 1978.

Richmond, D.R. and C.S. White. "Biological Effects of Blast and Shock." Washington, DC: Department of Defense, Defense Atomic Support Agency. April 1966.

Riley, M. "Modeling Gas Bubble Behaviour and Loading on a Rigid Target Due to Close-Proximity Underwater Explosions: Comparison to Tests Conducted at DRDC Suffield." DRDC Atlantic TM 2010-238. Canada: Defence R&D Canada–Atlantic. November 2010a.

Riley, M. "Analytical Solutions for Predicting Underwater Explosion Gas Bubble Behaviour." DRDC Atlantic TM 2010-237. Canada: Defence R&D Canada–Atlantic. November 2010b.

Rostberg, J.I. "Common Chemicals As Precursors of Improvised Explosive Devices: The Challenges of Defeating Domestic Terrorism." Master's thesis. Naval Postgraduate School. Monterey, California. September 2005. <http.//www.amazon.com/Chemicals-Precursors-Improvised-Explosive-ebook/dp/B007PRUQTG> (March 31, 2013)

Sandia. "CTH Shock Physics." Albuquerque, New Mexico: Sandia National Laboratories. <http://www.sandia.gov/CTH/index.html> (March 8, 2013.)

Slawson, T.R., S.B. Garner, and S.C. Woodson. "Yield Effects on the Response of a Buried Blast Shelter." Technical Report SL–86–5. Vicksburg, Mississippi: Department of the Army, Waterways Experiment Station, Corps of Engineers. April 1986.

Smith, P.D. and J.G. Hetherington. *Blast and Ballistic Loading of Structures*. Oxford, England: Butterworth-Heinemann. 1994.

University of California at Berkeley. "Of Nuclear Bombs and Earthquakes." Berkeley, California: University of California at Berkeley. 2009. <http://seismo.berkeley.edu/blog/seismoblog.php/2009/05/25/of-nuclear-bombs-and-earthquakes> (February 1, 2013).

U.S. National Counterterrorism Center. "DHS Bomb Threat Stand-Off Chart." 2006. <http://www.nctc.gov/docs/2006_calendar_bomb_stand_chart.pdf> (January 29, 2013).

Vortman, L.J. "Ground Motion From Earthquakes and Underground Nuclear Weapons Tests: A Comparison as it Relates to Siting a Nuclear Waste Storage Facility at NTS." SAND–81–2214. Albuquerque, New Mexico: Sandia National Laboratories. 1982.

Vortman, L.J. "A Comparison of Ground Motion from Earthquakes and Underground Nuclear Weapons Tests at NTS." Workshop on Seismic Performance of Underground Facilities, Augusta, Georgia. Albuquerque, New Mexico: Sandia National Laboratories. 1981.

Walter, W.R. "Monitoring Clandestine Nuclear Tests." Livermore, California: Lawrence Livermore National Laboratory. 2013. <https://www.llnl.gov/str/Walter.html.2013> (January 15, 2013)

Walter, W.R., A.J. Rodgers, K. Mayeda, S.C. Myers, M. Pasyanos, and M. Denny. "Preliminary Regional Seismic Analysis of Nuclear Explosions and Earthquakes in Southwest Asia." UCRL–JC–130745–Ext–Abs–Rev–1. Livermore, California: Lawrence Livermore National Laboratory. 1998.

Wang, Z., Y. Lu, and C. Bai. "Numerical Analysis of Blast-Induced Liquefaction of Soil." *Computers and Geotechnics*. Vol. 35, No. 2. pp. 196–209. 2008.

Wang, Z., Y. Lu, and H. Hao. "Numerical Investigation of Effects of Water Saturation on Blast Wave Propagation in Soil Mass." *Journal of Engineering Mechanics*. Vol. 130, No. 5. pp. 551–561. 2004.

Weidlinger, P. and E. Hinman. "Analysis of Underground Protective Structures." *Journal of Structural Engineering*. Vol. 114, No. 7. pp. 1,658–1,673. 1988.

White, C.S. "Biological Effects of Blast." Washington, DC: Department of Defense, Defense Atomic Support Agency. December 1961.

Wilt, T., G. Ofoegbu, and S. Hsiung. "Vulnerability Assessment of Buried Near-Surface Structures Subject to Ground Surface Blasts." San Antonio, Texas: Center for Nuclear Waste Regulatory Analyses. March 2012.

NRC FORM 335 (12-2010) NRCMD 3.7

U.S. NUCLEAR REGULATORY COMMISSION

BIBLIOGRAPHIC DATA SHEET

(See instructions on the reverse)

1. REPORT NUMBER (Assigned by NRC, Add Vol., Supp., Rev., and Addendum Numbers, if any.)

NUREG/CR-7201

2. TITLE AND SUBTITLE

Charactarizng Explosive Effects on Underground Structures

3. DATE REPORT PUBLISHED

MONTH	YEAR
September	2015

4. FIN OR GRANT NUMBER

5. AUTHOR(S)

A. H. Chowdhury
T. E. Wilt

6. TYPE OF REPORT

Technical

7. PERIOD COVERED (Inclusive Dates)

8. PERFORMING ORGANIZATION - NAME AND ADDRESS (If NRC, provide Division, Office or Region, U. S. Nuclear Regulatory Commission, and mailing address; if contractor, provide name and mailing address.)

Center for Nuclear Waste Regulatory Analyses
Southwest Research Institute®
6220 Culebra Road
San Antonio, Texas 78238-5166

9. SPONSORING ORGANIZATION - NAME AND ADDRESS (If NRC, type "Same as above", if contractor, provide NRC Division, Office or Region, U. S. Nuclear Regulatory Commission, and mailing address.)

Division of Security Policy
Office of Nuclear Security and Incident Response
U.S. Nuclear Regulatory Commission
Washington, DC 20555-0001

10. SUPPLEMENTARY NOTES

11. ABSTRACT (200 words or less)

The overall objective of this report is to identify and evaluate potential effects on underground structures of a VBIED explosion that is assumed to occur in air near or on the ground surface. This report describes the characteristics of VBIEDs; dynamics of explosion propagation through air, underground soil medium, and underwater; computational methods to quantify blast-induced pressures; empirical relationships and numerical analyses to calculate soil pressure distribution and estimate crater formation; computational methods to evaluate underground structural response; and relevant design standards and guidance applicable to underground structures. This report also provided numerical determination of the "zones of influence" in the underground medium due to air and surface explosions of different magnitudes. The explosive and seismic loads to which an underground structure may be subjected are compared. The report includes a qualitative assessment of the design of an underground structure that will need to be done for (i) two individual design spectra (one for explosive load and the other for seismic load) or (ii) only one of these two design spectra that may envelope the other spectrum.

12. KEY WORDS/DESCRIPTORS (List words or phrases that will assist researchers in locating the report.)

Blast-induced effects
Codes and Standards for Design of Underground Structures
Explosive loads and seismic loads
Improvised Explosive Device (IED)
Underground structures subjected to explosive loads
Vehicle Borne Improvised Explosive Device (VBIED)

13. AVAILABILITY STATEMENT

unlimited

14 SECURITY CLASSIFICATION

(This Page)

unclassified

(This Report)

unclassified

15. NUMBER OF PAGES

16. PRICE

NRC FORM 335 (12-2010)

Federal Recycling Program

UNITED STATES
NUCLEAR REGULATORY COMMISSION
WASHINGTON, DC 20555-0001

OFFICIAL BUSINESS